Isern, A.R., Anselmetti, F.S., Blum, P., et al., 2002
Proceedings of the Ocean Drilling Program, Initial Reports Volume 194

8. Site 1197[1]

Shipboard Scientific Party[2]

INTRODUCTION

Site 1197 (proposed Site CS-08A) is located on the Southern Marion Plateau, 40 km east of the Great Barrier Reef margin and ~5 km southeast of the downcurrent, windward slope of the Southern Marion Platform (SMP) (Fig. F1). The site is located on regional multichannel seismic lines MAR07 (shotpoint 3721) (Fig. F2), MAR65 (shotpoint 645), and MAR 66 (shotpoint 907) in 348 m of water. Two holes were drilled at Site 1197 (Hole 1197A: 0–203.8 meters below sea floor [mbsf]; Hole 1197B: 0–674.9 mbsf) through a 666.6-m-thick sedimentary succession and 8.3 m into a volcaniclastic breccia with underlying basalt, possibly representing acoustic basement. Sediments at this site consist of predominantly periplatform and hemipelagic deposits of wackestone to grainstone textures occurring in water depths >150 m, with the exception of the lowermost sedimentary unit, which was deposited in depths <100 m.

The main purpose of this site was to retrieve a proximal platform margin record of sedimentation on the adjacent carbonate platform for documenting and dating platform growth. In particular, this site reveals a pattern of platform shedding in a downcurrent direction and subsequent current reworking. Furthermore, results from Site 1197 indicate that fluids are flowing out of the adjacent carbonate platform. Site 1197 also documents the age and nature of acoustic basement.

OPERATIONS

Operations at Site 1197 (proposed Site CS-08A) began when a beacon was dropped on site coordinates at 0711 hr on 6 February 2001. The corrected precision depth recorder indicated a water depth of 352.3 m.

F1. Bathymetry map, p. 26.

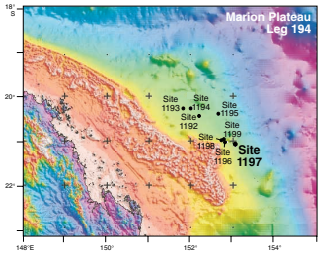

F2. Seismic line MAR07, p. 27.

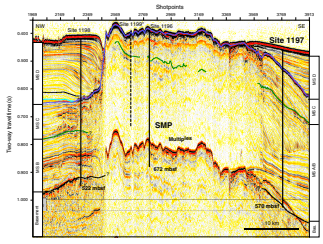

[1]Examples of how to reference the whole or part of this volume.
[2]Shipboard Scientific Party addresses.

Hole 1197A

After the drill string was deployed to 342 m, operations were put on standby to wait on weather. The maximum heave was exceeding 3 m, which was outside the limits permitted in operations in such shallow water. After 3.25 hr, the heave had dropped to 1.7 m. Hole 1197A was spudded with the advanced hydraulic piston corer (APC) at 1230 hr on 6 February (Table T2, p. 87, in the "Leg 194 Summary" chapter; Tables T1, T2). The water depth estimated from the recovery of the first core was 348.3 m. Piston coring advanced to 54.6 mbsf, where a hardground was contacted. The average recovery for this interval was 101.6%. Because of the expected shallow interval, the piston cores were not oriented. Coring continued with the extended core barrel (XCB) to 203.8 m, where operations were terminated because of very low recovery. The XCB cored 149.2 m and recovered only 0.71 m (0.48% average recovery). Eleven of the 16 XCB cores had zero recovery. After the bit was recovered, the bit seal, lockable float valve, and bit were inspected to see if there was some mechanical reason for the poor performance. No mechanical reason could be found, and it was decided to end operations at Site 1197 and consider a return at a later time.

T1. Coring summary, p. 63.

T2. Expanded coring summary, p. 64.

Starting at 1100 hr, the vessel remained in standby mode and on location to wait for the third helicopter arrival from Mackay, Australia, during Leg 194. The aircraft landed on the vessel at 1158 hr, took on 300 L of fuel, dropped off miscellaneous goods, and departed with Marine Specialist Shannon Center at 1227 hr. After the helicopter's departure, the beacon was recovered and the vessel proceeded to Site 1198 at 1345 hr on 7 February.

Hole 1197B (Return to Site 1197)

After completion of Site 1198 and a return to Site 1196, Site 1197 was revisited to drill the deep hole to basement in anticipation of better recovery through the critical interval below 60 mbsf. Thoughts were raised that perhaps the polycrystalline diamond compact (PDC) drill bit used with the XCB system, with its small-surface cutting wings, was crushing the friable formation and that the rotary core barrel (RCB) bit might in fact be a little easier on the weakly cemented reefal debris formation.

The second operation at Site 1197 began at 1700 hr on 13 February. Hole 1197B was spudded with the RCB, drilled to 50 mbsf with a center bit in place, and cored to 175.0 mbsf, where erratic torque was experienced after attempting a connection (this depth corresponded to a major unconformity at the bottom of the elusive Megasequence C). To maintain the integrity of the hole, a wiper trip was made up to 67 mbsf. Rotary coring then advanced from 175.0 to 348.0 mbsf. No hole problems were encountered, but a second wiper trip was made to 162.9 mbsf as a preventive measure. Coring was resumed and deepened the hole to 444.3 mbsf (Core 194-1197B-41R), where it was suspended for one hour to repair abrasion damage to the outer wrapping of the active heave compensator electrical and hydraulic umbilical. Coring once again was initiated and deepened the hole to 569.4 mbsf, where a third wiper trip was made to 345.8 mbsf. The driller experienced tight hole conditions in the interval from 451.5 to 422.6 mbsf on the way up the hole. RCB coring was resumed and finally penetrated basement with Core 194-1197B-65R. The final depth of 674.9 mbsf was 25 m below the 650.0 mbsf limit imposed by the Pollution Prevention and Safety Panel. Ap-

proval was given by Ocean Drilling Program (ODP)/Texas A&M University headquarters to exceed this depth.

The interval from 54.6 to 203.8 mbsf, which had an average recovery of 0.48% with the XCB in Hole 1197A, had 2.40 m recovery (1.56%) in Hole 1197B. The average recovery for the entire hole was 213.64 m (34.2%).

On 15 February, a planned rendezvous with the *Wyllaway* from Mackay took place. The vessel brought two bit releases, epoxy, video tapes, Schlumberger parts, and fresh produce and returned the stretcher used to evacuate Brooke Olson earlier in the leg. The vessel also returned operations engineer Leon Holloway to shore. Virtually at the last minute, Transocean Sedco Forex employee David Pence required evacuation for medical reasons. The vessel was alongside at 0700 hr and away by 0740 hr.

The hole was flushed and displaced with sepiolite mud, and the bit was released at the bottom of the hole in preparation for the logging program. As the bit was pulled up to the logging depth of 81.6 mbsf, several places in the hole required overpull to pass tight spots. In addition, the wind and sea conditions worsened by the time the logging equipment was being rigged up. The tool could not be advanced past the end of the open pipe. The tool suite was recovered and the logging equipment was partially rigged down. The pipe was repositioned with the end at 65.6 mbsf, and the tool was redeployed but only advanced to 81.6 mbsf, where the tool contacted an obstruction. When the tool was recovered, the compensating section of the digital dual induction tool was missing, presumably because the bit release top connector at the end of the pipe descended on the tool and severed this section. Logging was cancelled after attempts to clear the blockage with the drill string were unsuccessful. The drill string was recovered, both beacons were retrieved by 2335 hr on 17 February, and the vessel was slowly offset to Site 1199 (proposed Site CS-16A) using the dynamic positioning system.

LITHOSTRATIGRAPHY AND SEDIMENTOLOGY

Site 1197 is located on the downcurrent, windward margin of the SMP. Site 1197 is ideally positioned to observe the shedding of periplatform sediments from the carbonate growth phases of the southern platform. Site 1197 penetrated a 656.1-m-thick sediment package and recovered material from acoustic basement, which consists of volcaniclastic sediments and basalt. Core recovery at this site was ~100% from 0 to 59.6 mbsf, extremely poor (~0%) between 59.6 and 175.0 mbsf, poor (~10%) from 175.0 to 377.1 mbsf, and variable from 377.1 mbsf to the bottom of the hole. Sediments are unlithified in the upper interval with increased lithification below the hardground surface at 59.6 mbsf that separates hemipelagic drift deposits of lithologic Unit I from the last periplatform sediments of Unit II (Table **T3**).

The lithostratigraphy of Site 1197 has been divided into six units on the basis of changes in sedimentary texture, grain size, skeletal content, color variations, and the degree of bioturbation. Other criteria for distinguishing these units include changes in siliciclastic content (mostly as clays) and the presence of dolomite within the carbonate fraction (Fig. **F3**). The dominant lithologies throughout are skeletal packstone and grainstone with significant changes in grain size and fluctuations in the pelagic vs. neritic content. The intervals with abundant neritic

T3. Lithologic units and subunits, p. 71.

F3. Lithologic summary, p. 28.

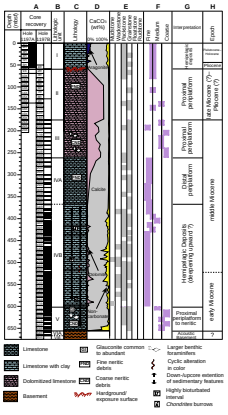

skeletal grains indicate increased shedding from the adjacent carbonate platforms of the Marion Plateau.

Lithologic Units

Unit I (0–59.6 mbsf; Pleistocene–Holocene)

Unit I is a homogeneous unit of white to pale yellow, unlithified skeletal packstone and grainstone rich in planktonic foraminifers, with minor amounts of bivalve fragments and echinoderms, rare scaphopods and pteropods (Fig. F3). Sponge spicules are common and, along with clays, contribute to the siliceous component of the sediment. Smear slide analysis confirms that only traces of silt-sized quartz and mica are present. Foraminifer fragments are abundant, but calcareous nannofossils are only of minor importance. X-ray diffraction (XRD) analysis indicates that aragonite is present above 43 mbsf, increasing in abundance upcore to a value of 21 wt% just beneath the seafloor.

Unit II (59.6–175.0 mbsf; Late Miocene?–Pliocene?)

Characterization of Unit II is hindered by extremely poor recovery, totaling just 0.8% for the entire 115.4-m drilled interval (Fig. F3). Seismic data indicate that the sediments of lithologic Unit II belong to a prograding package of clinoforms and therefore are likely to contain coarse-grained periplatform detritus shed from the SMP (see "Seismic Stratigraphy," p. 22). The upper boundary to this unit is marked by a hiatus with a maximum duration of 0.5 m.y. (see "Biostratigraphy and Paleoenvironments," p. 9), defined by a distinctive hardground surface.

The uppermost 0.42 m of Unit II is extremely well lithified, with available pore spaces tightly filled by calcite microspar cements. The surface of this unit has a 3- to 4-mm-thick, reddened hardground cap with a high phosphate content (Fig. F4). Borings are associated with this interval (Fig. F5), as is the selective dissolution of turret-shaped gastropods resulting in molds as long as 15 mm. Both of these features were infilled with either fine phosphatic silt or micrite. Color changes progressively downcore in this interval from reddish brown to brownish yellow to yellowish white. This color change was accompanied by a marked decrease in lithification and less pervasive micrite cements. Beneath the upper 0.42-m interval, the sediments are characterized by an increase in porosity and the presence of weak, fine-grained dolomite cements (rhombic crystals). This friable skeletal grainstone is probably responsible for the low recovery in this interval.

The remainder of lithologic Unit II is composed of dolomitized white skeletal grainstone rich in foraminifers (planktonic foraminifers and larger benthic foraminifers, particularly *Amphistegina* sp.) and coralline algae branch fragments (in the matrix groundmass) (Fig. F6). *Operculina* sp. and *Lepidocyclina* sp. are present along with rare echinoderm, bryozoan, and bivalve remains. Dolomite occurs as fine- to coarse-grained interparticle cement as confirmed by XRD analysis (see "Geochemistry," p. 17) (Fig. F3).

Unit III (175.0–261.5 mbsf; Late Middle Miocene)

The top of Unit III is defined by a significant unconformity (see "Biostratigraphy and Paleoenvironments," p. 9). The sediments of this

F4. Close-up photograph of indurated skeletal grainstone capped by a phosphatic crust, p. 29.

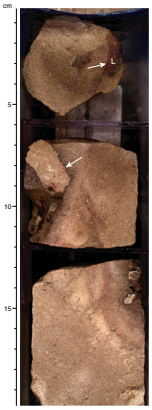

F5. Photomicrograph showing late-stage infilling of a boring, p. 30.

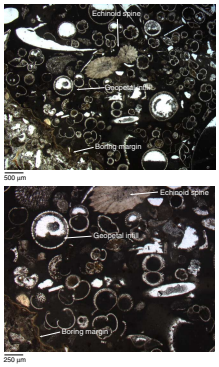

F6. Photomicrograph showing skeletal packstone dominated by planktonic foraminifers, p. 31.

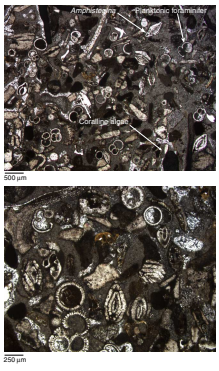

unit are characterized by dolomitized white to light gray, friable skeletal grainstone (Fig. F3). As with Unit II, recovery in this interval was poor. Larger benthic foraminifers, mainly *Lepidocyclina* sp., are the principal constituent and comprise almost the entire grainstone texture in some instances (Fig. F7). Other larger benthic foraminifers (*Operculina* sp. and *Amphistegina* sp.) are also present in the recovered sediments. Planktonic foraminifers and smaller benthic foraminifers are minor to abundant in the matrix, so the grainstone often appears to have a strongly bimodal sorting. Imbrication of foraminifer grains can be observed in many of the small pieces that were recovered along with a crude parallel lamination (Fig. F8). Many large lepidocyclinids show considerable damage to the test structure as compared to the smaller and more robust amphisteginids. Fragments of coralline algae are also an important contributor to skeletal allochems, whereas echinoderms and bivalves are of minor importance. Dolomite concentrations are often high (Fig. F3) (see "Geochemistry," p. 17). Glauconite is present mainly as infillings of foraminifers, becoming more common toward the base of this unit. Unit III represents the upper part of a progradational package as seen on seismic data (see "Seismic Stratigraphy," p. 22). The base of Unit III is characterized by an abrupt decrease in the presence of coarse neritic detritus and a decrease in the degree of dolomitization (Fig. F3).

F7. Photomicrograph showing skeletal grainstone containing abundant larger benthic foraminifers, p. 32.

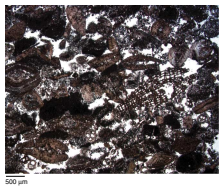

F8. Close-up photograph of skeletal grainstone containing abundant *Lepidocyclina* sp., p. 33.

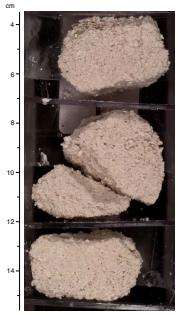

F9. Photomicrograph of a fine sand–sized skeletal grainstone, p. 34.

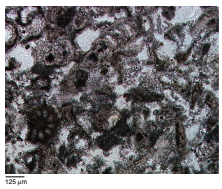

Unit IV (261.5–601.7 mbsf; Early to Middle Miocene)

Light gray, olive, and greenish gray fine skeletal packstone/grainstone and silt-sized grainstone/packstone characterize Unit IV (Fig. F3), which is distinguished from the overlying Unit III and underlying Unit V because of its fine sediment grain size. Coarse neritic detritus, particularly visible larger benthic foraminifers, are far less abundant in this interval. The majority of components are indistinct silt-sized skeletal particles whose identification can only be resolved in thin section (Fig. F9). This thick package of sediments is divided into two subunits based on changes in carbonate mineralogy, the degree of bioturbation, and the presence or absence of repetitive/cyclic intervals within the succession. Core recovery increases downcore within Unit IV.

Subunit IVA (261.5–367.4 mbsf)

Subunit IVA is characterized by a partially to highly dolomitized, pale yellow to light gray, silt-sized or fine skeletal packstone and grainstone rich in planktonic foraminifers. Planktonic foraminifers are poorly preserved and are often overgrown by dolomite cements. Larger benthic foraminifers, including *Lepidocyclina* sp., are common locally but not as abundant as in Unit III. Smaller benthic foraminifers, bryozoans, and echinoderm fragments are rare. Glauconite is a minor accessory component, often infilling intraskeletal porosity within foraminifers. Bioturbation ranges from rare to common throughout the unit but is not as abundant as in the underlying Subunit IVB. A further distinction of Subunit IVB is a marked downcore decrease in the abundance of dolomite (Fig. F3).

Subunit IVB (367.4–601.7 mbsf)

Subunit IVB marks a change to darker colored lithologies, with a slightly reduced calcium carbonate content resulting from increased siliciclastic input (Fig. F3). Planktonic foraminifers are common, as are smaller and larger benthic foraminifers. Bivalves, bryozoans, and small fragments of coralline algae are rare. Glauconite is low to moderately

abundant, often infilling the tests of larger benthic foraminifers or occurring as pellets. As with Subunit IVA, sediments are fine-grained sand- to silt-sized skeletal packstone and grainstone with light gray to olive color. However, finer-grained or muddier skeletal wackestone and mudstone are often present. The skeletal composition of these fine-grained limestones is difficult to distinguish because of their small size, fragmentation, and/or abrasion. Throughout Subunit IVB, there is a noticeable increase in the intensity of bioturbation as compared to Subunit IVA. Dolomitization is greatly reduced or absent (Fig. F3).

Repetitive alternations of darker and lighter colored intervals ranging in thickness from a few tens of centimeters to a few meters is the most obvious feature of Subunit IVB (Fig. F10). Such alternations are also seen in calcium carbonate data (Fig. F3) as a result of fluctuations in siliciclastic detritus, particularly clays, as confirmed by XRD analyses (see "Geochemistry," p. 17). The darkest intervals of these cycles contain up to 41% noncarbonate minerals. Bioturbation, mainly caused by *Chondrites* may mask the original depositional contacts in these cycles (Fig. F11).

Other small-scale sedimentary packages 10–20 cm thick are observed more sporadically throughout Subunit IVB, characterized by a distinct fining-upward trend and overall coarse texture. These packages are interpreted as turbidites (Fig. F12). The basal interval of each turbidite package is usually 5–10 cm thick and comprises a graded coarse grainstone with abundant visible larger benthic foraminifers plus subordinate bryozoans and fragments of coralline algae. The upper part of the package typically shows a well-developed parallel lamination.

Unit V (601.7–656.1 mbsf; Early Miocene)

Unit V is composed of white to light greenish gray skeletal grainstone and packstone, rudstone, and floatstone rich in larger benthic foraminifers. This abrupt change to lighter-colored lithologies is clearly observed in the color reflectance data (see "Core Physical Properties," p. 19). Large-sized lepidocyclinid foraminifers, up to 8 mm long, are the dominant skeletal component, along with other larger foraminifers and fragments of coralline algae, which are at times almost as abundant as the foraminifers (Fig. F13). Bivalve, echinoderm, and bryozoan remains are also commonly observed. Glauconite is abundant (typically 15%–25%), both as isolated pellets and infillings of intraskeletal porosity. Usually ~50% of the larger foraminifers show evidence of glauconite infilling and abrasion, whereas the remainder are freshly preserved. Fine- to coarse-grained quartz sand (up to 30%) is common to abundant in the basal interval of Unit V (646.7 to 656.1 mbsf) as was confirmed by XRD analyses (see "Geochemistry," p. 17). Well-developed parallel lamination and primary horizontal orientation of elongated (foraminifer) skeletal clasts are common in the skeletal packstone and grainstone. Small 10- to 30- cm-thick fining-upward intervals of coarse grainstone are seen throughout this unit, often capped by thin 0- to 5-cm darker-colored intervals of parallel-laminated finer-grained packstone (Fig. F14).

A distinctive greenish gray skeletal floatstone (Fig. F15) containing small oysters, pectenids, and abundant large bioclasts of massive celleporiform bryozoans (up to 25 mm in size) is present in the lowermost 0.35 m of Unit V (at 656.4 to 656.1 mbsf; Core 194-1197B-64R). The matrix is composed of larger benthic foraminifers, bryozoans, echinoderms, and coralline algae fragments. Cobbles and pebbles of basalt and

F10. Photograph showing alternating dark- and light-colored intervals of fine-grained skeletal packstone and grainstone, p. 35.

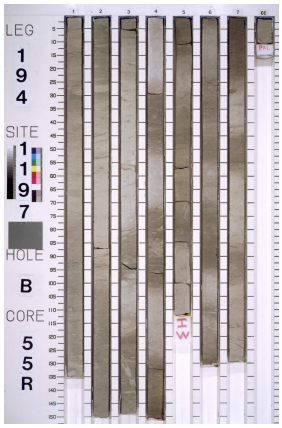

F11. Close-up photograph of extensive bioturbation at the contact between an interval of grainstone overlying a skeletal packstone, p. 36.

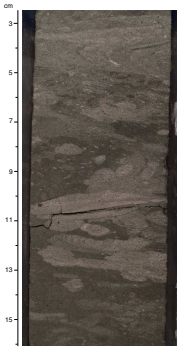

F12. Close-up photograph of small turbidite bed with a sharp planar base, p. 37.

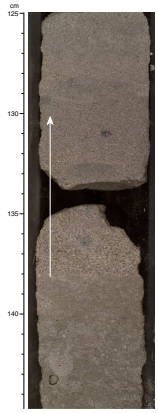

other volcanic rocks are included in the basal floatstones that immediately overlie Unit VI.

Unit VI (656.1–666.7 mbsf; Pre-Miocene)

Unit VI is characterized by multicolored pebble- to cobble-sized volcaniclastic sediments that represent acoustic basement. Two subunits are distinguished: a ~10.5-m-thick series of volcaniclastic sediments and an underlying, thin interval of basalt.

Subunit VIA (656.1–666.6 mbsf)

Subunit VIA consists of a highly altered, matrix-supported volcaniclastic breccia with coarse (up to 12 cm) angular clasts of light gray basalt derived from the underlying basement. Small dark red-colored pebble clasts (4–10 mm in size) and larger subangular to subrounded clasts (typically 5–50 mm in size) are also likely to be highly altered material of volcanic origin (Fig. F16). Thin section analysis indicates that bioclastic material is absent. Octahedral dark reddish black metallic crystals are observed within the matrix and are tentatively identified as sphalerite.

Subunit VIB (666.6–666.7 mbsf)

Highly altered, light to medium gray basalt with olivine and plagioclase phenocrysts (1–3 and 2–4 mm in diameter, respectively) set in a groundmass of fine crystalline plagioclase was recovered at the base of Hole 1197B (interval 194-1197B-65R-1, 129–142 cm). Rare vesicles up to 1 mm in diameter are present. The rock appears to be highly weathered, with the original mineralogy such as olivine crystals being altered to iddingsite. Only a small interval of this basalt was recovered, and it is uncertain whether this rock is in situ basement or a large breccia clast.

Discussion

The majority of sediments recovered at Site 1197, particularly in the interval from 59.6 mbsf to the top of the acoustic basement at 601.7 mbsf were deposited on the proximal slope of the SMP resulting in a reworked faunal assemblage of foraminifers, coralline algae, and other skeletal detritus derived from a neritic platform environment. Discussion of the depositional history for Site 1197 is given below.

Unit VI (Pre-Miocene)

The age and origin of the thin interval of olivine basalt observed at the base of Site 1197 (Subunit VIB) is uncertain, but it is interpreted as originating from basalt flows related to synrift tectonic activity. The surface of this flow was most likely exposed for a significant period of time and then covered by a veneer of volcaniclastic breccias (Subunit VIA) that accumulated from debris flows related to an alluvial fan or as slope colluvium. This surface likely maintained a significant paleorelief. Similar basaltic igneous rocks were encountered at Site 1198; however, no overlying volcaniclastic sediments were recovered. Unit VI represents the acoustic basement at Site 1197.

Unit V (Early Miocene)

Initial flooding of the basement is recorded by an interval of skeletal floatstone rich in oysters with their paired valves still attached. This im-

F13. Photomicrograph showing skeletal packstone containing abundant larger benthic foraminifers, p. 38.

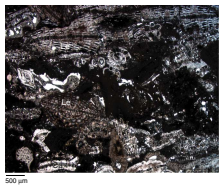

F14. Close-up photograph of fining-upward package of coarse skeletal grainstone, p. 39.

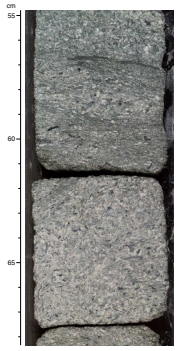

F15. Close-up photograph of skeletal floatstone containing bryozoan fragments, p. 40.

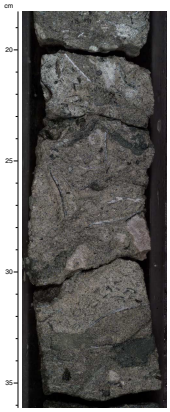

plies limited reworking across a shallow neritic platform in water depths <30 m. The upper 50 m of sediment in Unit V is coarse skeletal packstone to fine rudstone, indicating either deposition in an open shelf environment at depths of <100 m or, possibly, transport and deposition in a proximal periplatform setting (see "Biostratigraphy and Paleoenvironments," p. 9). Small- to medium-scale graded bedding and the strong laminar fabric of many of the deposits suggest deposition from unidirectional gravity flows, probably slope-proximal turbidites, related to shedding in a periplatform setting.

Unit IV (Early–Middle Miocene)

The very fine skeletal packstone, grainstone, and wackestone sediments of Unit IV indicate deposition in a hemipelagic through distal periplatform setting. Thin section analysis confirms that many of the fine skeletal particles are fragmented neritic grains from coralline algae and benthic foraminifers (Fig. F9). Clay content generally increases upward between 600 and 480 mbsf and likely indicates a progressive deepening through this interval, possibly followed by a broad shallowing from 480 mbsf to the top of Subunit IVB, where clay content gradually declines. Distinctive color-banded intervals are recognized within Subunit IVB with slight fluctuations in textural composition and clay content. Small-scale fining-upward intervals with well-preserved parallel lamination are characteristic of deposition from turbidites. Calciturbidites are enriched in coarse skeletal detritus such as larger benthic foraminifers transported from the platform margin. These turbidites are probably unrelated to the cyclicity producing the color-banded intervals discussed previously.

The absence of clays and the presence of fine-grained skeletal particles of neritic origin, including larger benthic foraminifers, is typical of Subunit IVA and indicates deposition in a periplatform setting at water depths of ~200 m (see "Biostratigraphy and Paleoenvironments," p. 9). The fine grain size and massive character of this subunit is surprising because it forms the basal part of an inclined, prograding slope package, as seen on seismic profiles (see "Seismic Stratigraphy," p. 22). However, the overall coarsening-upward trend is consistent with progradation of slope deposits.

Unit III (Late Middle Miocene)

The range of sedimentary structures and abundance of reworked larger benthic foraminifers filled by glauconite (particularly *Lepidocyclina* sp.) within Unit III imply reworking from the nearby SMP. Larger benthic foraminifers usually live in the euphotic zone (~50–100 m) but have been transported to a proximal periplatform environment with depths of ~150 m or greater (see "Biostratigraphy and Paleoenvironments," p. 9). The upper boundary of Unit III is loosely constrained because of poor core recovery, but nonetheless shows a marked nondepositional hiatus (see "Biostratigraphy and Paleoenvironments," p. 9). The seismic profile (see "Seismic Stratigraphy," p. 22) indicates that this horizon is also a downlap unconformity between two prograding seismic sequence packages, likely to represent the boundary of the middle and late Miocene platform growth phases.

F16. Close-up photograph of matrix-supported volcaniclastic breccia, p. 41.

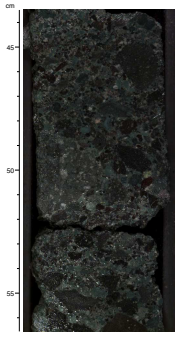

Unit II (Late Miocene?–Pliocene?)

Similar to Unit III, the sediments of Unit II often show rudimentary laminations, perhaps indicating deposition from unidirectional currents. The abundance of *Amphistegina* sp. in particular, along with fragments of coralline algae, is reminiscent of the Subunit IA and IB facies encountered at Sites 1196 and 1199 on the SMP (see **"Lithostratigraphy and Sedimentology,"** p. 5, in the "Sites 1196 and 1199" chapter). The main difference here is the mixing with planktonic foraminifers (Fig. **F6**), which enables the dating of these periplatform sediments. The adjacent SMP (observed at Sites 1196 and 1199) likely drowned in the latest Miocene, terminating neritic supply to the slopes. This platform demise is recorded by a relative increase in the amount of planktonic foraminifers in the uppermost part of Unit II in addition to the formation of an indurated hardground with a thin phosphatic cap. The base of Unit II is defined by a significant hiatus (see **"Biostratigraphy and Paleoenvironments,"** p. 9) and is coincident with a prominent downlap and unconformity surface on seismic profiles (see **"Seismic Stratigraphy,"** p. 22). All evidence suggests that Unit II sediments were shed contemporaneously with the growth of the SMP.

Unit I (Pleistocene–Holocene)

A 60-m-thick series of skeletal grainstone and packstone rich in planktonic foraminifers was deposited in an upper bathyal hemipelagic setting above the hardground surface. Mineralogical analyses show that aragonite is present from ~43 mbsf to the modern seafloor with abundance increasing upward. This indicates that aragonite is being produced in the environment, either from organisms living on the seafloor at this location or more likely from shedding and neritic supply related to a distal platform area. It is also likely that aragonite dissolution increases downcore. An identical trend in aragonite concentration vs. preservation can be recognized at Site 1198 on the western side of the SMP (see **"Lithostratigraphy and Sedimentology,"** p. 3, in the "Site 1198" chapter).

BIOSTRATIGRAPHY AND PALEOENVIRONMENTS

Shipboard analyses using calcareous nannofossils and planktonic foraminifers reveal a Pleistocene to upper Pliocene sequence in the top 54 mbsf and a poorly preserved upper Miocene interval from 54 to 20 mbsf. Sediment from Hole 1197B was cored from ~60 to ~670 mbsf and yielded age-diagnostic material of variable quality. The hole penetrated an upper Miocene to possible Pliocene sequence unconformably overlying an upper middle Miocene sequence. The majority of the cores from this hole contain no age-diagnostic fauna. Table **T4** lists the nannofossil and planktonic foraminifer datums used for age assignments. See **"Age Model,"** p. 16, for age vs. depth and sedimentation rate data. In addition, benthic foraminiferal assemblages and biogenic constituents were evaluated as environmental indicators. Core catcher samples were the basis for the primary analysis, and some additional samples from within selected intervals were studied to refine the biostratigraphy.

T4. Biostratigraphic datums, p. 72.

Calcareous Nannofossils

Hole 1197A

The top seven cores contain abundant late Pliocene through Pleistocene nannofossils. Sample 194-1197A-1H-2, 136 cm, contains common *Emiliania huxleyi* and abundant *Gephyrocapsa* spp. (>4 µm) among other taxa and can be assigned an age of 0.08–0.26 Ma. Sample 194-1197A-1H-CC contains only abundant *Gephyrocapsa* spp. (>4 µm) but no *E. huxleyi* or *Pseudoemiliania lacunosa*. This suggests an age of 0.26–0.46 Ma. The last occurrence (LO) of *P. lacunosa* (0.46 Ma) is placed between Samples 194-1197A-1H-CC and 2H-CC based on the presence of the species in the latter sample. The LO of *Calcidiscus macintyrei* (1.7 Ma) is located between Samples 194-1197A-4H-CC and 5H-CC. Discoasters were first encountered in Sample 194-1197A-7H-1, 28–30 cm, and this sample is thus older than 2.0 Ma. Sample 194-1197A-7H-1, 28–30 cm, contains *Discoaster brouweri,* but other species of discoasters are absent. This indicates that the sample has an age of 2.0–2.5 Ma. Below this core, the few core catcher samples available for analysis were barren of nannofossils. The only exception was Sample 194-1197A-20X-CC, which yielded rare specimens of nannofossils, including *Reticulofenestra pseudoumbilicus,* which suggests an age older than 3.7 Ma.

Hole 1197B

Samples 194-1197B-2R-CC through 34R-CC yielded generally rare specimens of nannofossils, and no age-diagnostic species were found. By contrast, Samples 194-1197B-35R-CC through 37R-CC yielded common nannofossils. The presence of *Cyclicargolithus floridanus* and the absence of *Sphenolithus heteromorphus* in these samples indicates an age of 11.9–13.6 Ma for this interval. Samples 194-1197B-38R-CC through 57R-CC yield generally common nannofossils, with index species *S. heteromorphus* consistently present. This relatively long interval can be dated by the species stratigraphic range as 13.6–18.2 Ma. Sample 194-1197B-61R-CC also contains common nannofossils. *Sphenolithus belemnos* and *Sphenolithus disbelemnos* were found, suggesting an age of 18.5–19.3 Ma (early Miocene). Samples 194-1197B-62R-CC and 63R-CC, which are above a conglomerate and basement, contain only rare or few nannofossils. Index taxa are not present in these two samples, but the flora resemble impoverished early Miocene assemblages.

Planktonic Foraminifers

Hole 1197A

Samples 194-1197A-1H-CC through 7H-CC reveal an upper Pleistocene (Zone N23) to upper Pliocene (Zones N20–N21) conformable sequence reaching a depth of 54.4 mbsf. Samples 194-1197A-8X-CC through 20X-CC are either barren, lack age-diagnostic fauna, or have 0% recovery. The exceptions are Samples 194-1197A-17X-CC and 20X-CC, which are tentatively assigned an early Pliocene to late Miocene age.

Samples 194-1197A-1H-CC through 5H-CC are Pleistocene based on the presence of *Globorotalia truncatulinoides,* combined with the LO datums of *Globorotalia tosaensis* and first occurrence of *Pulleniatina finalis*. Sample 194-1197A-1H-CC contains the "pin" morphotype of *Globigerinoides ruber* and therefore has a minimum age of 0.12 Ma based on the

Pacific LO datum of this species. Sample 194-1197A-5H-CC contains *Globigerinoides extremus,* which places its LO datum (1.8 Ma) between Samples 194-1197A-4H-3, 12–14 cm, and 5H-CC, whereas the LO of *Globigerinoides fistulosus* (1.77 Ma) is placed between 194-1197A-4H-CC and 5H-CC. The LO of *Globorotalia pseudomiocenica* is placed between Samples 194-1197A-7H-1, 28–30 cm, and 7H-CC, whereas *G. tosaensis* and *Globorotalia limbata* are observed in Samples 194-1197A-6H-CC and 7H-CC. This interval can therefore be assigned to the late Pliocene (top of Zones N21 and N20–N21, respectively). Some age-diagnostic taxa are conspicuously absent. For example, *Dentoglobigerina altispira* and *Sphaeroidinellopsis seminulina* are expected to occur in these samples but are not observed. In addition, altered specimens of the Pleistocene index fossil *G. truncatulinoides* were present.

Samples 194-1197A-8X-CC through 20X-CC were either barren, lacked age-diagnostic assemblages, or had 0% recovery and as a result cannot be precisely dated. Sample 194-1197A-17X-CC contains *Globorotalia plesiotumida* and *Globigerinoides bulloideus*. It is tentatively assigned to Zones N17 through N19, whereas Sample 194-1197A-20X-CC contains *Globigerinoides conglobatus, Globoquadrina dehiscens,* and *Globoquadrina baroemoenensis,* indicating a Zone N17 age.

Hole 1197B

Sample 194-1197B-3R-CC was the first sample to contain age-diagnostic planktonic foraminifers. Samples 194-1197B-3R-CC through 13R-CC are subject to variable preservation and intermediate to low abundances. Many index fossils are absent or difficult to identify; thus, disappearances or absences have limited diagnostic utility. The interval can be placed within Zones N16 to N18 (4.8–11 Ma), reflecting a late Miocene to earliest Pliocene age range. The upper age limit (4.8 Ma) can be defined between Samples 194-1197B-6R-CC and 8R-CC by specimens of *Globoquadrina* (e.g., *G. baroemoenensis, G. dehiscens,* and *G. globosa*), which were consistently present, whereas the lower age limit was defined by the sporadic occurrence of *G. plesiotumida, Globigerina apertura,* and *G. bulloideus*. The age range reference for these globoquadrinids is that of Kennett and Srinivasan (1983), who stipulated the LO datum of *G. baroemoenensis* as extending to the top of Zone N18 (late late Miocene). Since then, this zone has been moved into the early Pliocene; thus, there is a discrepancy as to the absolute date of the LO datum for this species. This species is unique in these samples because its last appearance can be reliably determined. This matter is dealt with by means of an error box in **"Age Model,"** p. 16.

The next age-diagnostic Sample is 194-1197B-15R-1, 1–4 cm (184.6 mbsf), which contains *Globorotalia siakensis* and indeterminate specimens of *Globorotalia (F.) robusta* that reflect a middle Miocene age between Zones N12 and N13 (12.3–11.65 Ma). Additional samples proved to be barren of planktonic foraminifers. Samples 194-1197B-15R-1, 29–31 cm, 15R-CC, and 21R-CC (251.9 mbsf) contain the same age-diagnostic fauna, suggesting a range between Zones N12 and N14. The apparent hiatus between Sections 194-1197B-13R-CC and 15R-1 (spanning the middle to late Miocene boundary) is supported by a prominent downlapping unconformity on the corresponding seismic profile (see **"Seismic Stratigraphy,"** p. 22). The hiatus is placed within Sample 194-1197B-14R-CC (175 mbsf), which is barren of fauna. Samples 194-1197B-24R-CC through to basement at ~670 mbsf contain poorly preserved, low-abundance, nondiagnostic fauna, or are barren.

Benthic Foraminifers

Hole 1197A

Microscopic analysis of biogenic constituents (>63 µm), particularly the diverse and often abundant benthic foraminifers, provided data for paleoenvironmental interpretation of the cores from Hole 1197A (Table T5).

T5. Summary of paleoenvironmental interpretations, p. 73.

Samples 194-1197A-1H-CC (6.13 mbsf) through 6H-CC (53.79 mbsf), in lithologic Unit I (see "Lithostratigraphy and Sedimentology," p. 3), are dominated by planktonic foraminifers and pteropods. Upper bathyal benthic foraminiferal taxa, including *Cibicidoides,* nodosarids, and agglutinated taxa, are common and diverse through this interval. In addition, bioclastic debris from deep hard-bottom communities, including small bryozoan colonies and fragments, solitary corals, alcyonarian spicules, and miliolid foraminifers, is a conspicuous component of this interval.

Sample 194-1197A-7H-CC (54.59 mbsf) marks the transition between the upper interval of predominantly pelagic input and the lower interval of predominantly neritic components. Sample 194-1197A-9X-1, 31–34 cm (59.91 mbsf), is characterized by recrystallized neritic debris and planktonic foraminifers. This sample is from the vicinity is of an apparently reworked hardground (see "Lithostratigraphy and Sedimentology," p. 3).

Samples 194-1197A-10X-CC (69.43 mbsf) through 20X-CC (165.4 mbsf), representing lithologic Unit II (see "Lithostratigraphy and Sedimentology," p. 3), recovered abundant neritic debris, including well-preserved specimens of larger benthic foraminifers, including *Lepidocyclina, Amphistegina, Cycloclypeus,* and *Operculina*. The foraminiferal assemblage also includes planktonic foraminifers, as well as *Cibicidoides* spp., *Hoeglandina elegans,* and other taxa characteristic of outer neritic/upper bathyal water depths.

Hole 1197B

Samples 194-1197B-2R-1, 84–86 cm (59.91 mbsf), to 22R-1, 22–24 cm (252.1 mbsf), represent lithologic Units II and III (see "Lithostratigraphy and Sedimentology," p. 3) and contain abundant neritic debris. A middle neritic source of origin is again indicated by the larger benthic foraminiferal assemblage, which includes *Lepidocyclina, Amphistegina, Cycloclypeus,* and *Operculina*. *Cibicidoides* spp., *H. elegans,* and other outer neritic/upper bathyal benthic foraminifers are also common. Preservation of fossils ranges from moderate to very poor within this interval. The fossil assemblages between Units II and III differ primarily in the more diverse assemblage in Unit II as compared with the dominance of relatively uniform *Lepidocyclina* in the sediments of Unit III (see Table T5).

Samples 194-1197B-23R-1, 44–46 cm (261.9 mbsf), through 33R-1, 52–55 cm (358.3 mbsf), represent lithologic Subunit IVA (see "Lithostratigraphy and Sedimentology," p. 3). They contain varying proportions of planktonic foraminifers, outer neritic/upper bathyal benthic foraminifers, and silt- to medium sand-sized neritic debris that sometimes includes smaller and larger benthic foraminifers from middle to inner neritic water depths. Samples 194-1197B-34R-1, 96–98 cm (368.4 mbsf), through 57R-CC (598.4 mbsf), representing lithologic Subunit IVB, contain relatively less identifiable neritic debris and substantial

amounts of terrigenous clays (see "Lithostratigraphy and Sedimentology," p. 3). Increasing lithification downsection complicated assessment.

Samples 194-1197B-58R-7, 66–67 cm (607.4 mbsf), through 62R-CC (641.5 mbsf) are coarse, larger benthic foraminifer-rich grainstones representing most of lithologic Unit V. Bryozoan fragments are also common. *Lepidocyclina* and *Amphistegina* are the dominant genera with *Cycloclypeus* and *Operculina* present. Samples 194-1197B-63R-4, 89–91 cm (651.0 mbsf), and 64R-2, 125–127 cm (658.3 mbsf), are dark-colored sandstones and conglomerates containing bivalves and *Operculina* foraminifers.

Interpretation

Hole 1197B did not reach basement but did penetrate dark-colored siliciclastic sandstone and conglomerates whose major clasts appear to be of volcanic origin (lithologic Unit V; see "Lithostratigraphy and Sedimentology," p. 3). Thus, the sediments retrieved may reflect an early stage in the flooding of volcanic terrain, as their biotic constituents indicate an origin in inner neritic water depths. The dark sandstone is overlain by *Lepidocyclina*-rich grainstones with clasts originally produced in middle-neritic water depths, possibly in an open-shelf setting where they were rounded and mixed. The shells also show evidence of transport and likely reworking, as many are well-rounded and blackened or glauconite-filled. Thus, the water depth of the depositional environment is uncertain. However, in two samples, 194-1197B-60R-CC (621.3 mbsf) and 61R-CC (641.5 mbsf), that were disaggregated, only taxa characteristic of middle neritic water depths were seen.

The fine bioclastic sediments of Unit IV appear to have been deposited in a distal periplatform setting in outer neritic to upper bathyal water depths, as indicated by the benthic foraminiferal assemblage. These sediments are dominated by a mixture of fine neritic and planktonic debris, with occasional pulses of slightly coarser sediments that originated in middle to inner neritic depths, as indicated by debris from larger benthic foraminifers that lived within the euphotic zone. The major biogenic constituent difference between subunits in Unit IV is that Subunit IVB received pulses of terrigenous input and the origin of the fine carbonate debris is difficult to determine, whereas Subunit IVA has very little noncarbonate and pulses of recognizable neritic debris. The sequence of sediments seen in lithologic Unit V and Subunit IVB appear to represent a transgressive episode to a distal periplatform setting, followed in Subunit IVA by a progressive increase in platform influence that becomes dominant in Unit III.

Lithologic Unit III (see "Lithostratigraphy and Sedimentology," p. 3) is characterized by abundant neritic debris, including well-preserved specimens of larger benthic foraminifers. A middle neritic source of origin is indicated by the larger benthic foraminiferal assemblage, whereas the prevalence of outer neritic/upper bathyal benthic foraminifers indicates that the neritic material was transported to a proximal periplatform depositional setting at outer neritic to upper bathyal paleowater depths.

Although there are intervals of fine to medium sand–sized grainstones within Unit III, the predominance of coarser neritic debris, particularly of larger benthic foraminifers, rather abruptly increases at the base of Unit II (175 mbsf). *Lepidocyclina* dominate sediments of Unit III, which were deposited in the late middle Miocene. A more mixed assem-

blage with particularly abundant *Amphistegina* (Fig. F17) is characteristic of the sediments deposited within the late Miocene. However, *Lepidocyclina* (Fig. F18) are common to abundant in the sediments that were transported from the platform top onto this proximal periplatform setting during the late Miocene. The prevalence of these sediments supports observations from Sites 1196 and 1198 that the range of *Lepidocyclina* likely extended through the late Miocene, as it does on the Queensland Plateau (Betzler, 1997).

Although depth differences between the platform at Site 1196 and the sediments in lithologic Units II and III at Site 1197 indicate that the latter were deposited ~100 m below the platform top, the sporadic occurrence of *Cibicidoides* and other outer bathyal/upper neritic benthic foraminifers indicates that the paleowater depths were likely outer neritic depths (150–200 m). This conclusion is supported by the absence of deep euphotic red algal crusts or in-place specimens of very large, flat larger foraminifers such as *Cycloclypeus* spp. or *Lepidocyclina* (*Eulepidina*) sp. that can take advantage of low-light conditions in the 100- to 150-m depth range. The prolific shedding of platform sediments ceased in the late Miocene or early Pliocene as transgression or subsidence deepened the site and hemipelagic sedimentation prevailed.

PALEOMAGNETISM

Paleomagnetic analyses were performed on the whole-round sections for the APC cores and on the archive halves for RCB cores using the three-axis pass-through cryogenic magnetometer. The core sections were first measured for natural remanent magnetization (NRM). They were then subjected to 5-mT and 30-mT field demagnetization in the alternating-field (AF) coils of the cryogenic magnetometer, and their magnetization was successively measured.

APC cores from Hole 1197A were drilled with a nonmagnetic Russian-made PDC bit in the bottom-hole assembly rather than a standard C3RBI bit, resulting in a good magnetic record. Cores from Hole 1197B were drilled with the RCB. Polarity reversal sequences were observed in intervals of good recovery. However, remagnetization is evident and caused difficulty for the interpretation. Nevertheless, some known chron boundaries can be identified when comparing the magnetic signal with biostratigraphic data (Table T6).

Results

Natural Remanent Magnetization

In Hole 1197A, NRM intensity generally varies between 10^{-3} and 10^{-2} A/m, with an average intensity of $10^{-2.5}$ A/m (Fig. F19). The mean intensity drops to 10^{-3} A/m after demagnetization at 30 mT. Core-top intensity anomalies were also observed and care was taken to not misinterpret these as polarity sequences. The NRM intensity for Hole 1197B is very low, ~$10^{-4.5}$ A/m (Fig. F20), and remains constant downcore. Even following demagnetization to 30 mT, a strong normal overprint persists throughout the section, even though the intensity was reduced to 10^{-5} A/m. This caused problems for the identification of polarity intervals.

F17. Photograph showing neritic sediments, p. 42.

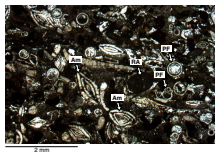

F18. Photograph illustrating vertical sections through *Lepidocyclina,* p. 43.

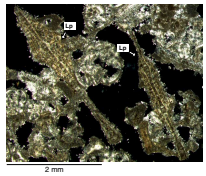

T6. Magnetic polarity transitions, p. 75.

F19. Long-core measurements, Hole 1197A, p. 44.

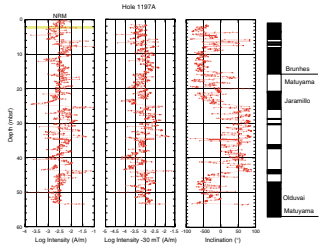

F20. Long-core measurements, Hole 1197B, p. 45.

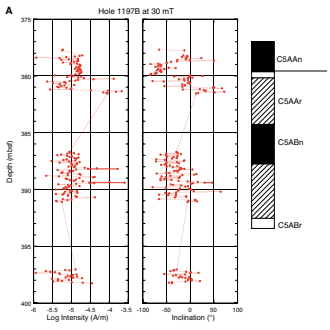

Magnetostratigraphy

Inclination and intensity are shown as a function of depth for the entire drilled section of Hole 1197A in Figure F19. Long intervals of negative inclination from 0 to 24 mbsf, positive inclination between 24 and 44 mbsf, and a short interval of negative inclination below 44 mbsf are clearly identifiable (Fig. F19). Within each of the long intervals, a number of short polarity intervals or excursions also appear. When these polarity interval patterns are compared to the geomagnetic-polarity time scale, the long normal and reversed intervals correlate with the Brunhes and Matuyama Chrons, respectively. However, the correlation in this interval is not in agreement with the biostratigraphic data, which would place the base of the Brunhes Chron at ~15 mbsf, between the Jaramillo Subchron (20–24.5 mbsf) and the Olduvai Subchron (43–50 mbsf).

Magnetic measurements in Hole 1197B are highly corrupted by a strong downward overprint. The weak magnetization of the sediments in this hole precludes the separation of the signal from the overprint by AF demagnetization. Therefore, identification of the polarity interval in Hole 1197B is difficult, even though the recovery was high. By distinguishing intervals of predominantly high negative inclination from intervals with partly zero to positive inclination, some reversed intervals could be recognized using the biostratigraphic data as a guide. In this way, it is possible to identify polarity intervals found in the middle to early Miocene (Figs. F20, F21). However, in most cases, it is difficult to locate the exact boundaries of the polarity reversals.

Below 655 mbsf, strongly magnetized basement rocks with an average NRM intensity of 10^{-1} to $10^{-0.5}$ A/m are encountered (Fig. F20D). These strongly magnetized basement cores have a mean inclination of 60° in a reversed direction. Results of complete thermal demagnetization indicated that the principal minerals carrying magnetization are titanomagnetite and hematite. Two components of magnetization have been identified; one with a mean inclination of –30° and another with 64°, the former being a remagnetization and the latter likely representing primary magnetizations. When compared with the Australian apparent polar wander curve, these two inclinations represent ages of 29 and >102 Ma, respectively.

Rock Magnetism

Between 4 and 50 mbsf, NRM, anhysteretic remanent magnetization (ARM), and isothermal remanent magnetization (IRM) demagnetization of six discrete samples from Hole 1197A were measured. The NRM and ARM results are identical for all of the samples. The IRM acquisition curves for some of the samples show no increase after 300 mT, indicating magnetite as the dominant mineral (Fig. F22A, F22B). For some other samples, an increase in acquisition after 300 mT occurs (Fig. F22C, F22D), which is not strong enough for hematite but suggests a magnetic phase having intermediate coercive force between magnetite and hematite. Complementary determination of ratios between ARM at 0.1 T and susceptibility indicates the possible presence of pyrrhotite, which is in good agreement with the signal of IRM acquisition. When the normalized IRM acquisition, IRM demagnetization, and ARM are plotted together as a function of the applied field (Fig. F22), they intersect at values 0.4 to 0.45, which indicates that the magnetite is predominantly single domain with little interaction. For pelagic limestone, this

F21. Comparison of observed magnetic stratigraphies, p. 49.

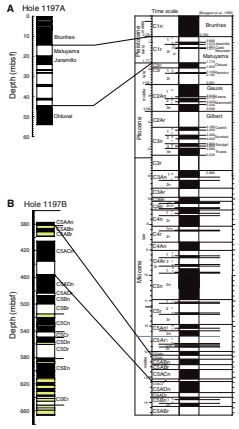

F22. Normalized ARM, IRM acquisition, and IRM demagnetization curves vs. demagnetizing steps, p. 50.

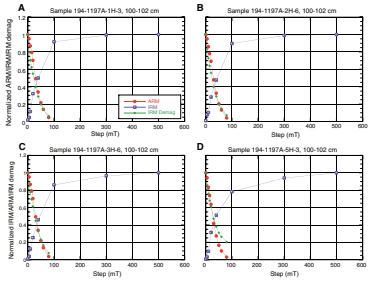

value is ~0.5 and considered to result from noninteracting single-domain magnetite (Johnson et al., 1975).

The IRM 0.1 T:1 T ratio gives a value of about 0.9 for the top 30 mbsf, indicating that magnetite is the dominant magnetic remanence carrier (Fig. **F23B**). Below 30 mbsf, this ratio drops to 0.75 to 0.81, indicating the presence of other magnetically hard minerals, possibly pyrrhotite (Fig. **F23B**). The downcore variation in NRM, ARM, and IRM is a function of magnetite concentration (Fig. **F23A**). This might suggest that dissolution of fine-grained primary magnetite in reducing diagenetic conditions mostly leads to the formation of pyrite and other iron sulfides, both of which decrease the magnetization of the sediments.

Twelve representative discrete samples have been analyzed from Hole 1197B. Because they were less magnetic, no significant interpretations could be made.

F23. NRM, ARM, and IRM plotted down the core, p. 51.

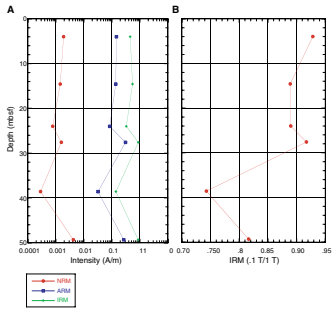

AGE MODEL

At Site 1197, 14 calcareous nannofossil and planktonic foraminifer age-depth control points and two age-diagnostic species ranges were established for the 675-m-thick sequence of early Miocene to Pleistocene age (Fig. **F24**; Table **T7**) (see **"Biostratigraphy and Paleoenvironments,"** p. 9). The upper ~59 mbsf, corresponding to the hemipelagic lithologic Unit I and seismic Megasequence D, yielded excellent core recovery and abundant and well-preserved nannofossils and planktonic foraminifers. A magnetostratigraphy could be established for this interval, but not for the poorly recovered sequence below it (see **"Paleomagnetism,"** p. 14) (Fig. **F24**). The age model is constructed based on the biostratigraphic control points.

Age-depth relationships are ill-constrained for lithologic Unit II (59.6–175 mbsf), which is equivalent to Megasequence C at this site, as well as for the underlying lithologic units of Megasequence B. Core recovery was extremely low over most of that section (a few centimeters per 9.6 m core interval). With the recovery of such small pieces of core, which is associated with grinding and flushing of 99% of the drilled material and borehole instability, downhole contamination becomes likely. In addition, microfossils in the few and small samples were rare and moderately to poorly preserved, and index fossils were difficult to identify. Within Megasequence C, a broad age range (Zones N16–N18; 11–4.8 Ma) defined by an assemblage of planktonic foraminifers is therefore the only age constraint (see **"Biostratigraphy and Paleoenvironments,"** p. 9) (Fig. **F24**).

Seismic and lithologic data suggest that two major hiatuses are at 59 and 175 mbsf, the top and bottom of Megasequence C. The age model constrains the total duration of both hiatuses and deposition of Megasequence C to 2–11 Ma; however, it does not constrain the duration of either of the two hiatuses or Megasequence C (Fig. **F24**). For a rough estimate, it can be argued that the hiatus at 59 mbsf should have lasted ~4 m.y. (6–2 Ma), given the missing section of Megasequence D dated at other sites. Assuming a sedimentation rate of ~60 m/m.y. for Megasequence C for the period of active platform shedding, Megasequence C deposition would have lasted ~2 m.y. (8–6 Ma). This would leave ~3 m.y. for the hiatus at 175 mbsf (11–8 Ma).

Average sedimentation rates at Site 1197 are 60 m/m.y. for the Miocene Megasequence B and 30 m/m.y. for the Pliocene–Pleistocene

F24. Age-depth model and sedimentation rates, p. 52.

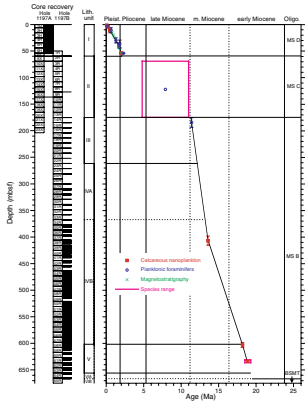

T7. Age-depth control points, p. 76.

Megasequence D. Age picks for lithologic and seismic unit boundaries are summarized in Table T8.

T8. Age picks, p. 77.

GEOCHEMISTRY

Volatile Hydrocarbons

Concentrations of volatile hydrocarbon gases were measured from every core using the standard ODP headspace sampling technique and gas chromatographic analysis. Methane occurred in only very minor concentrations (1.6–3.1 ppmv) (Table T9). The low gas content at Site 1197 is likely a function of appreciable pore water SO_4^{2-} concentrations, limiting methanogenesis and the lack of mature organic matter to provide a thermogenic component to the gas fraction.

T9. Headspace gas composition, p. 78.

Interstitial Water Chemistry

A total of 18 pore water samples were taken from Site 1197 sediments (Fig. F25; Table T10). Six samples were recovered from lithologic Unit I in Hole 1197A, covering the interval from 4.4 to 50 mbsf. In Hole 1197B, low recovery and the disturbed nature of the recovered sediment eliminated the possibility of taking pore water samples until a depth of 420.91 mbsf. This low-recovery interval corresponds approximately to seismic Megasequence C. Below 420.91 mbsf, samples were taken approximately every 10 m to a depth of 548.91 mbsf. Below this depth, sediments were highly indurated with low porosity. It was therefore not possible to extract pore water from the samples, despite repeated attempts and squeezing at pressures of 40,000 lb for up to 5 hr.

F25. Dissolved constituents, p. 53.

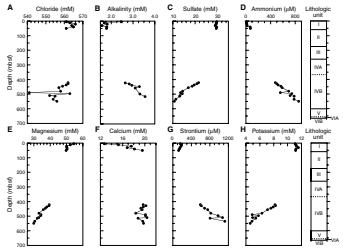

In sediments from the upper 50 mbsf of the hole, concentrations of dissolved constituents vary little from seawater values (Fig. F25), particularly for chloride, sulfate, ammonium, strontium, and potassium. Alkalinity decreases slightly from 2.5 to 1.7 mM in the upper 12 mbsf, then remains approximately constant to 50 mbsf (Fig. F25B). Magnesium concentration decreases from 55 to 50 mM in the upper 21.5 mbsf and then remains constant to 50 mbsf (Fig. F25E). Calcium alone shows a significant change, increasing steadily over the upper 50 mbsf from 11 to 20 mM (Fig. F25F).

T10. Interstitial water chemistry, p. 79.

The concentrations of various ions from the sample at 50 mbsf and at the top of the next sampled interval (420.91 mbsf) are similar. Calcium, for example, has essentially the same concentration, 20 mM, immediately above and below the sampling gap (Fig. F25F). Within the lower interval, chloride shows significant variation, with one value as low as 541 mM, the cause of which is uncertain (Fig. F25A). Alkalinity is 2.5 mM at 420 mbsf and increases slightly to 3.5 mM at 514 mbsf. Sulfate values decrease from 21.59 to 10.66 mM, whereas ammonium values increase from 477 to 856 µM in the lower sampled interval (Fig. F25C, F25D). Magnesium decreases from 39.36 mM at the top of this interval to 29.89 mM at the base. Calcium changes little, remaining near 20 mM. Strontium increases from 594 to 1124 µM (Fig. F25G). Finally, potassium values decrease from 8.2 to 4.6 mM in the lower interval (Fig. F25H).

Because of the paucity of samples, few inferences may be drawn from the pore fluid chemistry at this site. Nevertheless, the relative lack of change in chemistry of the pore waters immediately above and below the sediments of Megasequence C may be significant. The data show

that the fluids within this sequence have a composition similar to seawater, as at Site 1198 on the other side of the carbonate platform. It is thus possible that fluid flow occurs within these sediments, as was clearly expressed in the pore water chemistry at Site 1198.

X-Ray Diffraction Carbonate Mineralogy

A total of 133 sediment samples were analyzed for carbonate mineralogy from Site 1197 (Fig. F26; Table T11). The sediments of lithologic Unit I have typical mineralogy for shallow-water hemipelagic sediments deposited above the aragonite compensation depth. The sediments are comprised of ~20 wt% aragonite at the surface, with abundant high-magnesium calcite (HMC). Over the upper 60 mbsf, aragonite and HMC content decrease and a minor dolomite component appears. Below the unconformity marking the boundary between lithologic Units I and II, there is a sharp disappearance of aragonite and a sharp increase in dolomite concentration to ~70 wt%. High dolomite content is maintained to a depth of 280 mbsf and then decreases to ~5–20 wt% at 380 mbsf, the base of lithologic Subunit IVA. Both dolomite and total calcium carbonate are quite variable in lithologic Subunit IVB. Dolomite disappears completely below 600 m and only calcite is present in lithologic Unit V.

F26. Carbonate minerals determined by X-ray diffraction, p. 54.

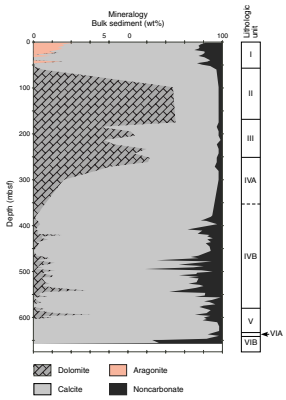

T11. Aragonite, calcite, dolomite, and noncarbonate mineral percentages, p. 80.

Sedimentary Geochemistry

Results

Calcium carbonate ($CaCO_3$) content at Site 1197 ranges from ~4 to 104 wt%. Carbonate measurements are calibrated for calcite; thus, the presence of dolomite can generate values >100 wt%. $CaCO_3$ content covaries inversely with total organic carbon (TOC) content, which ranges from 0.0 to 0.54 wt% (Fig. F27; Tables T12, T13). Note that TOC values from Rock-Eval pyrolysis and carbon-nitrogen-sulfur (CNS) analyses provide similar downsection profiles but differ in absolute values. However, the Rock-Eval profile indicates the lack of TOC in the uppermost 100 mbsf, whereas the CNS profile displays values up to ~0.1%.

Hydrogen index (HI) values at Site 1197 range from 0 to 171 mg HC/g TOC (Fig. F27; Table T13), but the low TOC values of some intervals limit the reliability of some of these results. We performed duplicate and triplicate analyses on these samples, and the results were within 10 wt% of the mean value. Oxygen index (OI) values vary from 0 to 51,100 mg CO_2/g TOC (Table T13). The high OI values are attributed to the thermal degradation of carbonate minerals during pyrolysis and are not considered in this interpretation. T_{max} values range from 305° to 418°C (Table T13), although the most reliable values lie between 405° and 415°C.

Total sulfur content in Site 1197 sediments ranges from 0.0 to 1.56 wt% (Fig. F27; Table T13), and its distribution is somewhat similar to that of TOC. C/N ratios and HI values show an inconsistent relationship (Fig. F27; Table T13). C/N values from Site 1197 indicate the presence of marine organic matter, whereas HI values indicate the presence of terrestrial or oxidized organic matter in the sediments. It must be noted that the low TOC content, and particularly the low total N content of these sediments, must be considered when assessing these data sets.

F27. Carbon, HI, and sulfur results, p. 55.

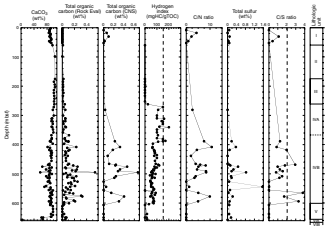

T12. Carbon, nitrogen, sulfur, and hydrogen results, p. 81.

T13. Rock-Eval pyrolysis results, p. 83.

Discussion

Variations in the generally high $CaCO_3$ content and the inversely covariant relation between $CaCO_3$ and TOC content at Site 1197 mostly reflect variations in carbonate mineralogy as these values were not recalculated to account for the presence of dolomite and the ratio of biogenic carbonate and terrigenous sedimentation through time. Calcium carbonate content displays an overall increase from ~90 wt% near the seafloor to >100 wt% $CaCO_3$ at ~100 mbsf. Between ~100 and 300 mbsf, in an interval characterized by high dolomite, TOC content is effectively zero.

Below ~260 mbsf, TOC and carbonate content display high frequency variability. The amplitude of these variations increases downsection through lithologic Unit IV. The maximum amplitude of variability is observed at ~495 mbsf in lithologic Subunit IVB. Here, the highest TOC value (0.54 wt%), lowest above-basement $CaCO_3$ value (~59 wt%), and second lowest total sulfur value (0.83 wt%) at Site 1197 were measured. These variations correspond to lower-frequency alternations that are well defined by natural gamma ray data (see **"Core Physical Properties,"** p. 19). The highest total S value (~0.83 wt%) measured at Site 1197 was also obtained within this interval (at ~544 mbsf). The variations in $CaCO_3$ content become less pronounced below ~550 mbsf, whereas TOC variations continue to display amplitudes similar to those observed above.

Interestingly, HI values suggest that lithologic Subunit IVB contains either terrestrial or oxidized organic matter. The presence of highly oxidized organic matter within an interval characterized by high total S content is unlikely; therefore, organic matter content may have been dominated by terrestrial input. This conclusion is supported by the presence of clay in Subunit IVB, suggesting that enhanced terrigenous input to the seafloor diluted $CaCO_3$ content during this time.

At ~600 mbsf, more consistent $CaCO_3$ values ranging from ~92 to 98 wt% and TOC values of zero roughly correspond to lithologic Unit V. Beneath this unit, $CaCO_3$ values decline through lithologic Unit VI and reach a low value of ~4 wt% in the basement.

CORE PHYSICAL PROPERTIES

Physical properties at Site 1197 were measured and evaluated on whole cores, split cores, and discrete core samples. The multisensor track was used on whole cores to perform nondestructive measurements of bulk density, magnetic susceptibility, and natural gamma radiation. Color reflectance was measured on the archive halves of split cores. Compressional wave velocity was measured in the x-, y-, and z-directions on split cores and core samples. Moisture and density (MAD) analyses were performed on core samples. Thermal conductivity was evaluated on unlithified whole cores and on samples from semilithified and lithified cores.

Density and Porosity

Bulk density at Site 1197 was computed from gamma ray attenuation (GRA) using unsplit cores, and from MAD measurements on discrete plug samples. Each measurement method provides two independent estimates of bulk density. Bulk density averages 1.75 g/cm^3 in the upper

50 mbsf with the GRA values being larger then the MAD density data by ~0.1 g/cm³. Limited core recovery from 50 to 375 mbsf, principally within seismic Megasequence C (see "Seismic Stratigraphy," p. 22) prevented GRA measurements. The MAD data over this interval show a gradual increase from 1.75 to 1.95 g/cm³. Below 375 mbsf, both GRA and MAD measurements were taken with the MAD measurements being, on average, 0.2 g/cm³ greater than GRA. However, the general trends are similar: bulk density increases from ~2.1 to 2.3 g/cm³ over the interval of 375 to 600 mbsf. Below 600 mbsf, bulk density is nearly constant at 2.3 g/cm³.

Grain density above 50 mbsf is highly scattered between 2.6 and 2.85 g/cm³. The higher grain densities may reflect the presence of aragonite (see "Geochemistry," p. 17), which has a density of 2.93 g/cm³. From 240 to 500 mbsf, grain density decreases downcore from 2.85 to ~2.7 g/cm³ and then begins to increase slowly until the base of lithologic Unit V where it has a value of 2.75 g/cm³. Grain density again decreases within lithologic Subunits VIA and VIB, ranging from 2.6 to 2.7 g/cm³. These lithologic units consist of altered volcanic breccia composed of olivine basalt clasts and pumice set in a groundmass of finer-grained volcanic material (see "Lithostratigraphy and Sedimentology," p. 3).

Porosity at Site 1197 is ~70% at the seafloor and decreases to ~20% at 660 mbsf. The porosity-depth trend can be described with a negative exponential curve of the form (Athy, 1930):

$$\phi(z) = \phi_o\, e^{-kz},$$

where ϕ_o is the surface porosity and k is the porosity decay parameter (see the "Explanatory Notes" chapter). Least-squares estimation of these parameters is ϕ_o = 67% and k = 0.0016 m^{-1} (correlation coefficient = 0.94; Fig. F28). These parameters are similar to those established for hemipelagic sediments at other Leg 194 sites. Even though there is a significant data gap between 50 and 300 mbsf, the porosity trend is consistent within lithologic Unit I and the lower lithologic units of the site (lithologic subunits IVA–VIB; Fig. F28).

F28. Bulk density, grain density, and porosity, p. 56.

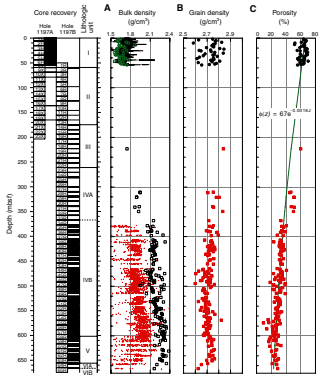

Compressional Wave Velocity

Compressional wave velocity was measured using the PWS3 contact probe system on both split cores (within the core liner) and ~9.5-cm³ cube samples of semilithified and lithified sediments. The cubes were used to measure velocity in the transverse (x and y) and longitudinal (z) directions.

Velocity values increase slowly from ~1650 to a maximum of 3175 m/s at a depth of 667 mbsf. Extreme velocity values correlate with the location of hardgrounds, such as the high 4796 m/s value at a depth of 59.6 mbsf (Fig. F29; see "Lithostratigraphy and Sedimentology," p. 3). The increased scatter in velocity value between 170 and 250 mbsf may reflect the high dolomite content associated with lithologic Unit III (see "Geochemistry," p. 17). Acoustic basement velocity (lithologic Subunits VIA and VIB) ranges from 3084 to 3870 m/s.

Velocity anisotropy is moderate and ranges from –10 to 10% (Fig. F29; also see "Geochemistry," p. 18, in the "Explanatory Notes" chapter). A positive anisotropy represents the common situation where sound transmission is relatively more efficient parallel to bedding rather than it is across. The anisotropy, which is positive for 59% of the

F29. *P*-wave and velocity, p. 57.

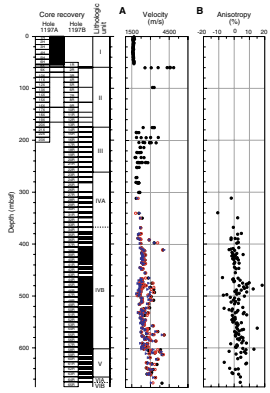

samples, appears to be randomly distributed with depth and does not show any simple relationship with either lithologic unit boundaries or grain size (see "Lithostratigraphy and Sedimentology," p. 3).

A crossplot of velocity vs. porosity for Site 1197 shows a general inverse relationship (Fig. F30). The velocity data from Site 1197 show significant negative deviations (average ~500 m/s) from the time-average equation (dashed line, Fig. F30; Wyllie et al., 1956). They can better be described with a power law relation:

$$V_P(\phi) = a\phi^{-b},$$

where V_P is the compressional wave velocity, and a (16,860 m/s) and b (0.56) are empirical constants determined from a least-squares regression (correlation coefficient = 0.88; Fig. F30).

Thermal Conductivity

Thermal conductivity at Site 1197 has an overall downhole increase from 0.95 to ~2.4 W/(m·K) (Fig. F31) that is consistent with measurements at other Leg 194 sites. Thermal conductivity variability increases below 440 mbsf. Thermal conductivity can be described as having a power law dependence on the solid matrix grain thermal conductivity and the thermal conductivity of the interstitial fluid (see the "Explanatory Notes" chapter). The values from Site 1197 follow this relationship within the range for the encountered sediments (Fig. F32), which gives confidence to the observations. Given the high carbonate content of this site (~90%; see "Geochemistry," p. 17), the range in thermal conductivity is consistent with the theoretic limestone curve.

Magnetic Susceptibility, Natural Gamma Radiation, and Color Reflectance

Magnetic susceptibility (MS) and natural gamma radiation (NGR) contain independent information concerning terrigenous sediment source and magnetic mineral derivation. Because of poor core recovery within lithologic Unit II through Subunit IVA at Site 1197, it is not possible to define a general trend in the NGR, MS, or the lightness (L*) parameter of color (Fig. F33). MS values range from 0 to 1725 × 10^{-6} SI, with the majority of values being less than 5 × 10^{-6} SI. Lithologic Unit I and Subunits VIA and VIB have the highest amplitudes. Lithologic Unit I is characterized by a general decrease in MS from ~25 to 5 × 10^{-6} SI. Superposed on this trend is a higher order ~10-m scale variability. Below 350 mbsf down to 625 mbsf, MS has a background value of 2 × 10^{-5} SI upon which are superposed a high-frequency signal with a length scale of 5–10 m. A prominent peak at 650 mbsf, with an amplitude of (>15 × 10^{-6} SI), appears to be responding to volcanic clasts within the base of lithologic Unit V (see "Lithostratigraphy and Sedimentology," p. 3). Volcaniclastic lithologic Subunits VIA and VIB (650 mbsf to base of hole) are characterized by the highest MS values that exceed 10^{-3} SI. For lithologic Subunit IVB and Units V and VI, NGR correlates with the MS and inversely correlates with the L* parameter of color (Fig. F33). The high lightness values from 610 to 645 mbsf correlate with high carbonate content (see "Geochemistry," p. 17).

A large NGR spike occurs at 60 mbsf and is associated with the existence of a hardground (see "Lithostratigraphy and Sedimentology,"

F30. Crossplot of velocity vs. porosity, p. 58.

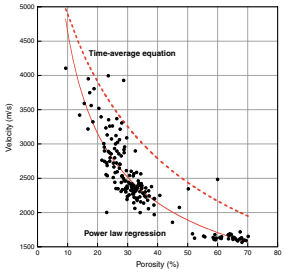

F31. Average thermal conductivity, p. 59.

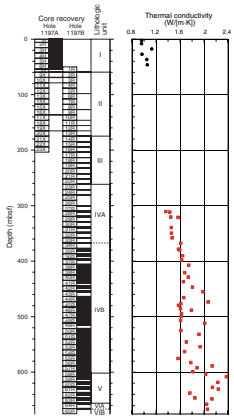

F32. Crossplot of porosity and thermal conductivity, p. 60.

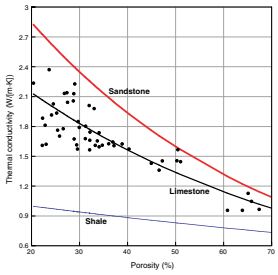

F33. Comparison of magnetic susceptibility, natural gamma radiation, and color reflectance, p. 61.

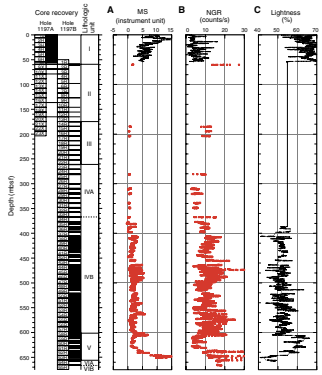

p. 3). High NGR values have characterized the response of other hardground and exposure surfaces cored during Leg 194, although the detailed form of the NGR signal varies from site to site. NGR values are highly variable throughout the entire site, ranging from 0 to >30 counts/s. Within the scatter, three general trends can be recognized. The interval from 300 to 610 mbsf shows a slight increase in average NGR. This is underlain by an interval of low-amplitude NGR (610 to 640 mbsf), coinciding with the upper portion of lithologic Subunit IVA. Then, NGR increases near the base of lithologic Unit V and remains relatively high in lithologic Subunits VIA and VIB. Variations in lightness between 610 and 400 mbsf in association with large variations in both MS and NGR likely indicate fluctuations in terrigenous clastic input to the basin.

SEISMIC STRATIGRAPHY

Site 1197 penetrated a 674.9-m-thick sedimentary succession and recovered 10 cm of volcanic basement. The site is located on regional multichannel seismic line MAR07 at shotpoint 3721 and on local grid lines MAR65 and MAR66 at shotpoints 645 and 907, respectively (Fig. **F34;** also see Fig. **F8,** p. 68, in the "Leg 194 Summary" chapter). Site 1197 is positioned ~5 km southeast of the leeward margin of the SMP (Figs. **F34, F2**). The main purpose at this site was to retrieve a platform proximal record, which documents and dates the platform growth history of SMP. Seismic data indicate that the sedimentary package at Site 1197 can be separated by three major unconformities into three megasequences (B, C, and D) and acoustic basement (Fig. **F34**).

F34. Multichannel line MAR07, p. 62.

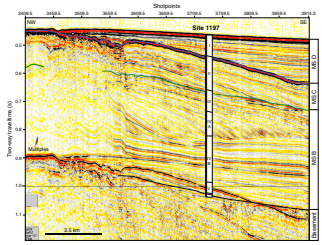

Time-Depth Conversion

Because of unstable hole conditions after drilling, downhole logging operations could not be completed at Site 1197. As a result, the time-to-depth conversion for this site was achieved using the shipboard velocity data collected from recovered sediments (see **"Core Physical Properties,"** p. 19). The continuity of the velocity values is hindered by the low recovery in part of Site 1197. *P*-wave sensor velocities also might have a systematic shift to lower values in respect to true formation velocities, as they were not measured under in situ conditions. In order to avoid a significant error in the two-way traveltime (TWT)-to-depth conversion, two prominent physical and lithological surfaces were used as tie points to relate the seismic traveltimes to coring depth. The first horizon is a hardground at 59 mbsf at the base of the hemipelagic drift deposits of lithologic Unit I (see **"Lithostratigraphy and Sedimentology,"** p. 3). This first downcore hard surface can be correlated to the high-amplitude reflection of the Megasequence C/D boundary at 536 ms TWT (Fig. **F34**). The second fix point corresponds to the basalt at the bottom of the hole at 666.6 mbsf, which produces the basement reflection at 1022 ms TWT. The resulting time-depth correlation is shown in Figure **F11,** p. 73, in the "Leg 194 Summary" chapter. Because no continuous velocity data are available, no synthetic seismogram was generated.

Megasequence D

Seismic Facies and Geometries

Megasequence D is characterized by laterally continuous low- to medium-amplitude reflections, which dip gently toward the southeast. They onlap along Megasequence C/D boundary onto underlying Megasequence C and form a wedge that disappears upslope, ~5 km to the northwest (Fig. F34). This onlap surface suggests a significant hiatus at the boundary to underlying Megasequence C. Megasequence D infills the topographic relief created by the SMP, indicating the dominance of currents on the sedimentation pattern. No major seismic unconformity can be recognized within Megasequence D.

Correlation with Cores

Megasequence D coincides with lithologic Unit I (0–59 mbsf), which consists of a skeletal grainstone and packstone with planktonic foraminifers deposited in a hemipelagic setting (see "Lithostratigraphy and Sedimentology," p. 3). Biostratigraphic data confirm a hiatus at the base of lithologic Unit I from at least 2.2 to 4.8 Ma, but likely even further back into the late Miocene (see "Age Model," p. 16).

Megasequence C

Seismic Facies and Geometries

The top of Megasequence C is marked by a high-amplitude reflection that dips to the southeast (~1°–1.5°) and forms a paleoslope topography of the SMP to the northwest (Fig. F34). Reflections within Megasequence C have the same dip as the C/D boundary and show no major intrasequence unconformities. Upslope, some of the reflections can be traced onto the carbonate platform, where they gradually turn horizontal, suggesting a continuous and gradual platform to slope transition, at least for the upper part of Megasequence C. The lower Megasequence B/C boundary is a downlap surface, indicating southeastward progradation of the slope deposits. As a result of this downlap, the lower half of Megasequence C wedges out within the upper 10 km of slope downward from the paleoplatform margin (Fig. F34).

Correlation with Cores

Megasequence C correlates well with the late Miocene lithologic Unit II (see "Lithostratigraphy and Sedimentology," p. 3, and "Age Model," p. 16), which consists of a fine-grained dolomitized skeletal grainstone deposited in a proximal periplatform setting. The high-amplitude reflection at the top correlates to the hardground surface observed in the cores, representing the hiatus at the Unit I/II boundary.

Megasequence B

Seismic Facies and Geometries

At Site 1197, Megasequence B forms a thick prograding slope sequence with two major seismic facies separated by a time-transgressive boundary (Fig. F34). The upper part of Megasequence B consists of inclined slope reflections that dip toward the southeast. At the base of the

slope, these reflections flatten out and form an almost horizontally layered section. This slope-to-plateau system is prograding out over at least 10 km. Because of their high-amplitude signature and their greater thickness than the horizontal open plateau time-equivalent reflections, the slope reflections terminate and downlap at the toe of the slope and form a pseudo-unconformity along the seismic facies boundary. This unconformity, which is the result of beds thinning below seismic resolution, crosscuts timelines, as shown in synthetic seismic sections of similar settings (Schlager, 1992). The slope reflections within Megasequence B display a slightly wavy and hummocky seismic facies in the upper ~150 ms, whereas the underlying plateau reflections yield a cleaner, more continuous seismic reflection pattern.

Correlation with Cores

At Site 1197, Megasequence B coincides with middle to early Miocene lithologic Units III through V. Lithologic Unit III consists of coarse detritus of skeletal grainstones. Unit III corresponds on the seismic data to the top of Megasequence B, displaying a slightly hummocky seismic facies, possibly indicative of the depositional/erosional process linked to the coarse grain size or the observed dolomitization. Underlying Subunit IVA consists of a partly dolomitized, very fine skeletal grainstone deposited in a more distal periplatform setting. The boundary to lithologic Subunit IVB marks the transition between the seismic slope and open plateau facies. Subunit IVB is comprised of similar sediments, as in the slope unit above, but contains a significant amount of clay (5%–40%) that is lacking in Subunit IVA. Surprisingly, despite the difference in bedding angle, no major grain size difference can be observed. Unit V corresponds to the base of Megasequence B and consists of more proximal periplatform skeletal grainstone and rudstone. Because the base of Megasequence B at Site 1197 is partly covered on the seismic data by the first multiple reflections, no detailed seismic facies analyses can be performed.

Acoustic Basement

Seismic Facies and Geometries

Acoustic basement at Site 1197 is defined by a strong reflection and a drastic change in seismic facies. Basement is slightly dipping to the southeast and, similar to Site 1198, cannot be traced below the SMP because the overlying platform sediments attenuate the signal and multiples mask most subsurface information.

Correlation with Cores

Acoustic basement at this site is formed by 10 m of volcaniclastic breccia-conglomerate with large angular basalt clasts (lithologic Unit VI) that overlies, at 666.6 mbsf, an olivine basalt likely representing the volcanic basement. The acoustic basement is also masked by multiple reflections so that it is not clear whether the breccia-conglomerate is a laterally continuous unit or just a local feature.

REFERENCES

Athy, L.F., 1930. Density, porosity, and compaction of sedimentary rocks. *AAPG Bull.,* 14:1–24.

Betzler, C., 1997. Ecological control on geometries of carbonate platforms: Miocene/Pliocene shallow-water microfaunas and carbonate biofacies from the Queensland Plateau (NE Australia). *Facies,* 37:147–166.

Berggren, W.A., Hilgen, F.J., Langereis, C.G., Kent, D.V., Obradovich, J.D., Raffi, I., Raymo, M.E., and Shackleton, N.J., 1995a. Late Neogene chronology: new perspectives in high-resolution stratigraphy. *Geol. Soc. Am. Bull.,* 107:1272–1287.

Berggren, W.A., Kent, D.V., Swisher, C.C., III, and Aubry, M.-P., 1995b. A revised Cenozoic geochronology and chronostratigraphy. *In* Berggren, W.A., Kent, D.V., Aubry, M.-P., and Hardenbol, J. (Eds.), *Geochronology, Time Scales and Global Stratigraphic Correlation*. Spec. Publ.—Soc. Econ. Paleontol. Mineral. (Soc. Sediment. Geol.), 54:129–212.

Johnson, H.P., Lowrie, W., and Kent, D.V., 1975. Stability of anhysteretic remanent magnetization in fine and coarse magnetite and maghemite particles. *Geophys. J. R. Astron. Soc.,* 41:1–10.

Kennett, J.P., and Srinivasan, M.S., 1983. *Neogene Planktonic Foraminifera: A Phylogenetic Atlas:* Stroudsburg, PA (Hutchinson Ross).

Schlager, W., 1992. Sedimentology and sequence stratigraphy of reefs and carbonate platforms. *AAPG Contin. Educ. Course Note Ser.,* 34:71.

Wyllie, M.R.J., Gregory, A.R., and Gardner, L.W., 1956. Elastic wave velocities in heterogeneous and porous media. *Geophysics,* 21:41–70.

Figure F1. Bathymetry map showing locations of Leg 194 sites. Site 1197 is shown in bold.

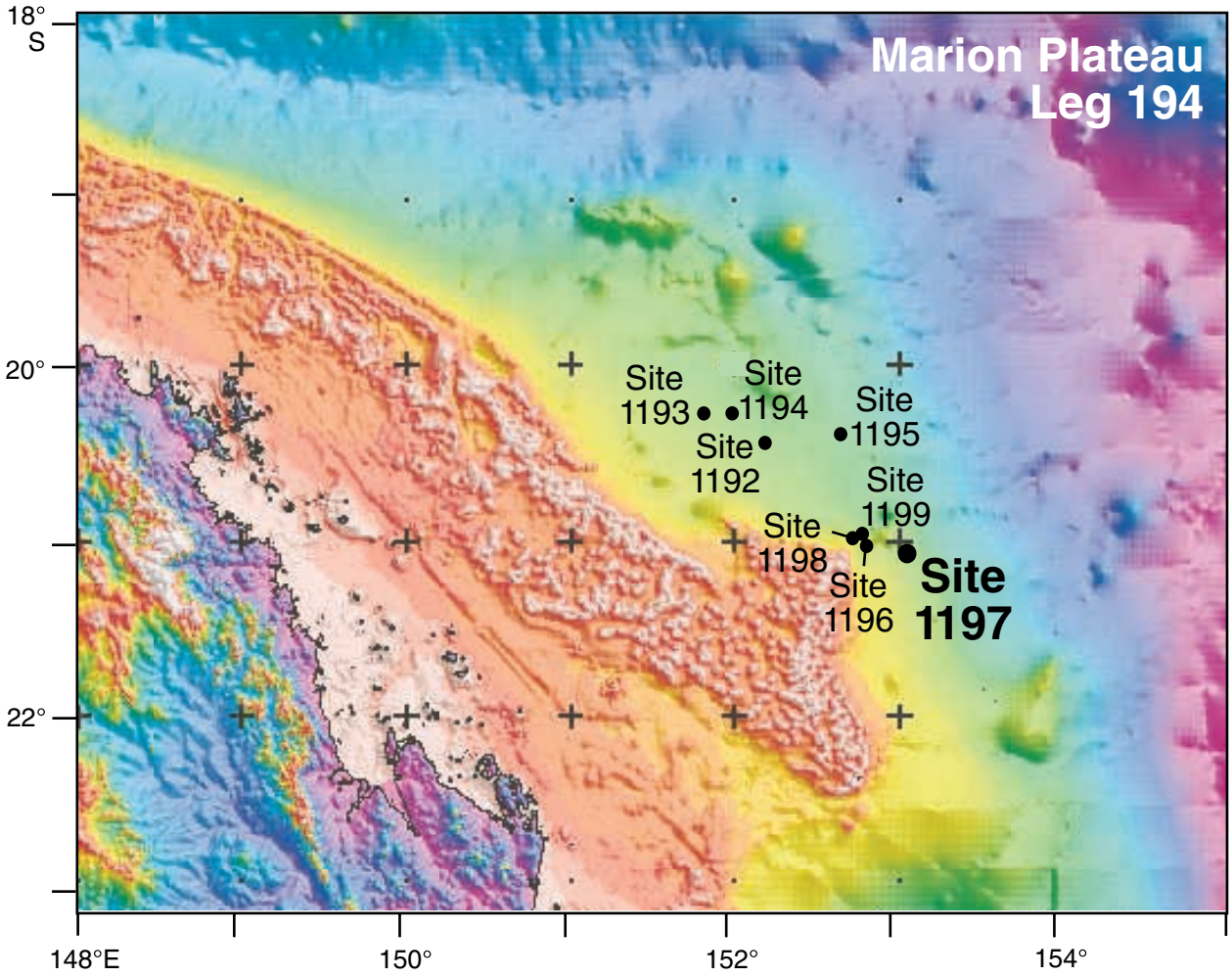

Figure F2. Seismic line MAR07 with locations of Sites 1196, 1197, 1198, and 1199. Site 1197 is positioned on the downcurrent, windward slope of the adjacent southern carbonate platform. * = projected into the seismic section parallel to the northwestern Southern Marion Platform (SMP) margin.

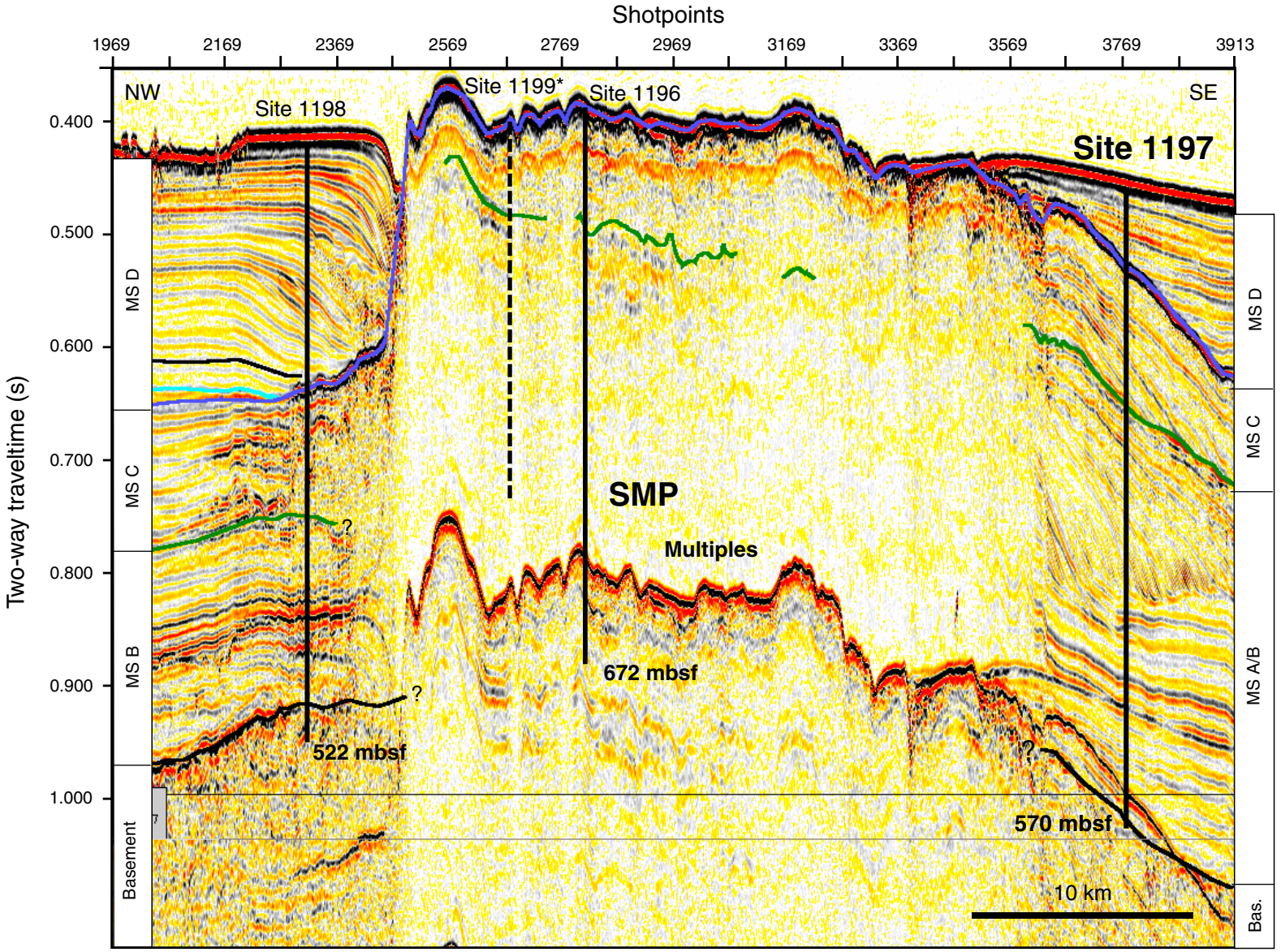

Figure F3. Lithologic summary for Site 1197. **A.** Core recovery. Black = recovered, white = gap. **B.** Lithologic units. **C.** Graphic lithology. **D.** Calcium carbonate content (see "Geochemistry," p. 17). **E.** Dunham texture classification. **F.** Grain size. **G.** Paleoenvironmental interpretation. **H.** Geologic age (see "Biostratigraphy and Paleoenvironments," p. 9).

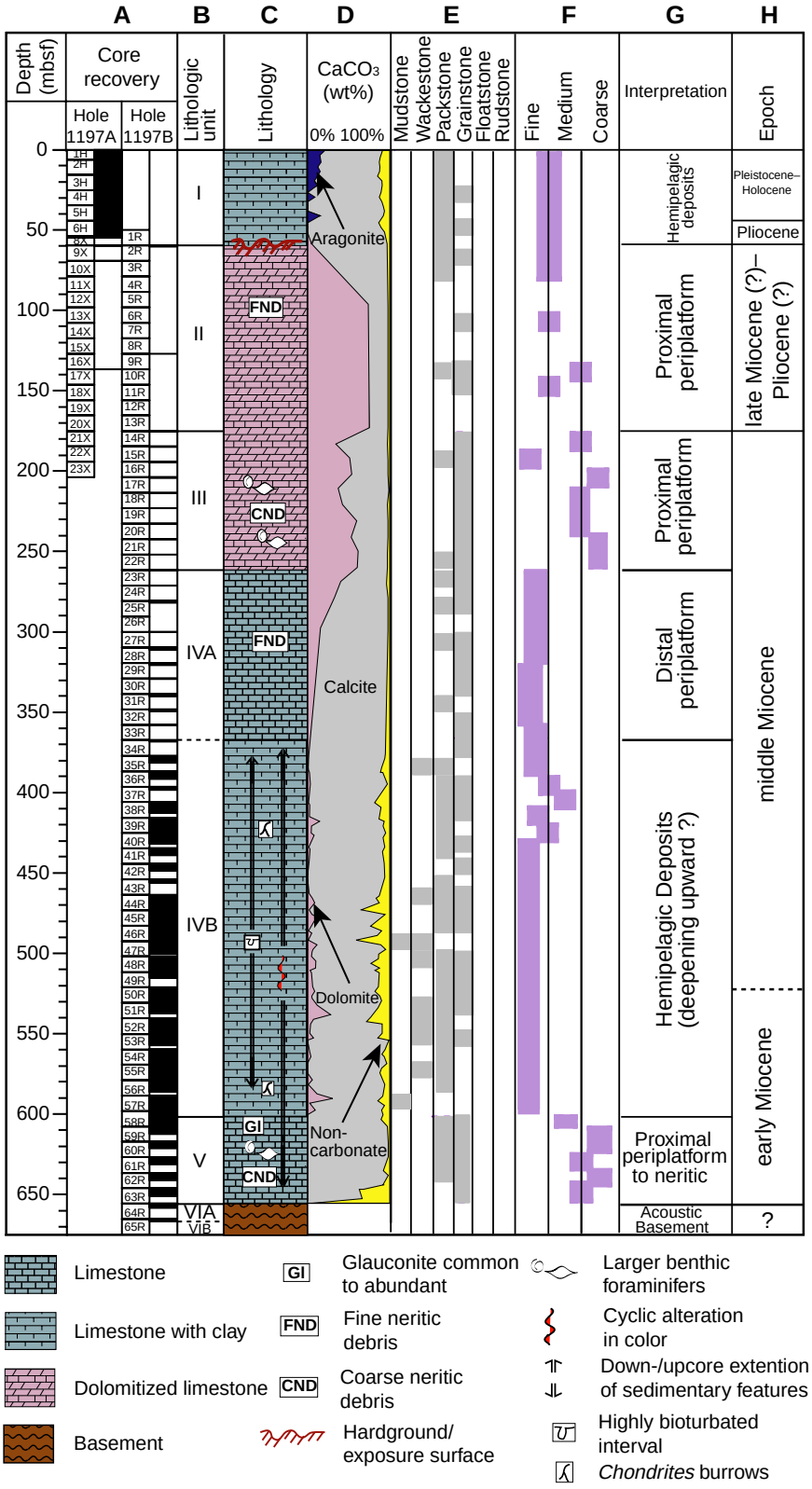

Figure F4. Close-up photograph of indurated skeletal grainstone at the top of Unit II capped by a reddened 2- to 4-mm-thick phosphatic crust (interval 194-1197B-2R-1, 0–20 cm). Large borings are present (arrows), infilled with phosphatic sand or foraminifer grainstone (L).

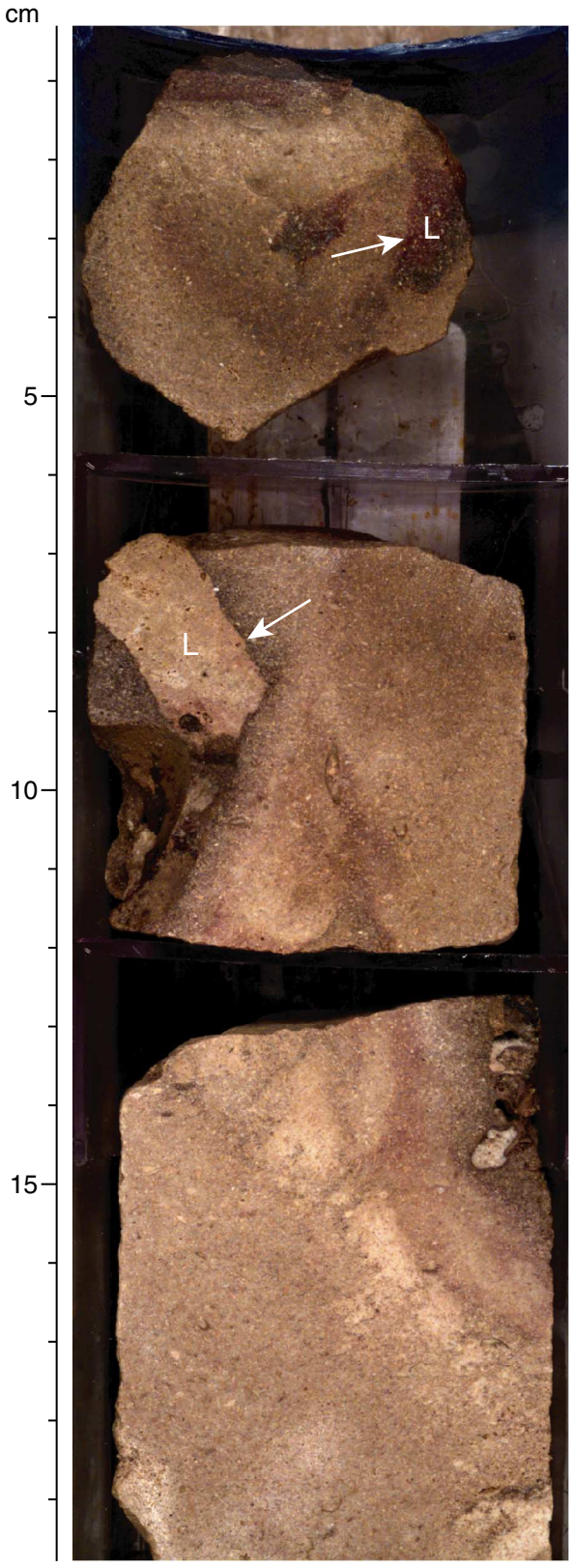

Figure F5. Photomicrograph showing the late-stage infilling of a boring excavated into the phosphatized upper interval of Unit II. Abundant planktonic foraminifers with geopetal infills can be observed in a dark brown micrite matrix (Sample **194-1197B-2R-1, 6–8 cm**).

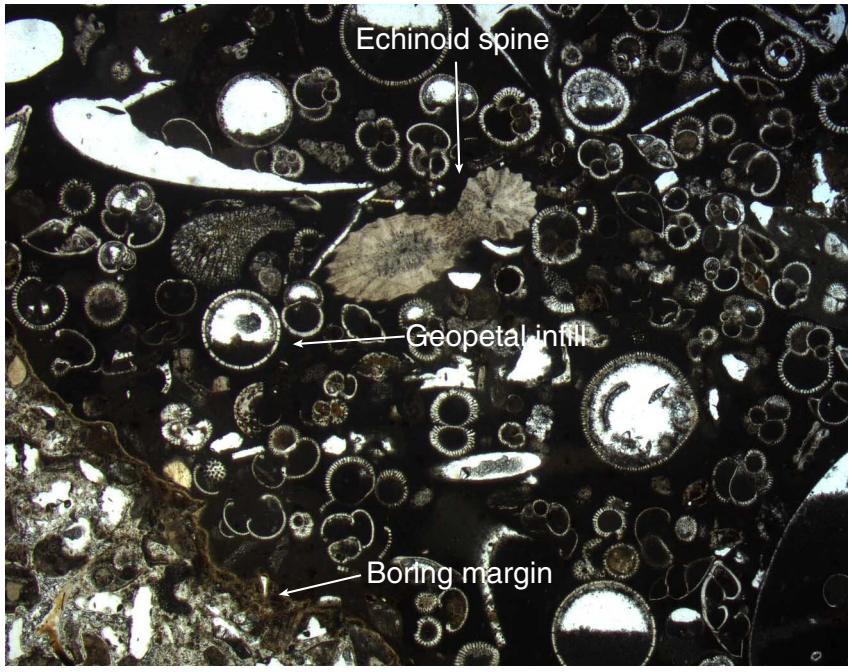

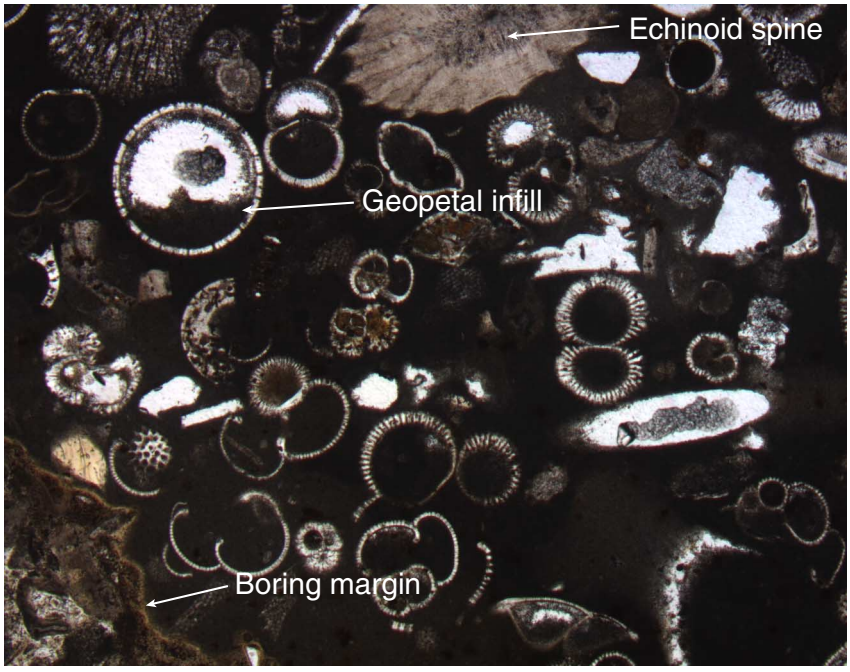

Figure F6. Photomicrograph showing skeletal packstone dominated by planktonic foraminifers in a phosphatized micrite cement (Sample **194-1197B-2R-1, 1–4 cm**). Largely unabraded *Amphistegina* sp. are common, along with fragments of coralline algae, indicating reworking of neritic detritus to the slope area.

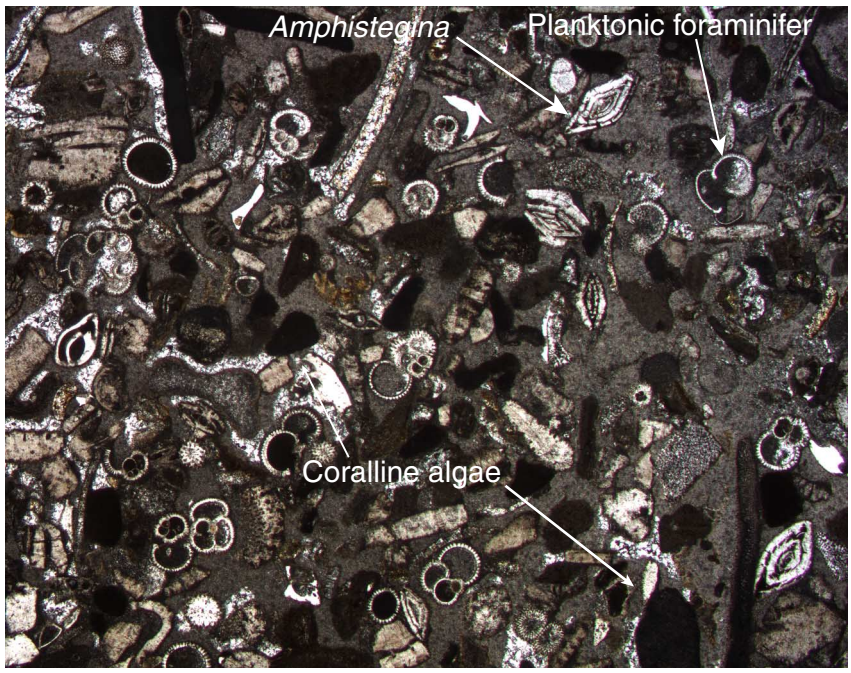

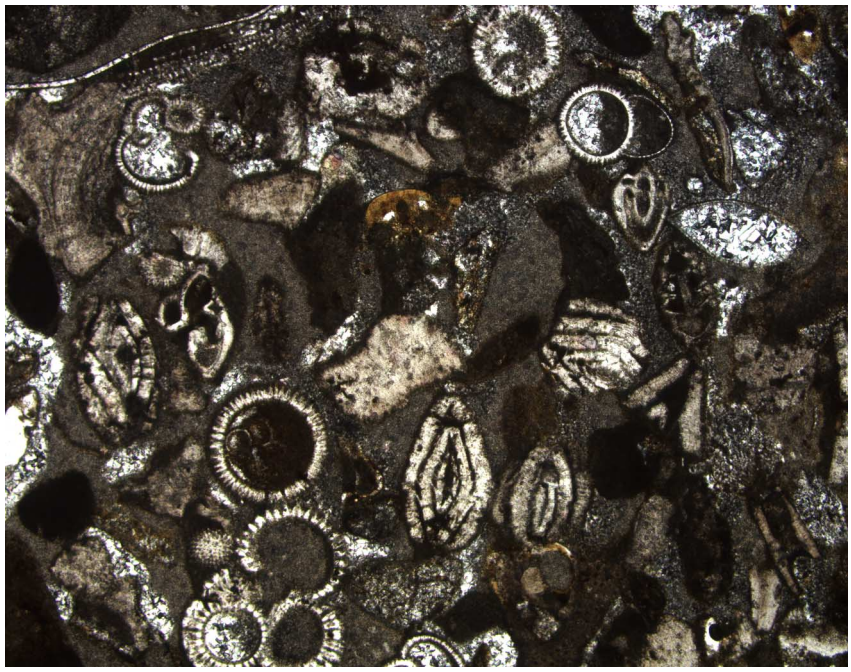

Figure F7. Photomicrograph showing skeletal grainstone that contains abundant larger benthic foraminifers, including *Lepidocyclina* sp., *Operculina* sp., and *Amphistegina* sp. (Sample **194-1197B-21R-1, 42–45 cm**). Coralline algae are a common component and planktonic foraminifers are present. Porosity is high and minor dolomite cement rims occur around skeletal grains.

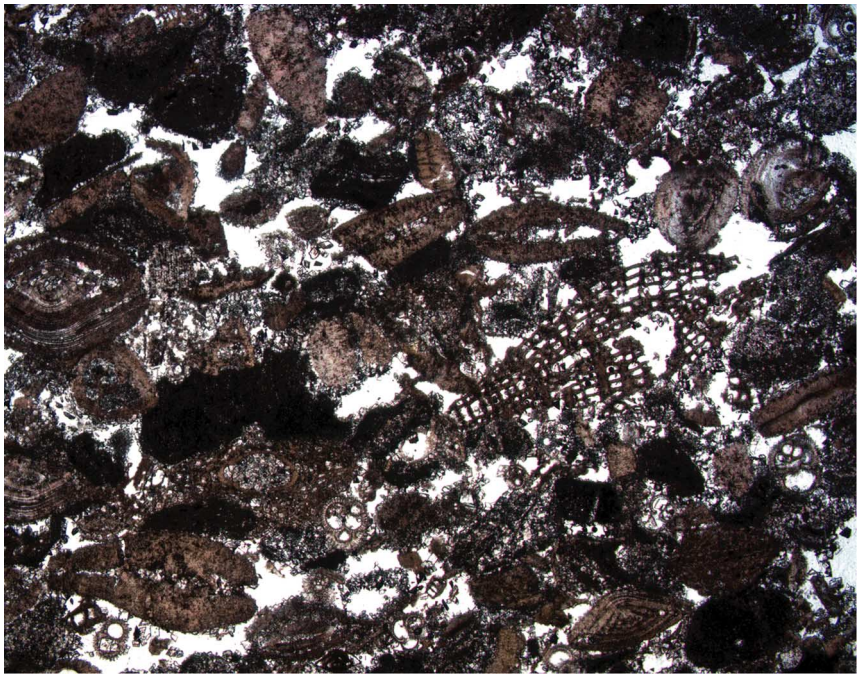

Figure F8. Close-up photograph of skeletal grainstone containing abundant *Lepidocyclina* sp. larger benthic foraminifers *Operculina* sp. and *Amphistegina* sp. (interval 194-1197B-16R-1, 4–15 cm). A crude lamination can be observed in the lithology and imbrication of foraminifer tests.

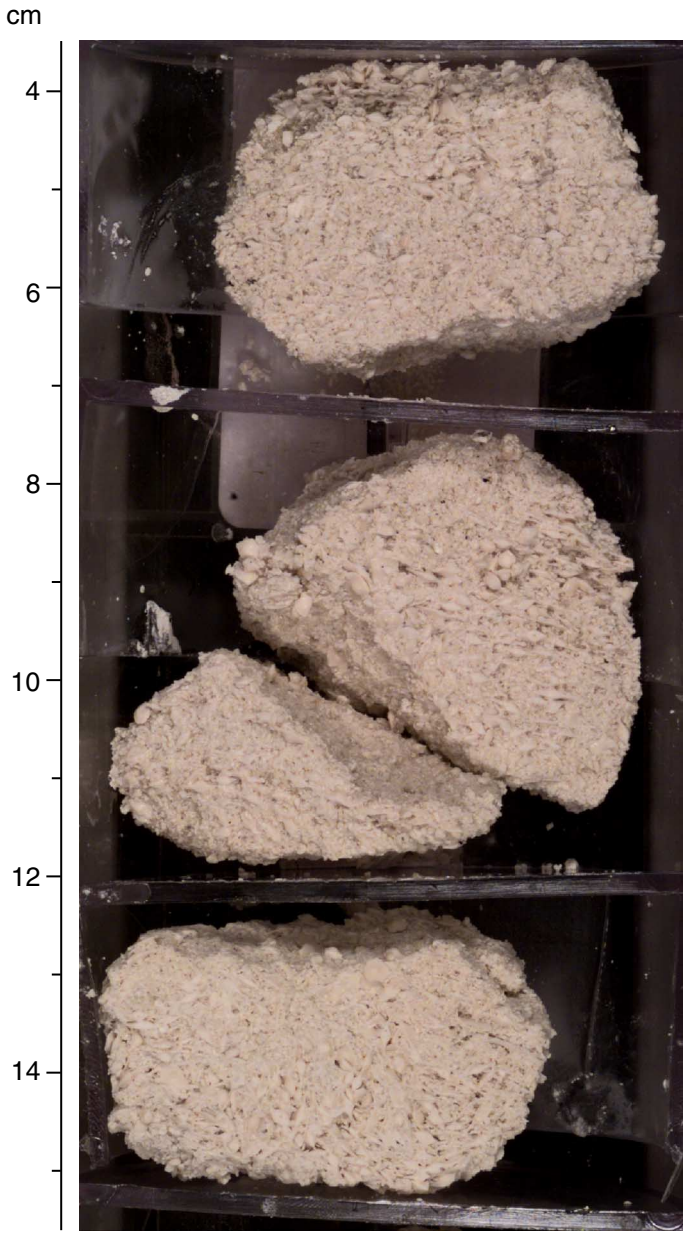

Figure F9. Photomicrograph of a fine sand-sized skeletal grainstone with abundant small benthic foraminifers and common fragments of coralline algae, suggesting skeletal particles are derived from a neritic source area (Sample **194-1197B-32R-1, 0–4 cm**). Planktonic foraminifers are present and often overgrown by fine dolomitic cements.

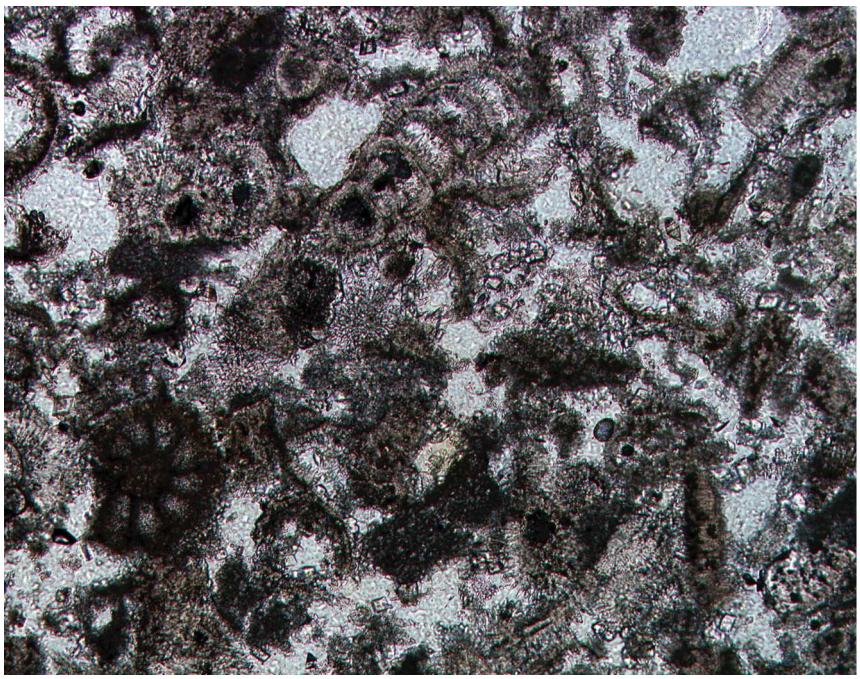

Figure F10. Photograph of Core 194-1198B-55R, showing alternating dark- and light-colored intervals of fine-grained skeletal packstone and grainstone indicate high-frequency cyclicity. Up to 15 individual cycles can be observed in which fluctuation of clay content is considered to control the color changes.

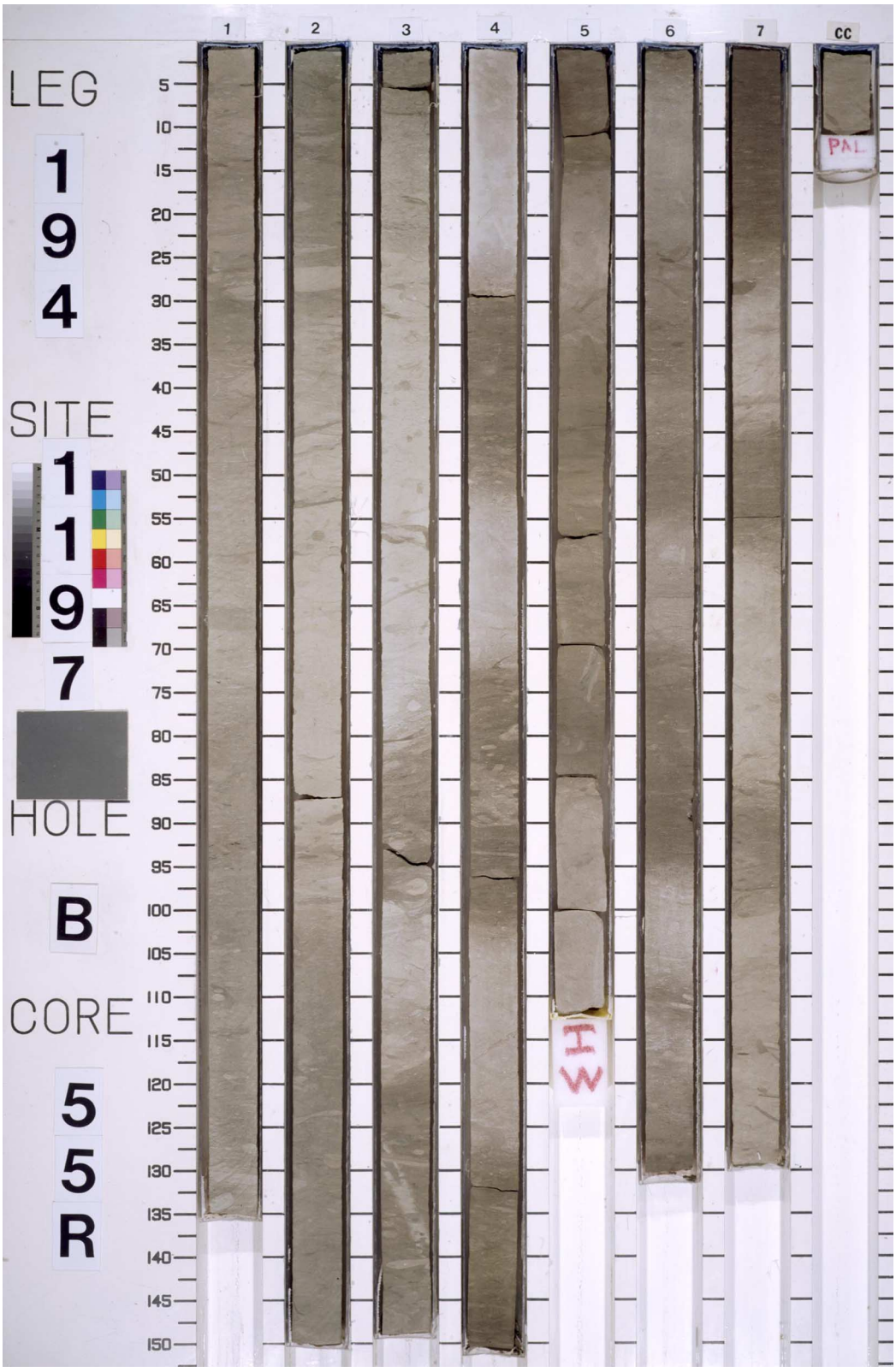

Figure F11. Close-up photograph of extensive bioturbation at the contact between an interval of light gray silt-sized grainstone overlying a darker olive-gray skeletal packstone with clay (interval 194-1197B-45R-2, 3–16 cm).

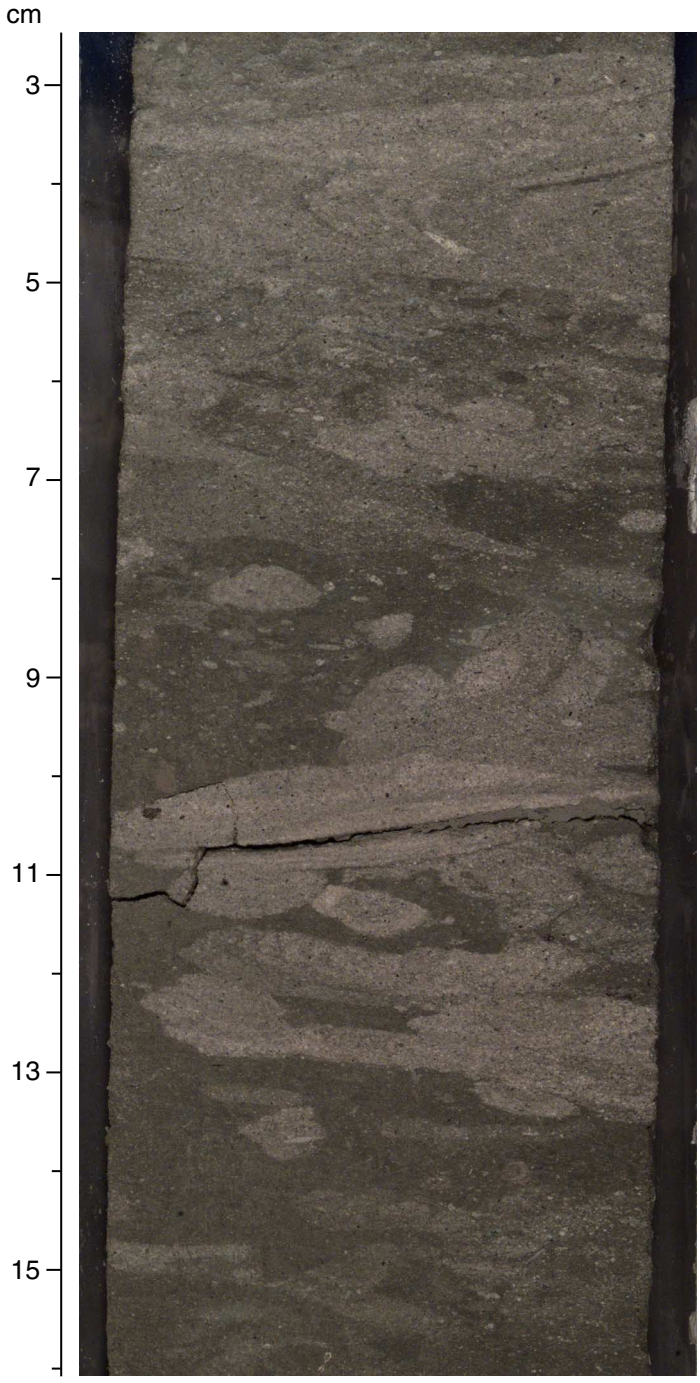

Figure F12. Close-up photograph of thin turbidite bed with a sharp planar base and a distinctive fining-upward grainsize (arrow) and clear parallel laminations (arrow) (interval 194-1197B-37R-1, 125–145 cm).

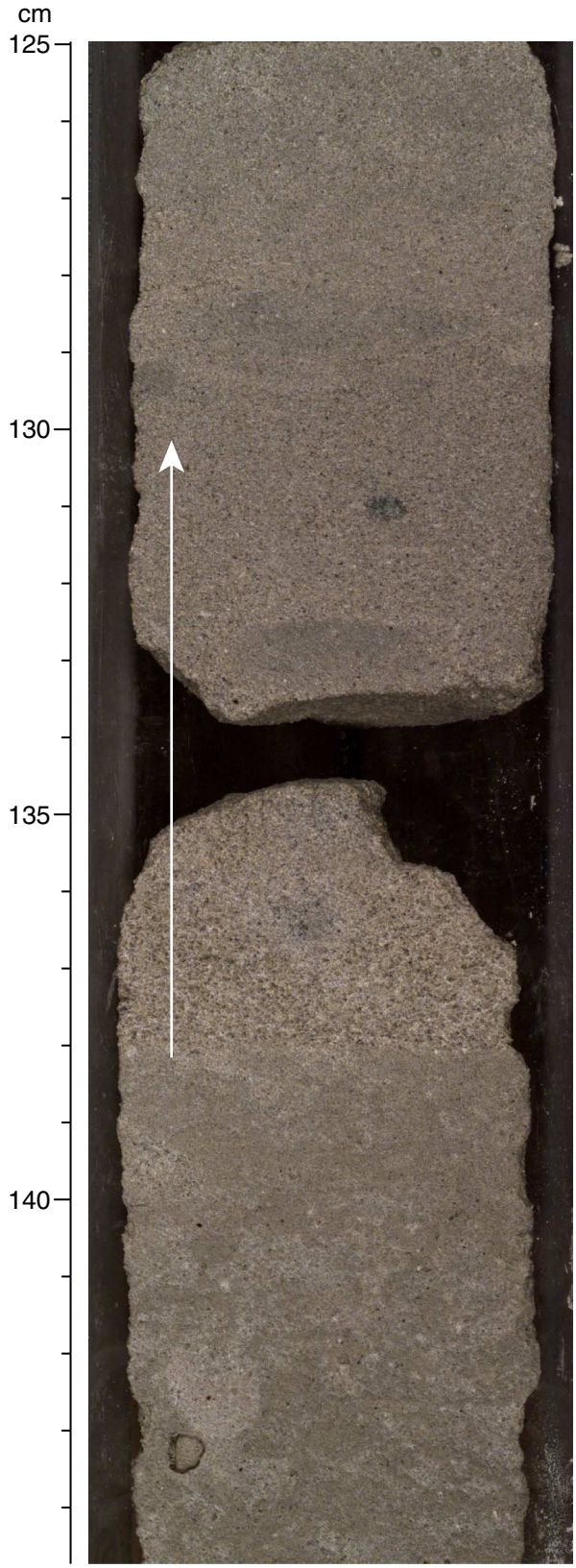

Figure F13. Photomicrograph showing skeletal packstone containing abundant larger benthic foraminifers and fragments of coralline algae (Ca) (Sample **194-1197B-59R-2, 109–113 cm**). *Lepidocyclina* sp. (Le) are extremely abundant but are often abraded and damaged. Planktonic foraminifers are also present.

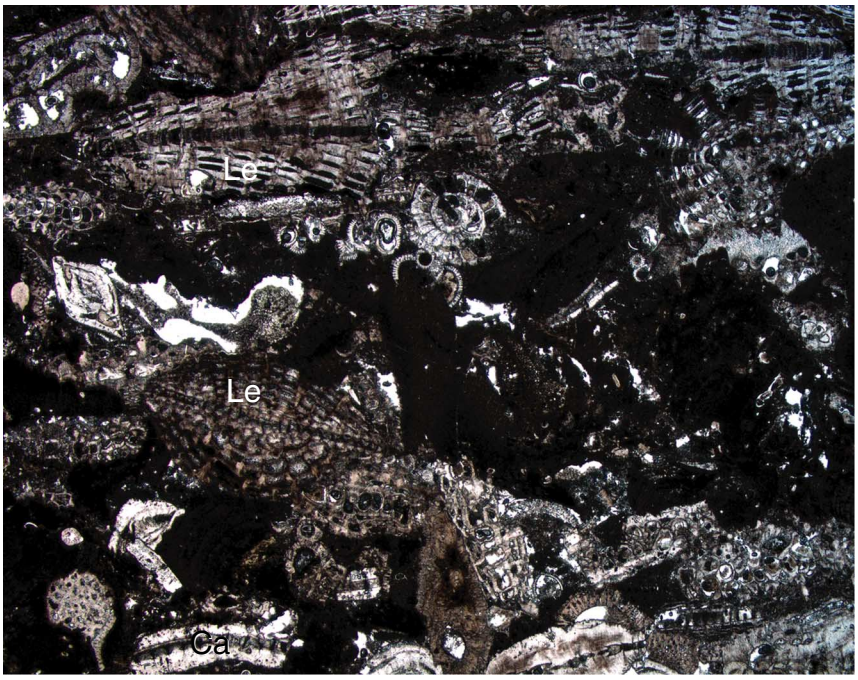

Figure F14. Close-up photograph of fining-upward package of coarse skeletal grainstone containing larger benthic foraminifers, capped by a thin parallel-laminated interval of finer, dark packstone (interval 194-1197B-59R-2, 55–68 cm). Glauconite is abundant, adding a green color to this lithology.

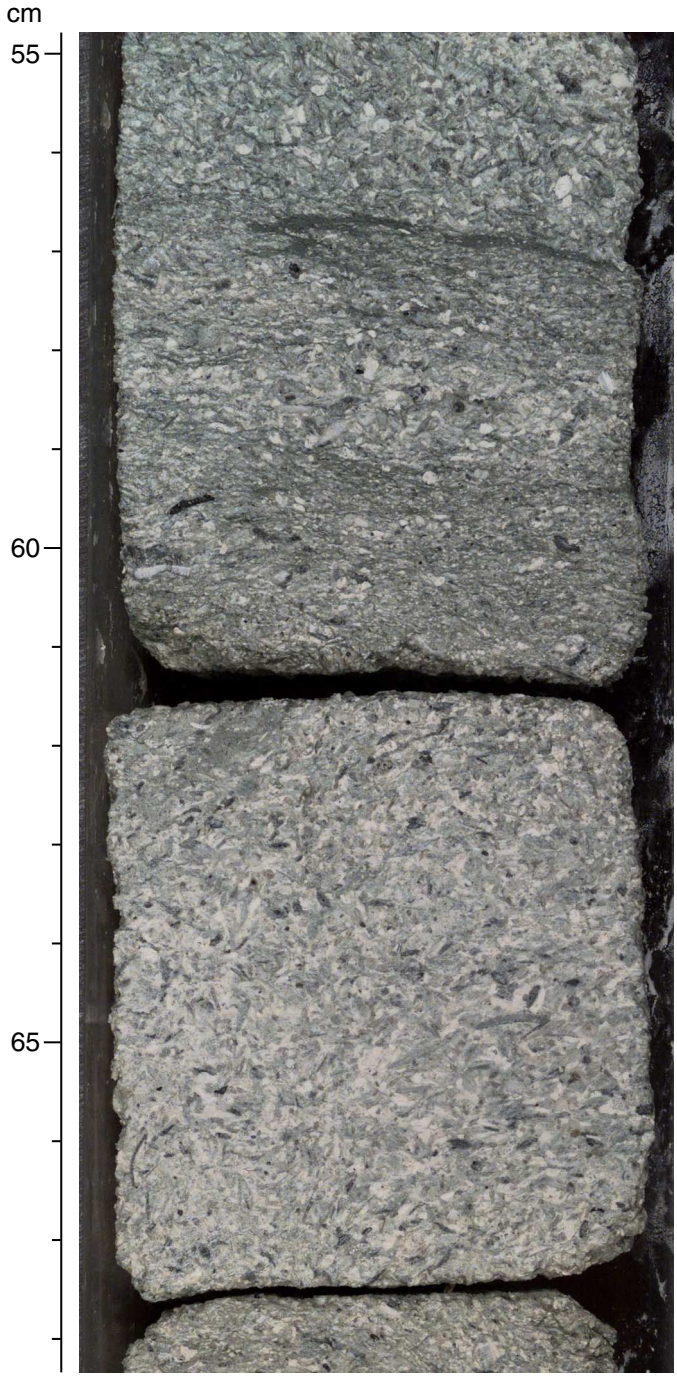

Figure F15. Close-up photograph of skeletal floatstone containing bryozoan fragments and large bivalves (interval 194-1197B-64R-1, 19–36 cm). Small pebbles of volcanic rock are also observed in a matrix of fine skeletal detritus, quartz, and glauconite.

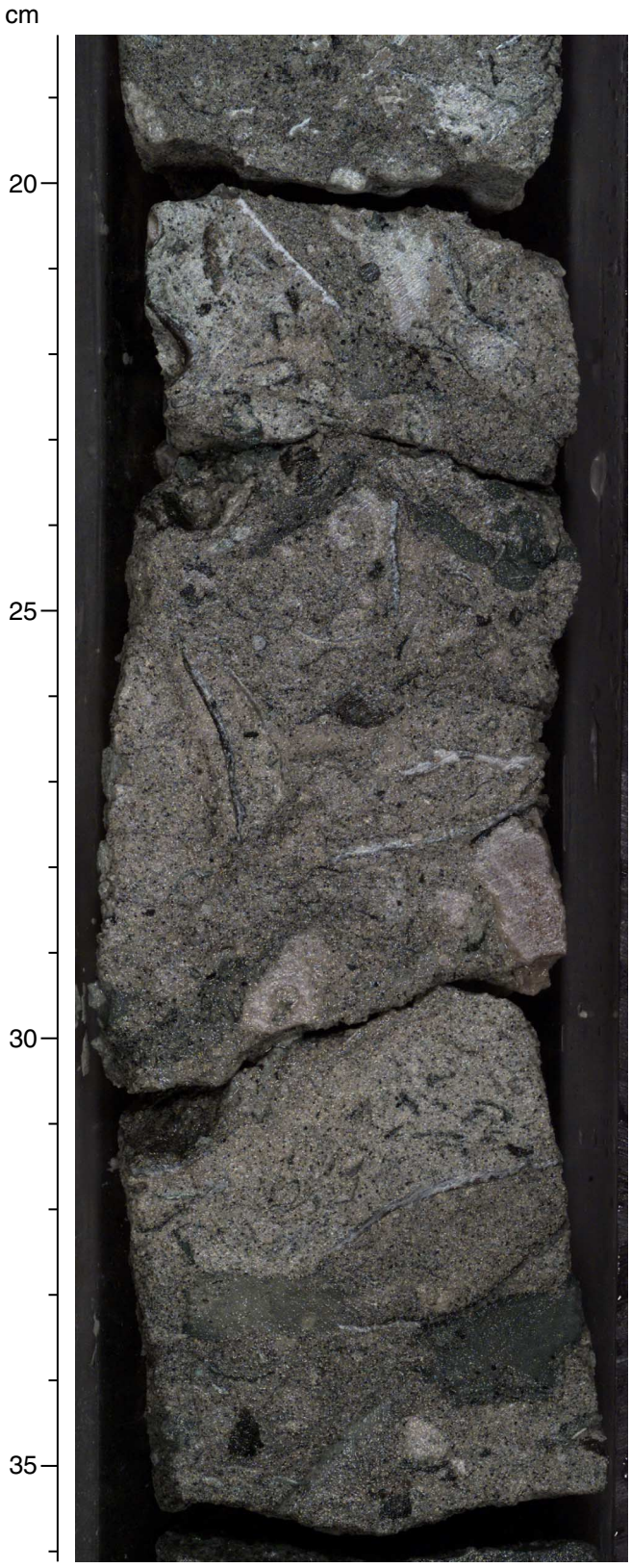

Figure F16. Close-up photograph of matrix-supported volcaniclastic breccia containing highly altered angular to subrounded clasts of basalt (interval 194-1197B-64R-1, 44–56 cm). This rock is interpreted as a debris flow, which originated in a continental setting with considerable paleorelief.

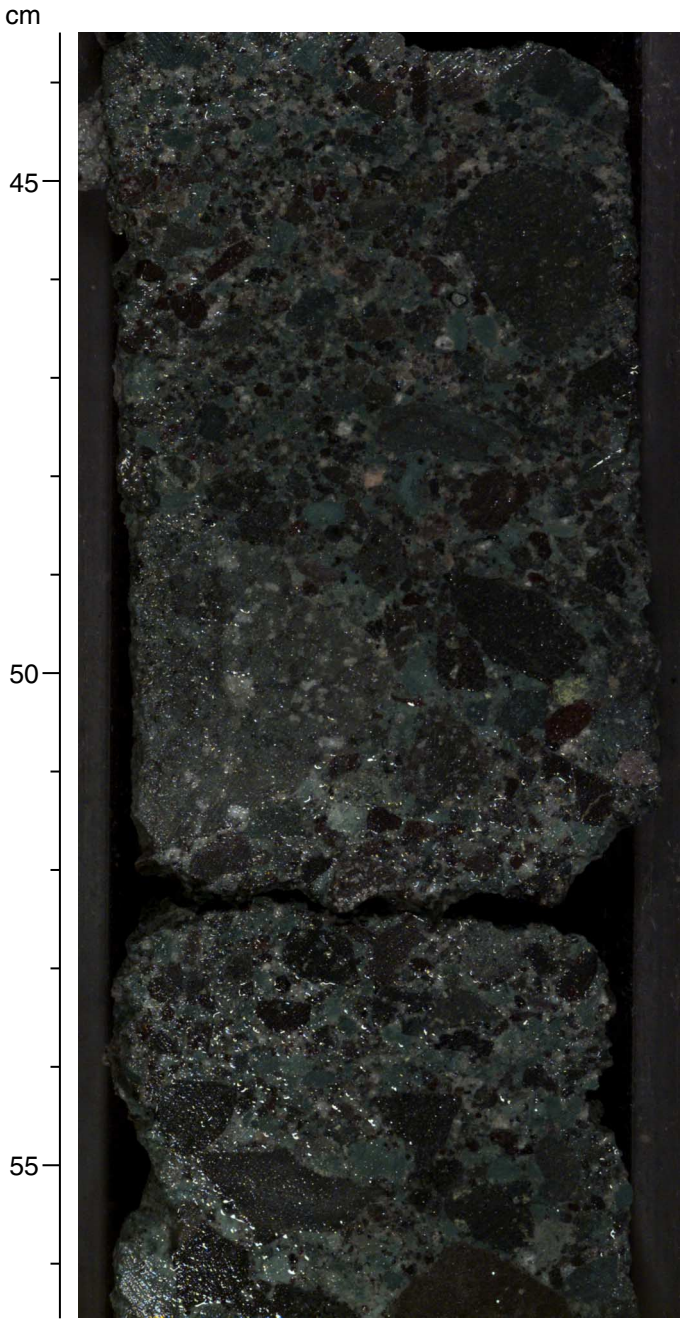

Figure F17. Photomicrograph of Sample **194-1197B-2R-1, 0–1 cm** (lithologic Unit II), showing neritic sediments, including *Amphistegina* (Am), red algal fragments (RA), and mixed planktonic foraminifers (PF).

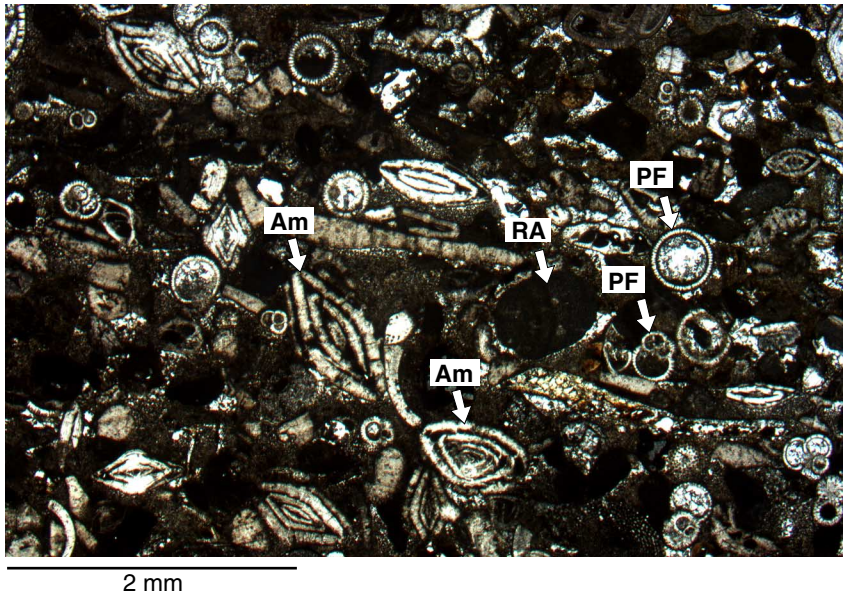

Figure F18. Photomicrograph of Sample **194-1197B-2R-1, 42 cm** (lithologic Unit II), illustrating vertical sections through two *Lepidocyclina* (Lp).

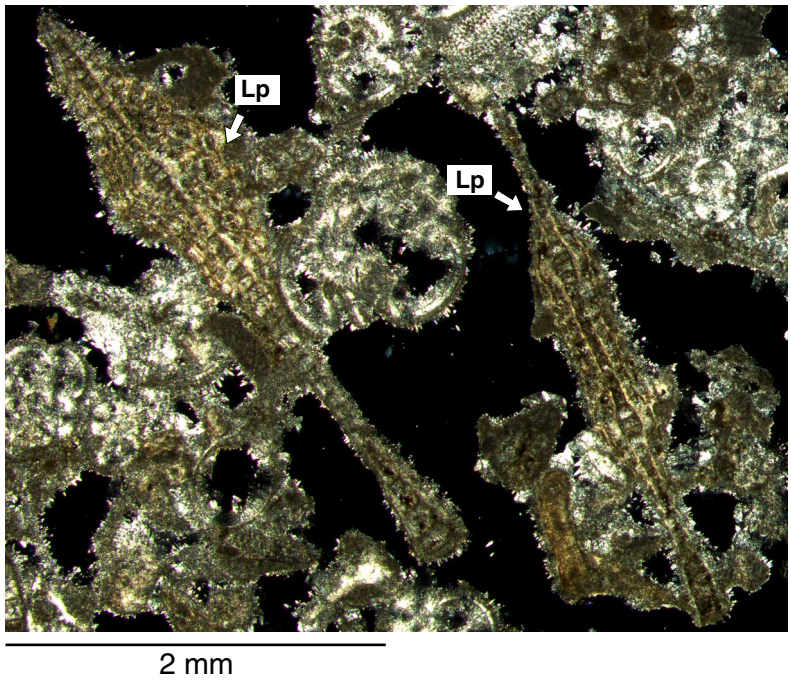

Figure F19. Long-core measurements for Hole 1197A, showing natural remanent magnetization (NRM) intensity after 30-mT demagnetization and inclination as a function of depth.

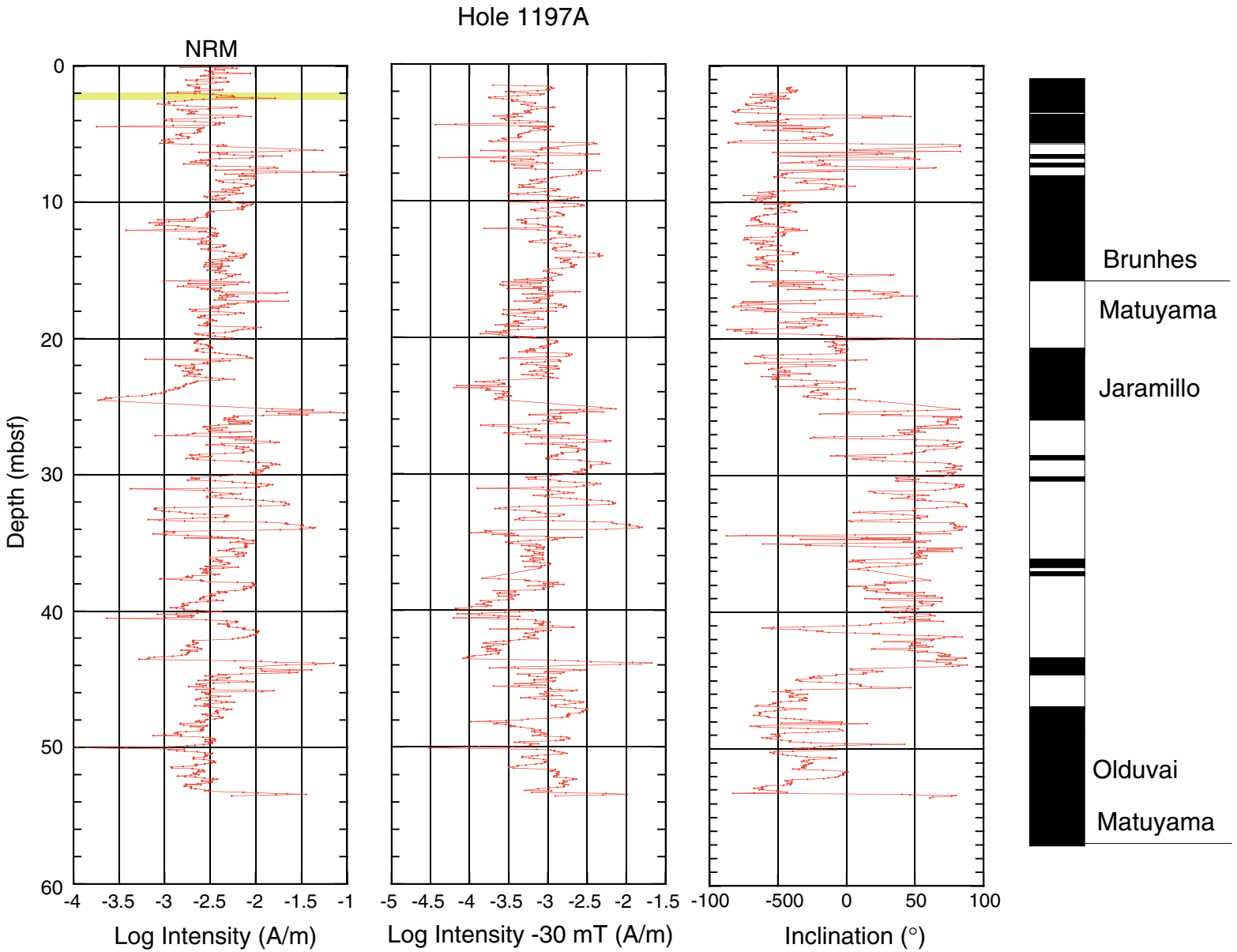

Figure F20. Long-core measurements for Hole 1197B, showing intensity and inclination as a function of depth. **A.** 375–400 mbsf. (Continued on the next three pages.)

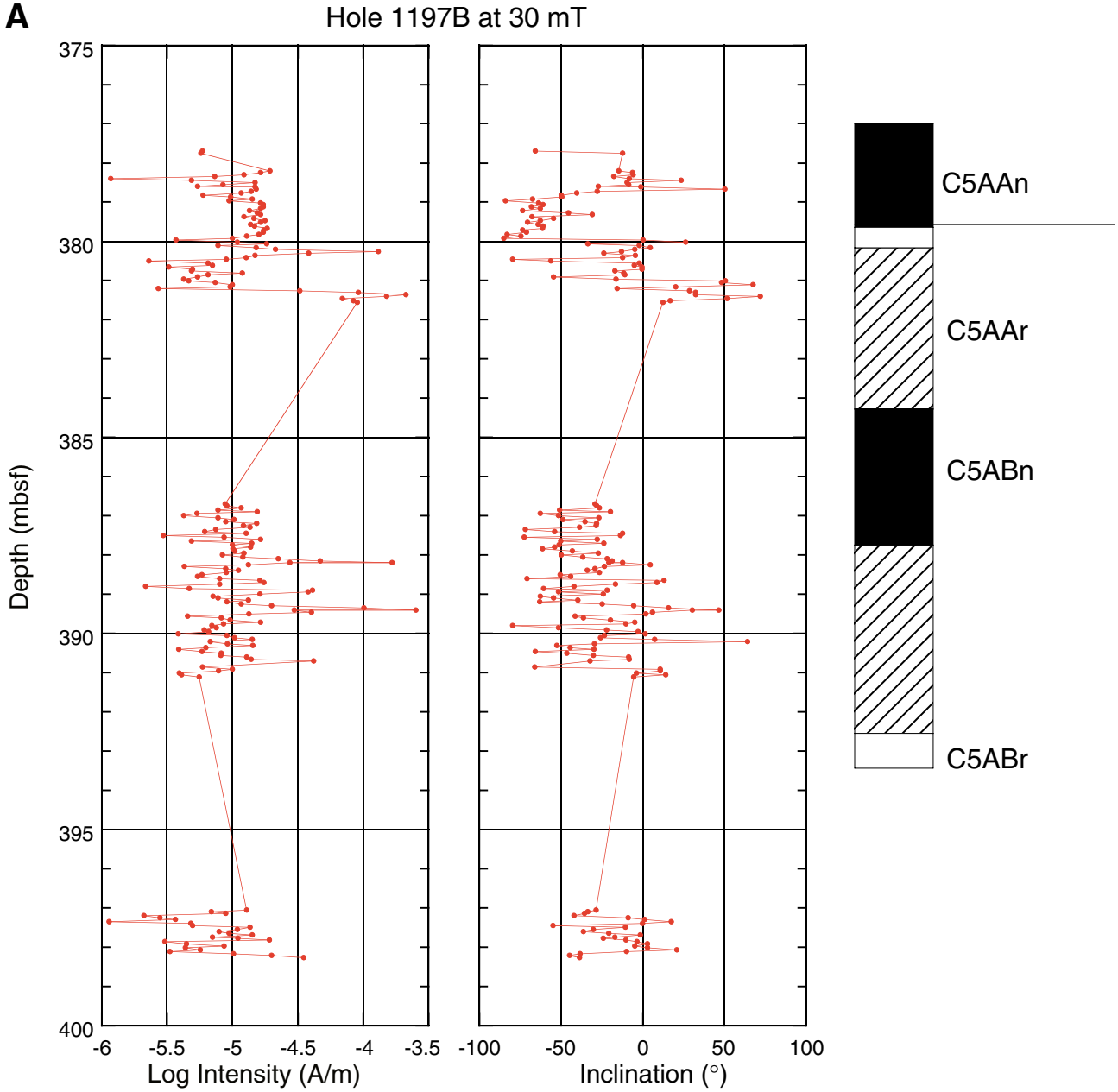

Figure F20 (continued). B. 400–500 mbsf.

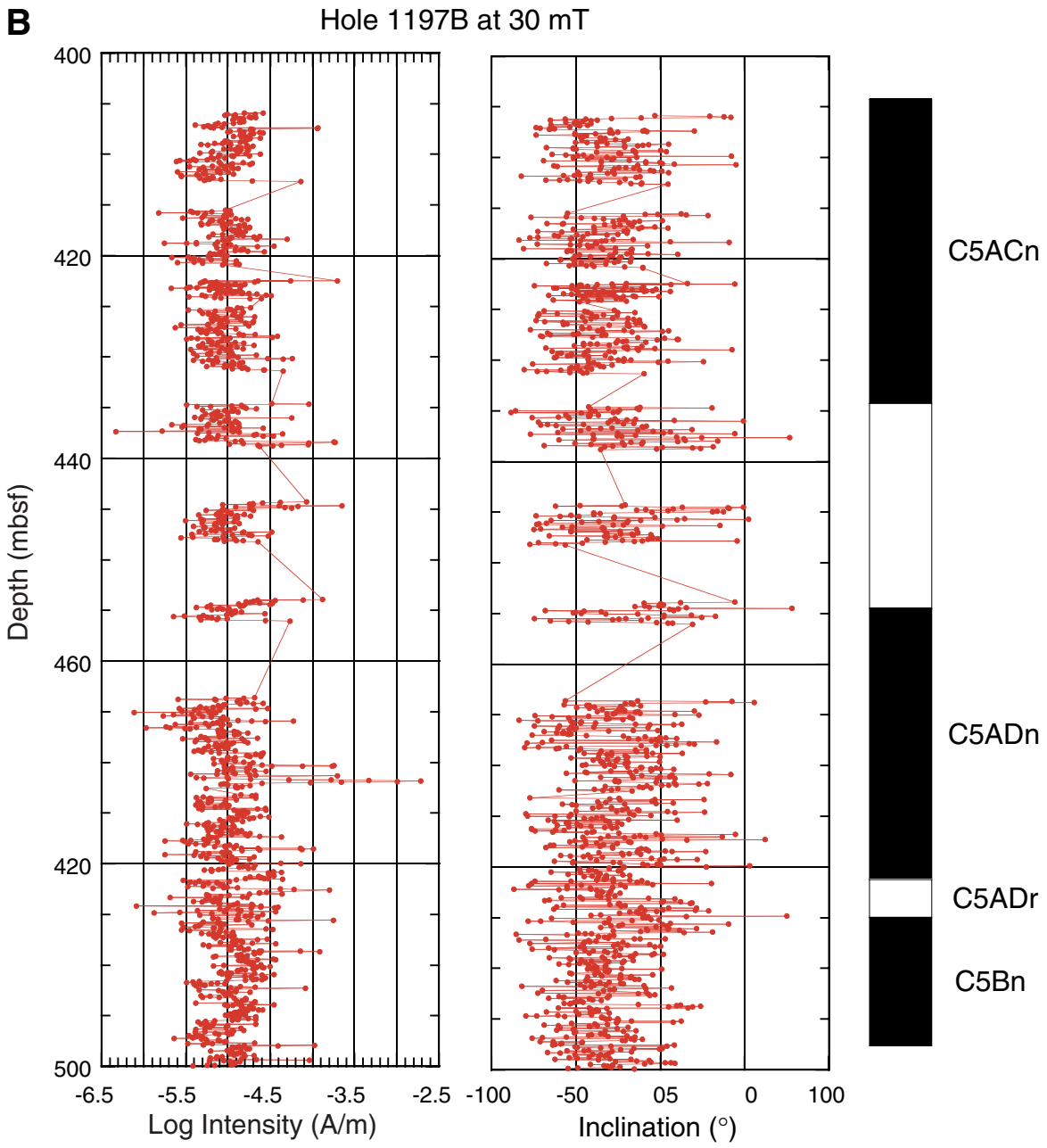

Figure F20 (continued). C. 500–600 mbsf.

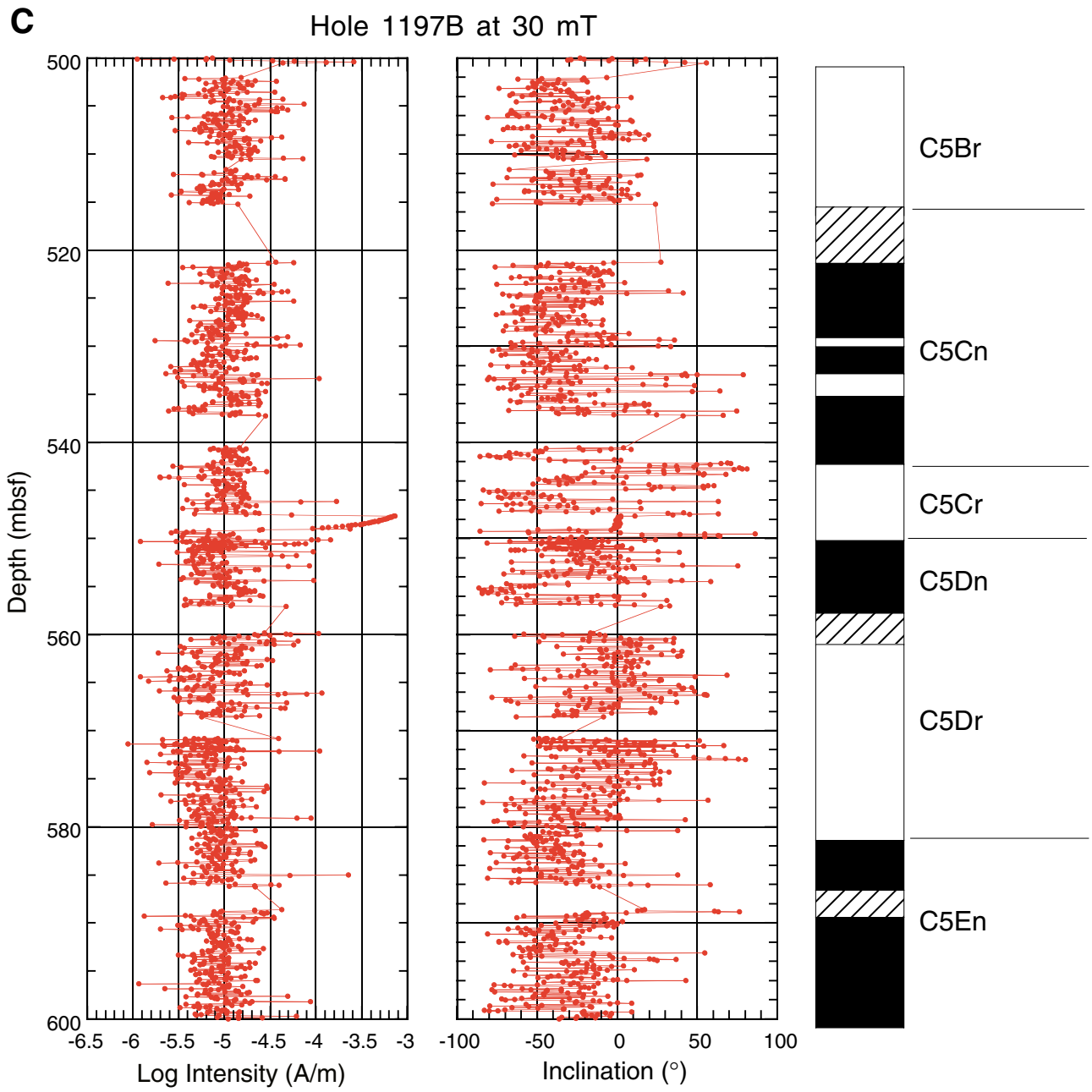

Figure F20 (continued). D. 600–670 mbsf.

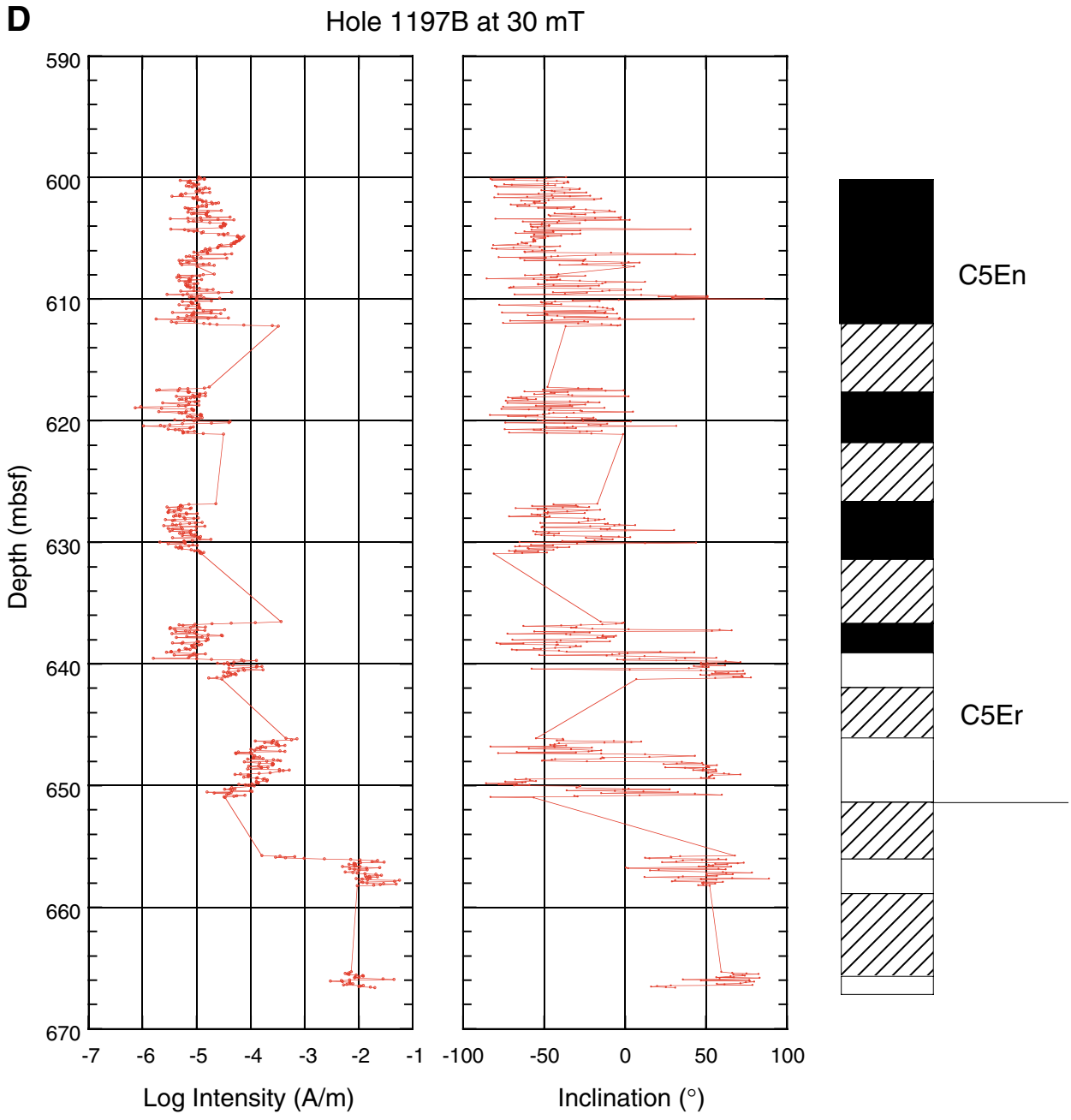

Figure F21. Comparison of observed magnetic stratigraphy in (**A**) Hole 1197A and (**B**) Hole 1197B, with the geomagnetic polarity timescale of Berggren et al. (1995a; 1995b).

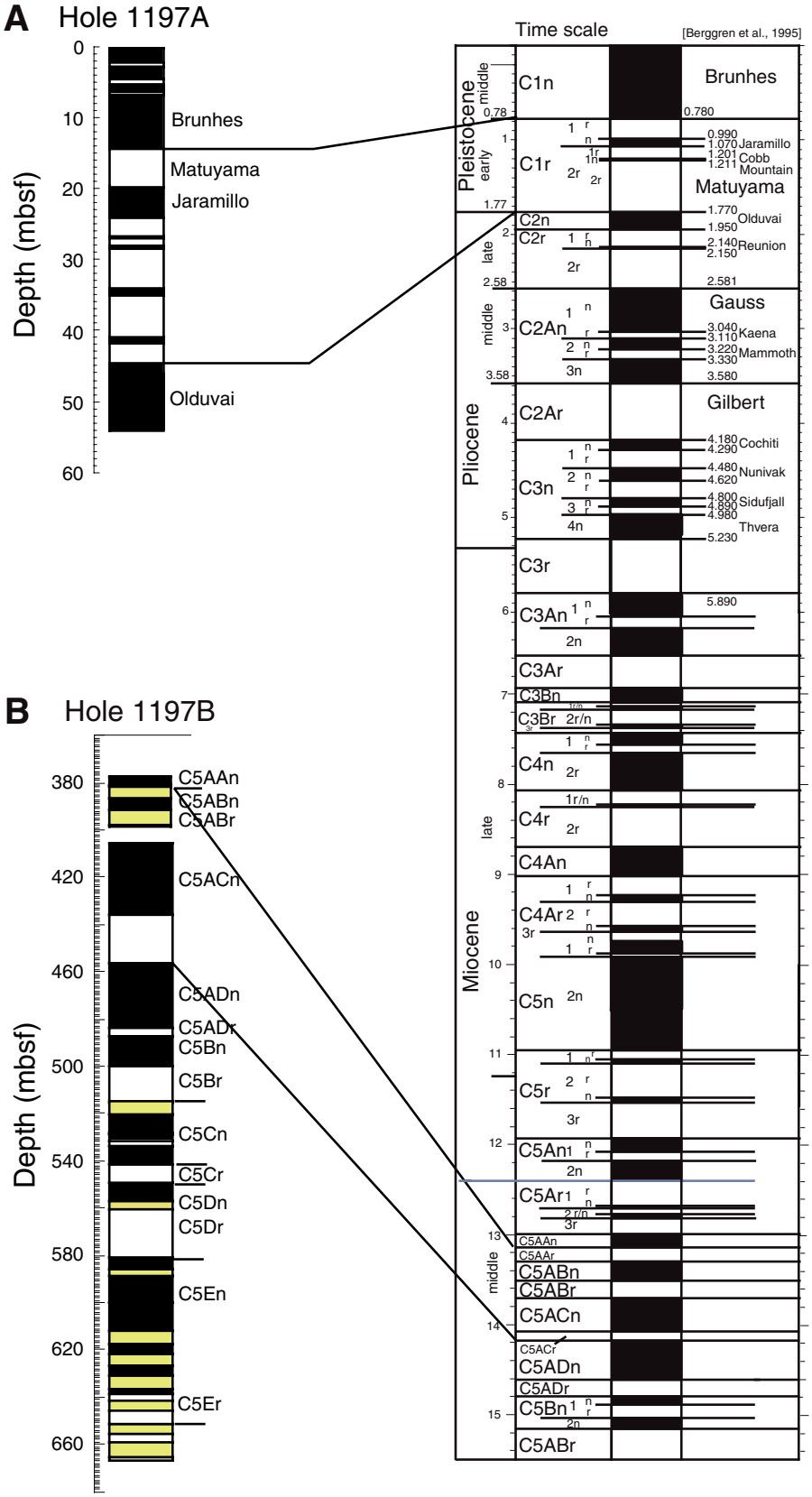

Figure F22. Normalized anhysteretic remanent magnetization (ARM), isothermal remanent magnetization (IRM) acquisition, and IRM demagnetization (demag) curves vs. demagnetizing steps in mT for (**A**) Sample 194-1197A-1H-3, 100–102 cm, (**B**) Sample 194-1197A-2H-6, 100–102 cm, (**C**) Sample 194-1197A-3H-6, 100–102 cm, and (**D**) Sample 194-1197A-5H-3, 100–102 cm.

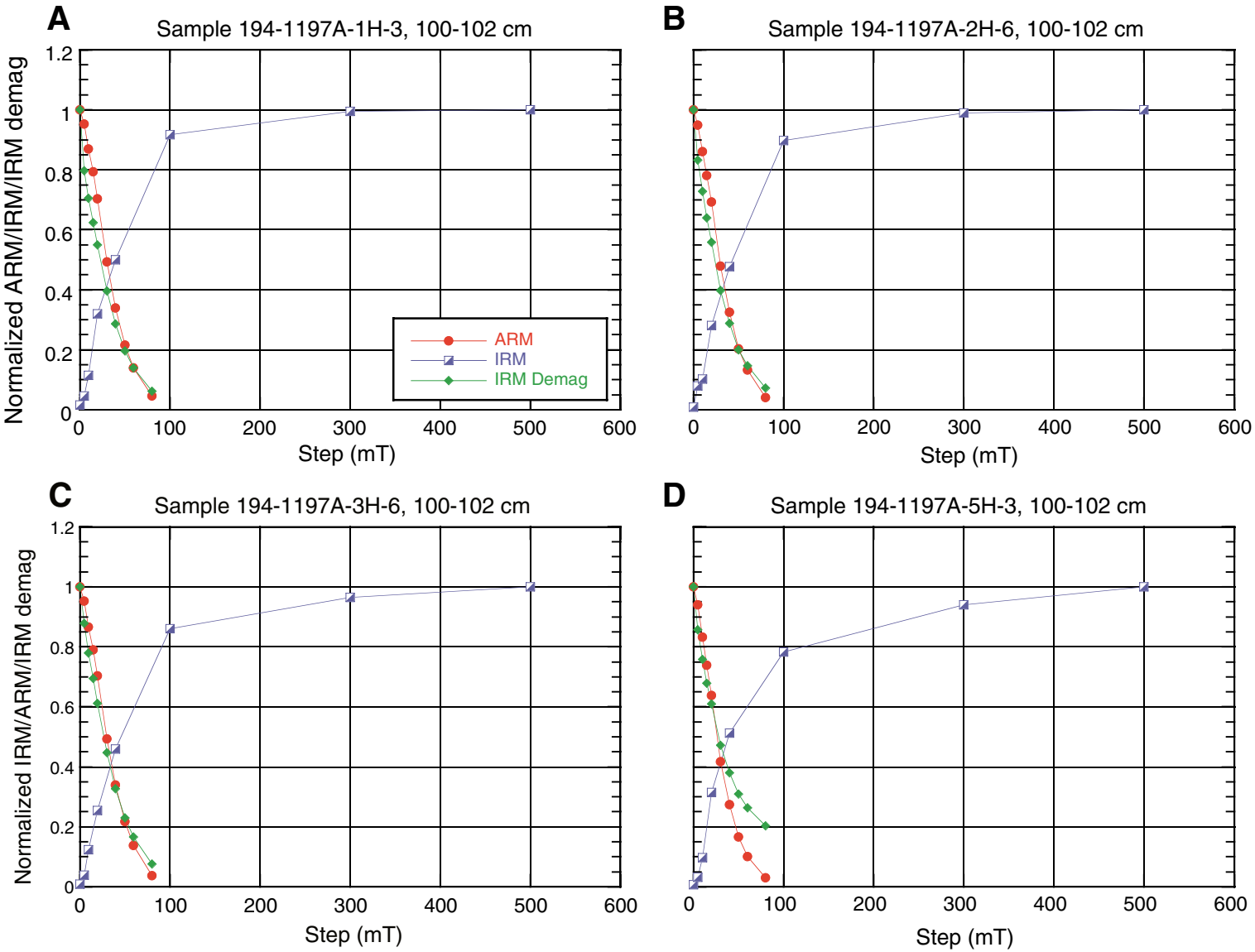

Figure F23. A. Natural remanent magnetization (NRM), anhysteretic remanent magnetization (ARM), and isothermal remanent magnetization (IRM) are plotted down the core. **B.** IRM (.1 T/1 T) ratio vs. depth.

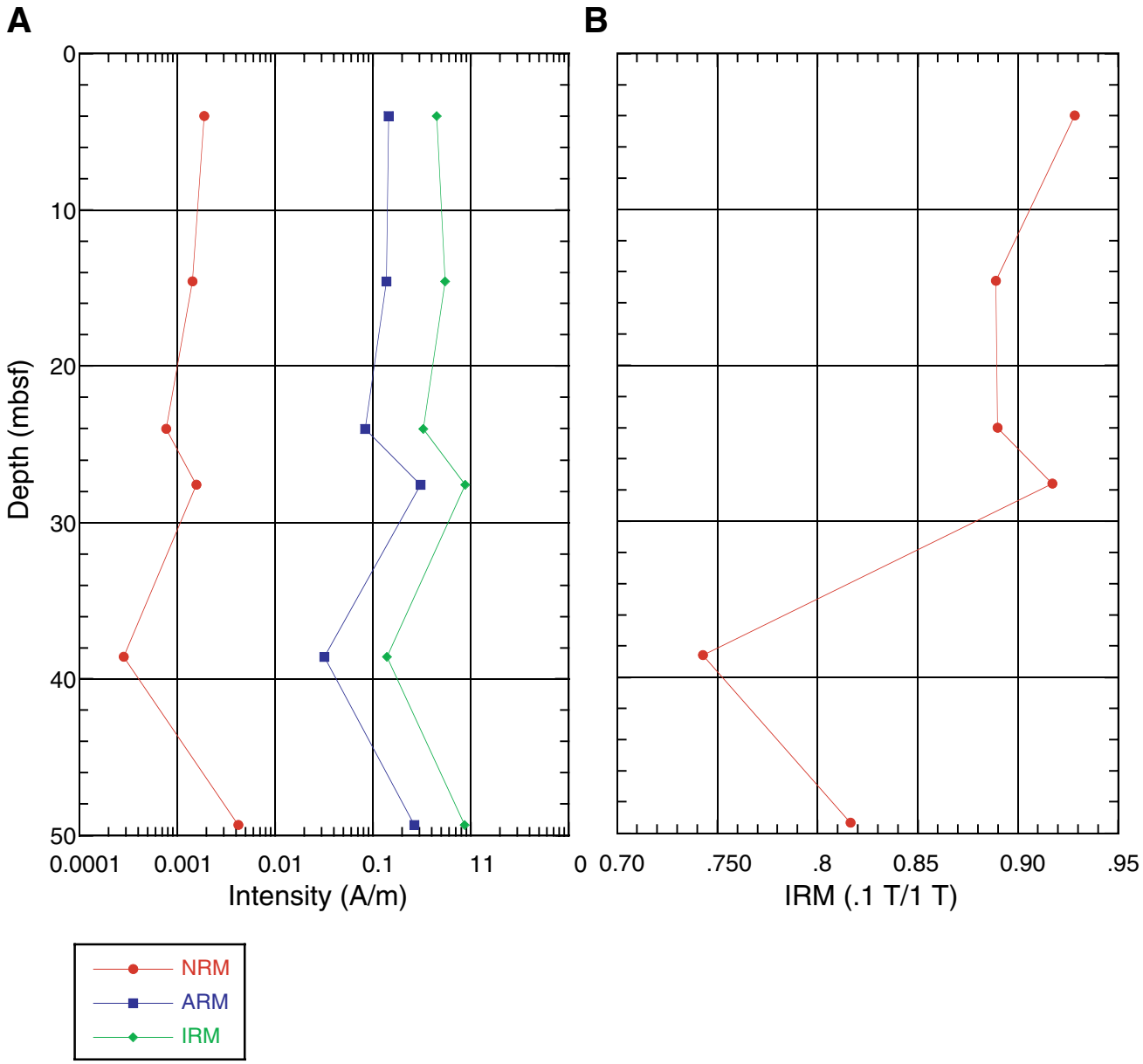

Figure F24. Age-depth model and sedimentation rates at Site 1197. Horizontal lines spanning from the left figure margin to the age-depth curve are lithologic unit (solid) and subunit (dashed) boundaries. Horizontal lines spanning from the right margin of the figure to the age-depth curve are seismic megasequence boundaries (solid) and major reflectors within megasequences (dashed). Vertical lines are epoch boundaries as labeled at the top of the diagram. MS = Megasequence.

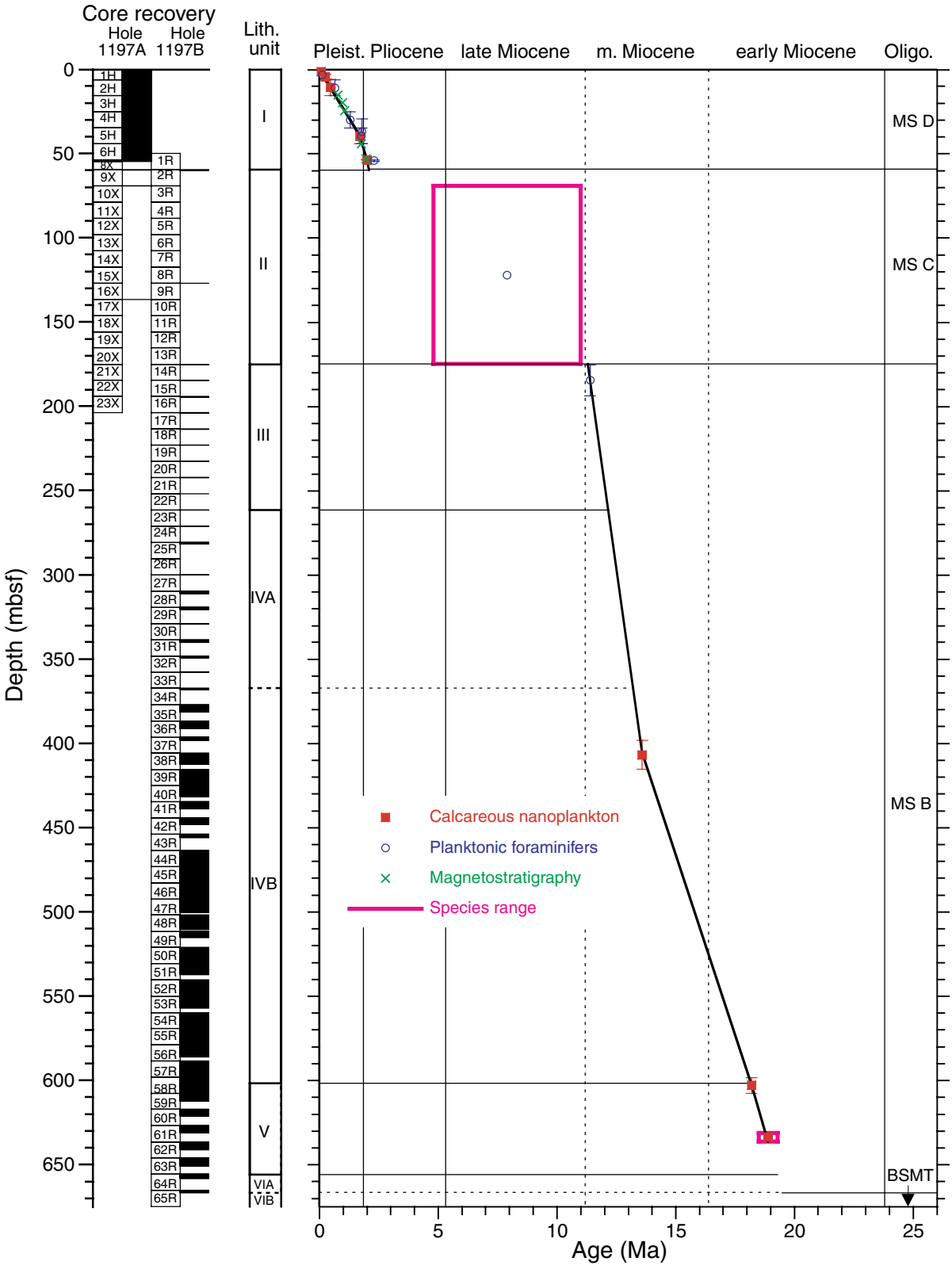

Figure F25. Concentrations of dissolved constituents vs. depth, Site 1197. **A.** Chloride. **B.** Alkalinity. **C.** Sulfate. **D.** Ammonium. **E.** Magnesium. **F.** Calcium. **G.** Strontium. **H.** Potassium. Solid circles = Hole 1197A, open circles = Hole 1197B.

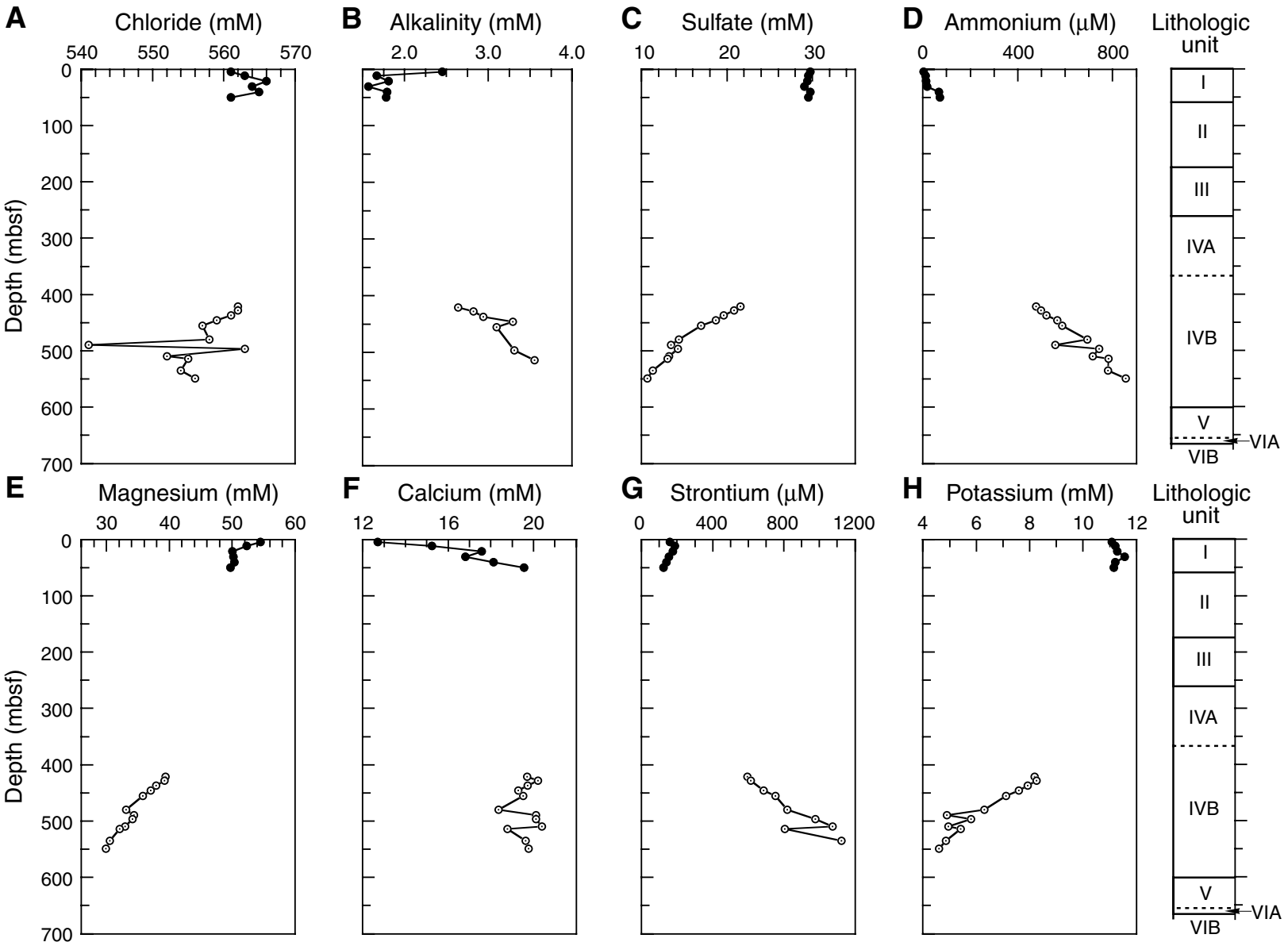

Figure F26. Percentages of carbonate minerals and noncarbonate fraction, Site 1197.

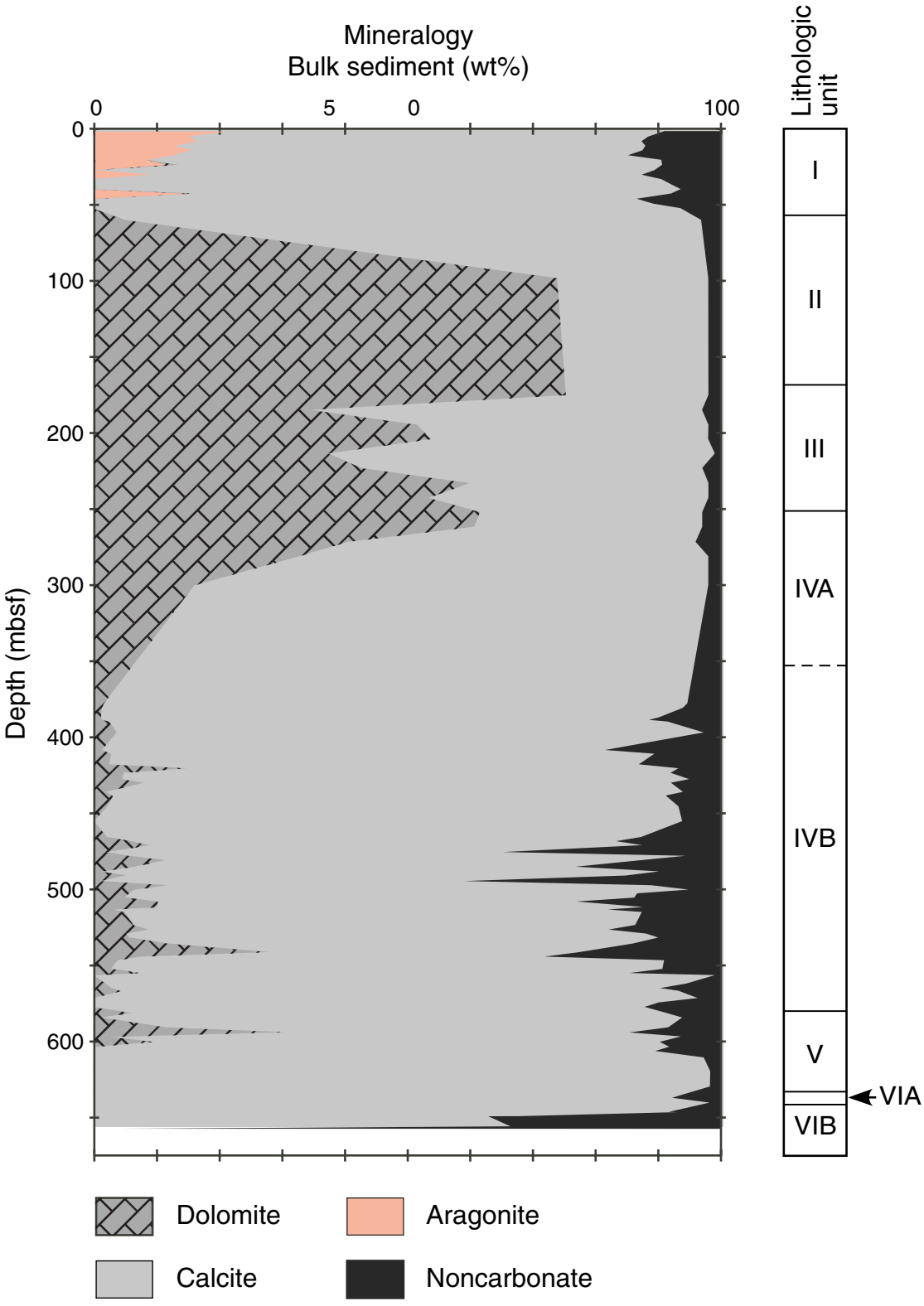

Figure F27. Plots of carbonate and total organic carbon content, hydrogen index values, total sulfur content, and C/N and C/S ratios, Site 1197. The solid vertical lines at HI = 150 and C/S = 2 mark the approximate boundary between terrigenous (<150) and marine organic matter and the transition between marine (<2) and brackish environments of formation, respectively.

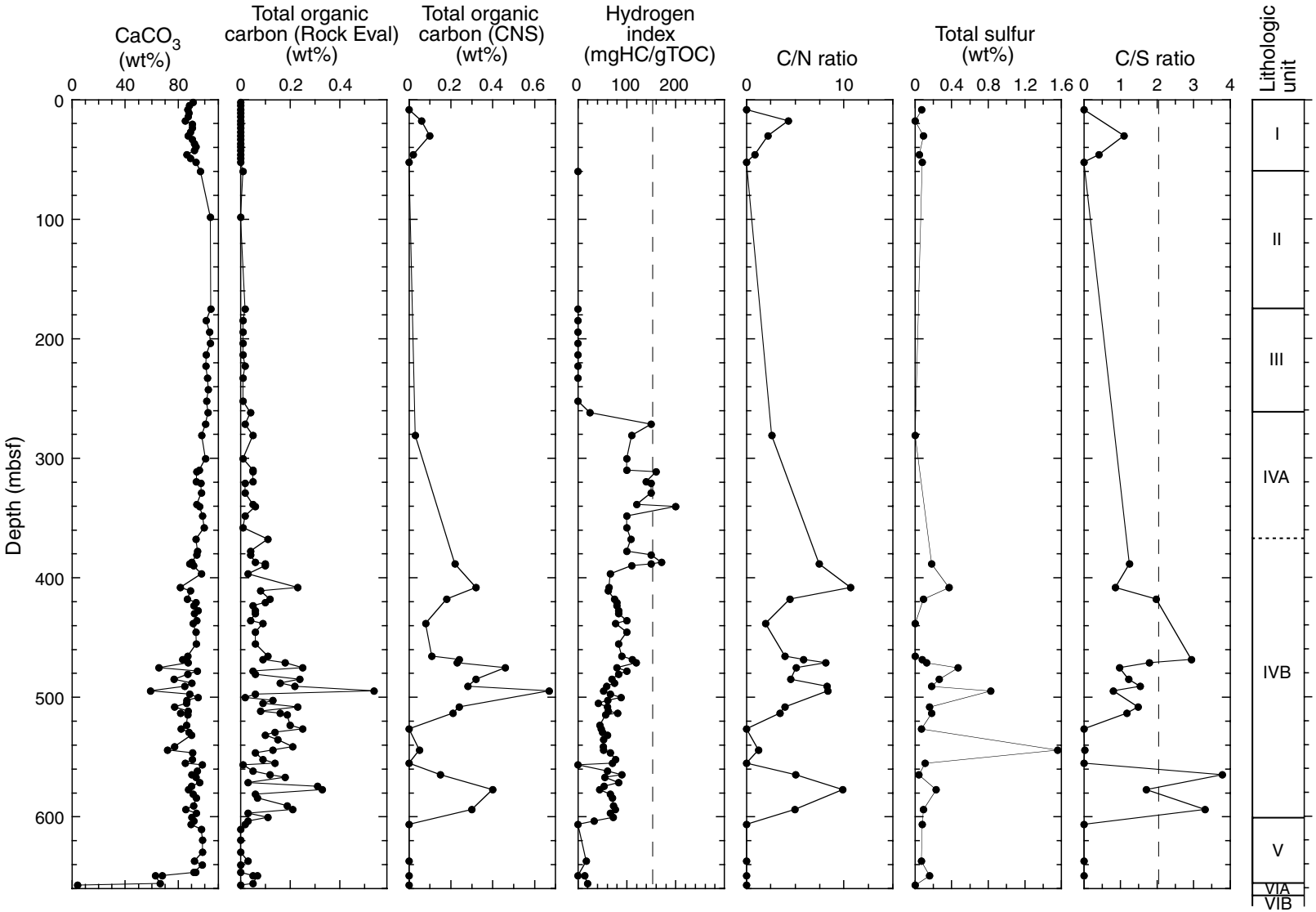

Figure F28. A. Bulk density. Open circles = MAD bulk density for Hole 1197A, squares = MAD bulk density for Hole 1197B, line = GRA bulk density for Hole 1197A, dots = GRA bulk density for Hole 1197B. **B.** Grain density. Solid circles = Hole 1197A, squares = Hole 1197B. **C.** Porosity. Solid circles = Hole 1197A, squares = Hole 1197B. Exponential least-squares regression of porosity using the combined Hole 1197A and Hole 1197B data set (line) is superposed on the porosity values.

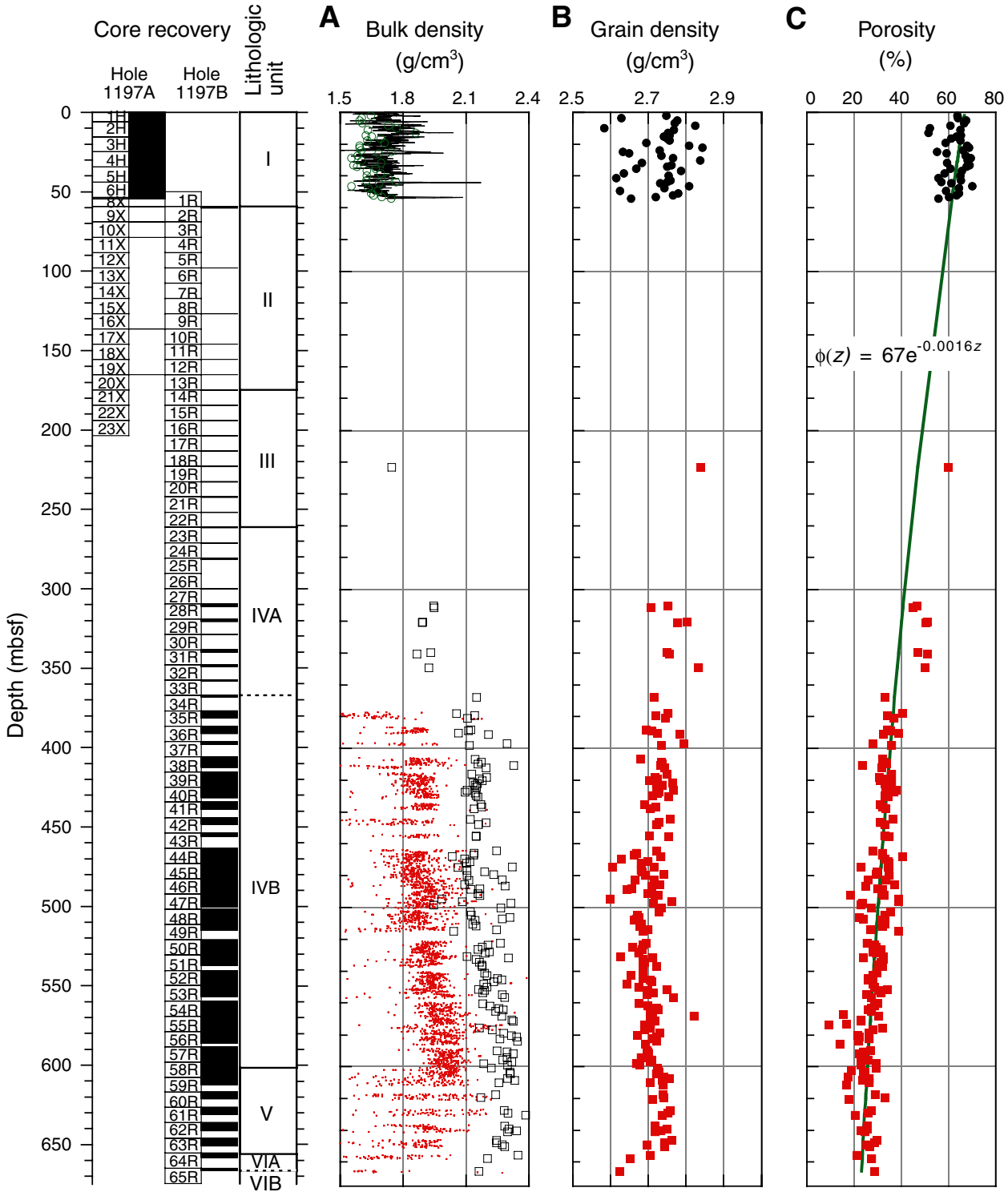

Figure F29. A. *P*-wave velocity as a function of depth at Site 1197 using the PWS3 contact probe system. Solid circles = x-direction, open circles = y-direction, triangles = z-direction. **B.** Seismic anisotropy between the average transverse and longitudinal velocities as a function of depth.

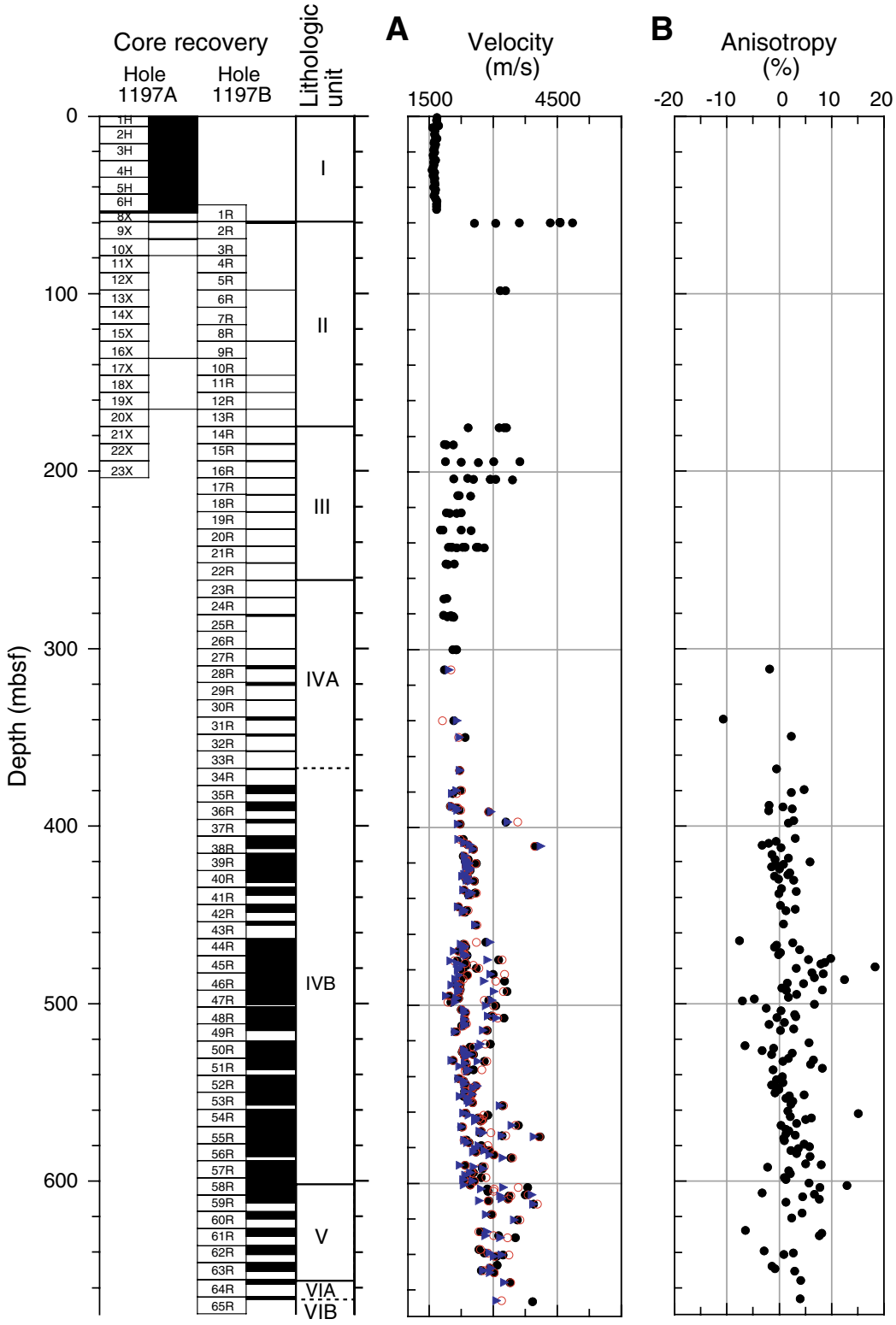

Figure F30. Crossplot of velocity vs. porosity for Site 1197. Dashed and solid lines represent the time-average equations for calcite (Wyllie et al., 1956) and a power law least-squares fit to the velocity data, respectively.

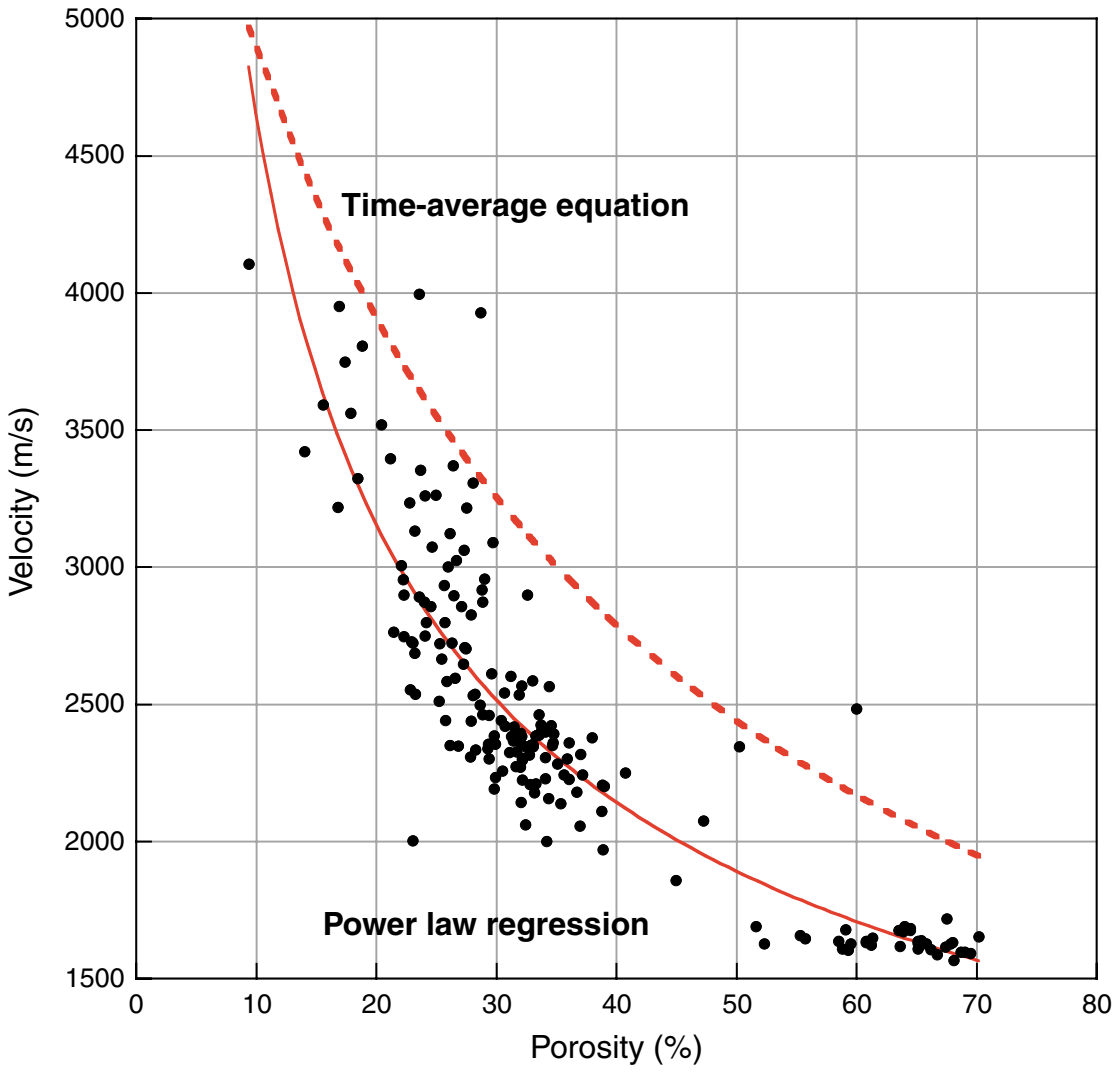

Figure F31. Average thermal conductivity as a function of depth for Site 1197. Circles = Hole 1197A, squares = Hole 1197B.

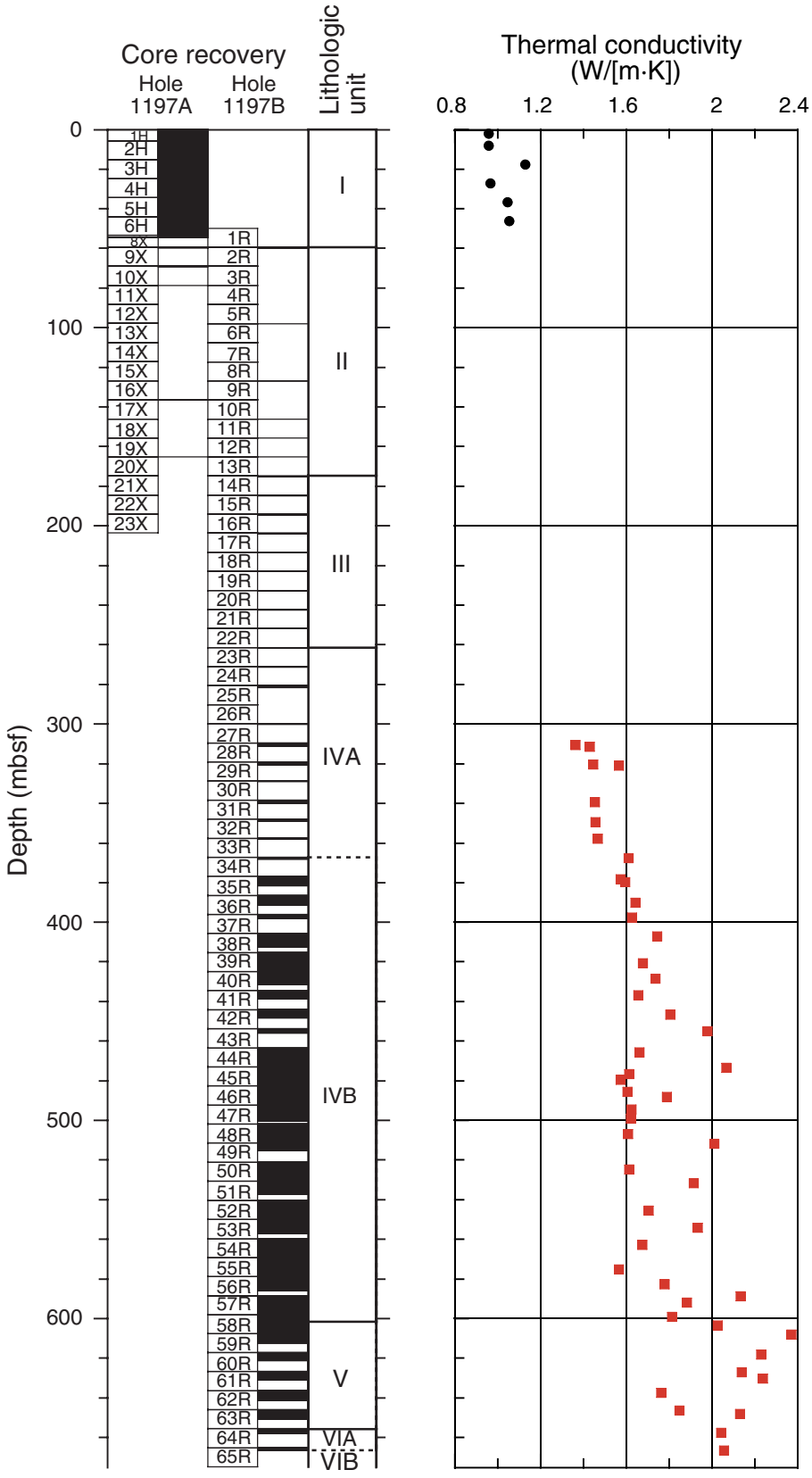

Figure F32. Crossplot of Site 1197 porosity and thermal conductivity. Superimposed are the power law curves, constructed from the observed range in porosity, for ideal end-member sedimentary facies: sandstone (red/upper curve), limestone (blue/center curve), and shale (black/lower curve).

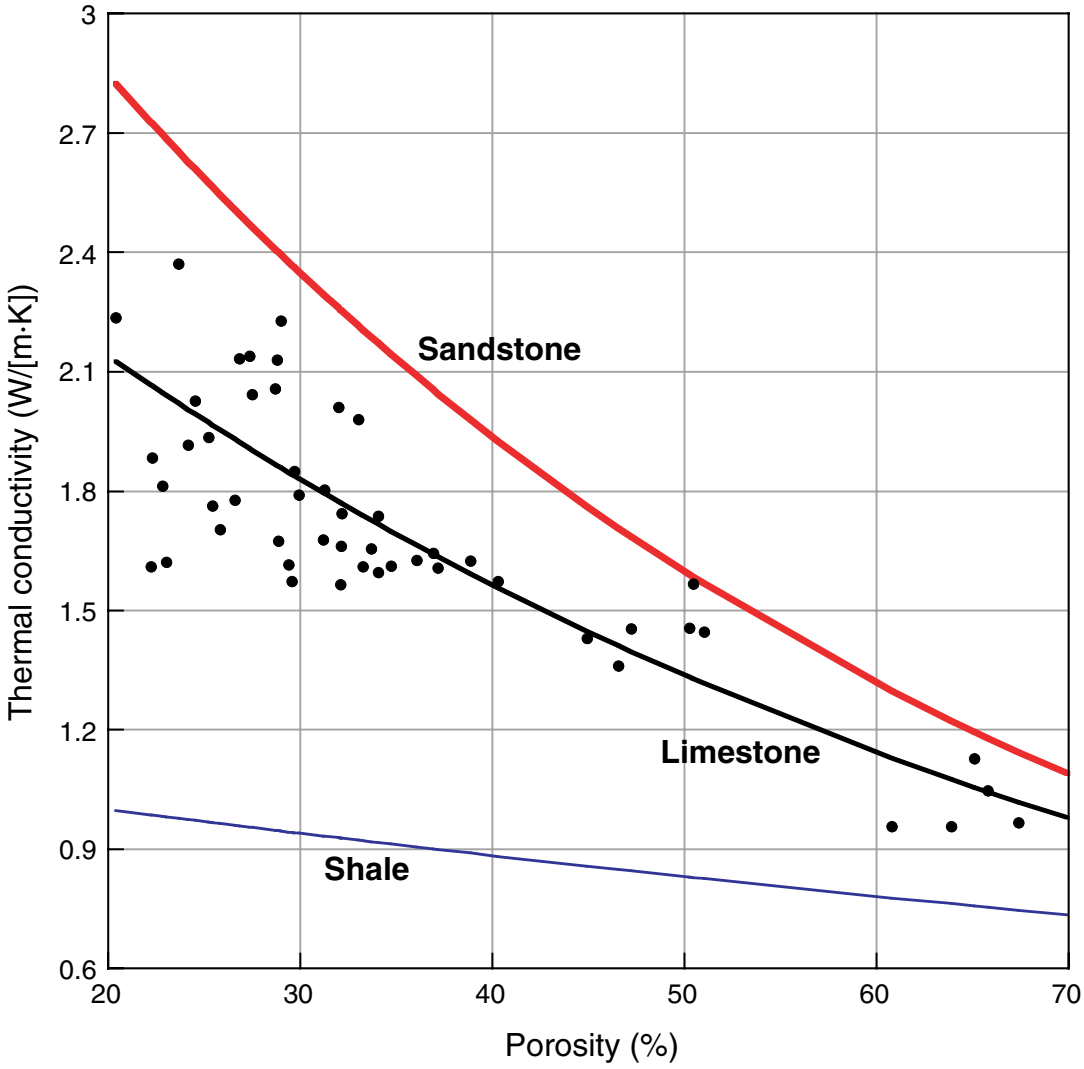

Figure F33. Comparison of (**A**) magnetic susceptibility (MS) (line = Hole 1197A; squares = Hole 1197B), (**B**) natural gamma radiation (NGR) (line = Hole 1197A; dots = Hole 1197B), and (**C**) color reflectance (lightness) for Site 1197.

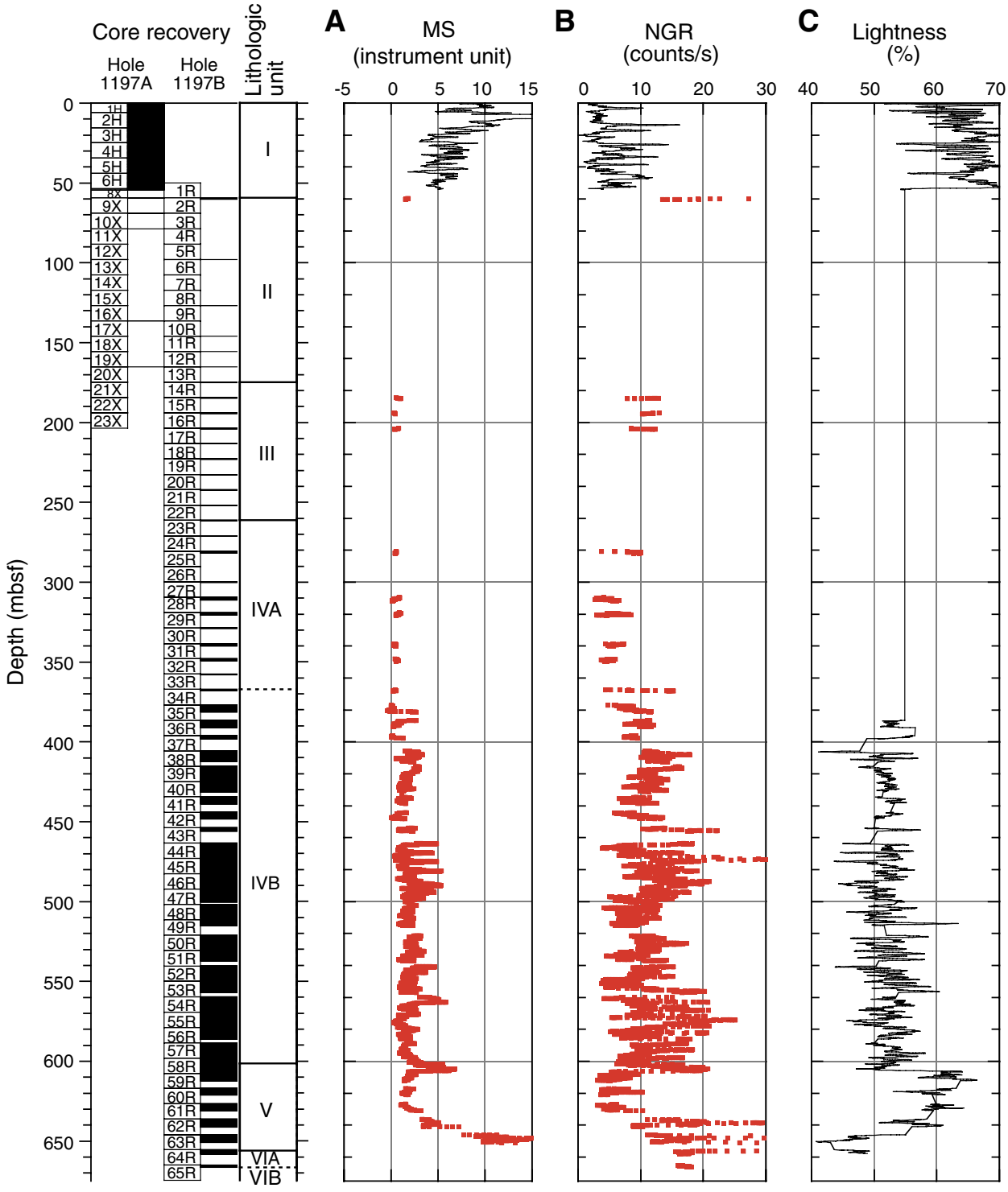

Figure F34. Multichannel line MAR07, with location and penetration depth of Site 1197, located at shotpoint 3721. The seismic sequences and basement are marked and traced along the section.

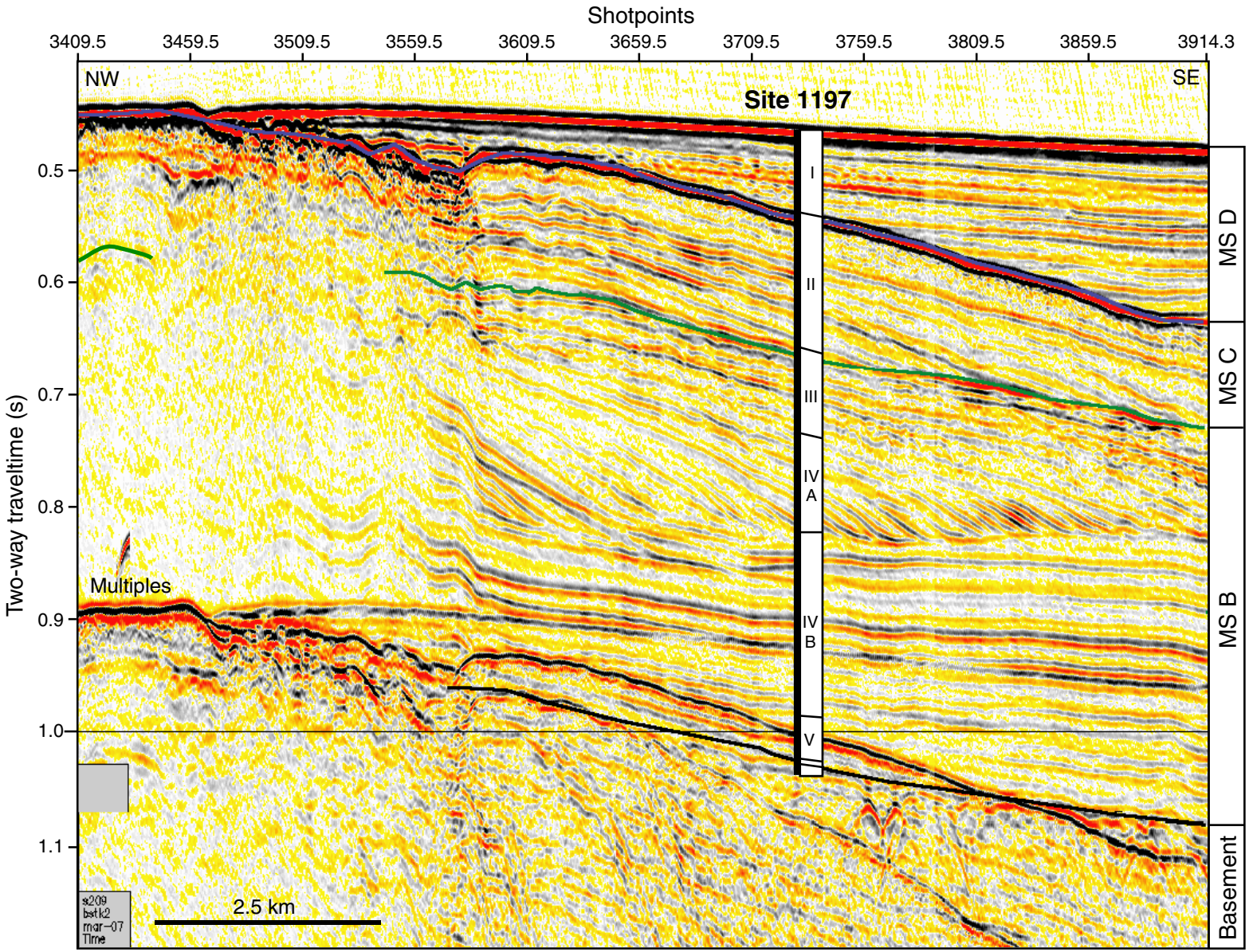

Table T1. Coring summary, Site 1197.

Core	Date (Feb 2001)	Time (local)	Depth (mbsf) Top	Depth (mbsf) Bottom	Length (m) Cored	Length (m) Recovered	Recovery (%)
194-1197A-							
1H	6	1235	0.0	6.1	6.1	6.15	100.8
2H	6	1325	6.1	15.6	9.5	9.53	100.3
3H	6	1405	15.6	25.1	9.5	9.64	101.5
4H	6	1455	25.1	34.6	9.5	9.79	103.1
5H	6	1525	34.6	44.1	9.5	9.62	101.3
6H	6	1550	44.1	53.6	9.5	9.71	102.2
7H	6	1610	53.6	54.6	1.0	1.01	101.0
8X	6	1730	54.6	59.6	5.0	0.00	0.0
9X	6	1925	59.6	69.2	9.6	0.26	2.7
10X	6	2020	69.2	78.8	9.6	0.25	2.6
11X	6	2125	78.8	88.5	9.7	0.05	0.5
12X	6	2230	88.5	98.1	9.6	0.00	0.0
13X	6	2310	98.1	107.7	9.6	0.00	0.0
14X	7	0005	107.7	117.3	9.6	0.00	0.0
15X	7	0050	117.3	127.0	9.7	0.00	0.0
16X	7	0135	127.0	136.6	9.6	0.00	0.0
17X	7	0215	136.6	146.2	9.6	0.10	1.0
18X	7	0305	146.2	155.8	9.6	0.00	0.0
19X	7	0345	155.8	165.4	9.6	0.00	0.0
20X	7	0425	165.4	175.0	9.6	0.05	0.5
21X	7	0515	175.0	184.6	9.6	0.00	0.0
22X	7	0615	184.6	194.2	9.6	0.00	0.0
23X	7	0725	194.2	203.8	9.6	0.00	0.0
				Cored total:	203.8	56.16	27.5
				Drilled total:	0.0		
				Total:	203.8		
194-1197B-							
10	13	2205	0.0	50.0	0.0	0.00	NA
1R	13	2250	50.0	59.6	9.6	0.00	0.0
2R	13	2350	59.6	69.2	9.6	0.78	8.1
3R	14	0040	69.2	78.8	9.6	0.03	0.3
4R	14	0120	78.8	88.5	9.7	0.00	0.0
5R	14	0220	88.5	98.2	9.7	0.01	0.1
6R	14	0300	98.2	107.8	9.6	0.06	0.6
7R	14	0350	107.8	117.4	9.6	0.00	0.0
8R	14	0425	117.4	127.0	9.6	0.02	0.2
9R	14	0500	127.0	136.6	9.6	0.10	1.0
10R	14	0550	136.6	146.2	9.6	0.00	0.0
11R	14	0625	146.2	155.8	9.6	0.05	0.5
12R	14	0700	155.8	165.4	9.6	0.05	0.5
13R	14	0725	165.4	175.0	9.6	0.05	0.5
14R	14	1055	175.0	184.6	9.6	0.30	3.1
15R	14	1140	184.6	194.2	9.6	0.45	4.7
16R	14	1215	194.2	203.8	9.6	0.50	5.2
17R	14	1250	203.8	213.4	9.6	0.42	4.4
18R	14	1340	213.4	223.0	9.6	0.23	2.4
19R	14	1415	223.0	232.7	9.7	0.29	3.0
20R	14	1505	232.7	242.3	9.6	0.25	2.6
21R	14	1540	242.3	251.9	9.6	0.30	3.1
22R	14	1625	251.9	261.5	9.6	0.16	1.7
23R	14	1705	261.5	271.2	9.7	0.25	2.6
24R	14	1745	271.2	280.8	9.6	0.26	2.7
25R	14	1840	280.8	290.4	9.6	1.03	10.7
26R	14	1940	290.4	300.0	9.6	0.00	0.0
27R	14	2025	300.0	309.7	9.7	0.30	3.1
28R	14	2125	309.7	319.3	9.6	1.62	16.9
29R	14	2220	319.3	328.9	9.6	1.46	15.2
30R	14	2315	328.9	338.6	9.7	0.31	3.2
31R	14	2355	338.6	348.2	9.6	1.67	17.4
32R	15	0425	348.2	357.8	9.6	1.10	11.5
33R	15	0520	357.8	367.4	9.6	0.44	4.6
34R	15	0630	367.4	377.1	9.7	0.88	9.1
35R	15	0725	377.1	386.7	9.6	4.59	47.8
36R	15	0815	386.7	396.3	9.6	4.74	49.4
37R	15	0930	396.3	405.9	9.6	2.00	20.8
38R	15	1045	405.9	415.5	9.6	6.79	70.7
39R	15	1205	415.5	425.1	9.6	9.03	94.1
40R	15	1320	425.1	434.6	9.5	6.62	69.7
41R	15	1430	434.6	444.3	9.7	4.40	45.4
42R	15	1710	444.3	453.9	9.6	4.24	44.2
43R	15	1840	453.9	463.6	9.7	2.30	23.7
44R	15	2005	463.6	473.2	9.6	9.35	97.4
45R	15	2105	473.2	482.8	9.6	9.43	98.2
46R	15	2230	482.8	492.4	9.6	9.73	101.4
47R	15	2355	492.4	502.0	9.6	8.17	85.1
48R	16	0115	502.0	511.6	9.6	8.66	90.2
49R	16	0235	511.6	521.2	9.6	3.71	38.6
50R	16	0420	521.2	530.8	9.6	9.88	102.9
51R	16	0545	530.8	540.5	9.7	6.56	67.6
52R	16	0710	540.5	550.1	9.6	9.92	103.3
53R	16	0840	550.1	559.8	9.7	7.17	73.9
54R	16	1020	559.8	569.4	9.6	9.59	99.9
55R	16	1710	569.4	579.0	9.6	9.95	103.6
56R	16	1945	579.0	588.6	9.6	7.32	76.3
57R	16	2205	588.6	598.2	9.6	9.83	102.4
58R	17	0005	598.2	607.9	9.7	9.17	94.5
59R	17	0115	607.9	617.2	9.3	4.60	49.5
60R	17	0235	617.2	626.8	9.6	4.15	43.2
61R	17	0350	626.8	636.5	9.7	4.36	44.9
62R	17	0515	636.5	646.1	9.6	4.98	51.9
63R	17	0635	646.1	655.7	9.6	4.96	51.7
64R	17	0805	655.7	665.3	9.6	2.64	27.5
65R	17	0920	665.3	674.9	9.6	1.43	14.9
				Cored total:	624.9	213.64	34.2
				Drilled total:	50.0		
				Total:	674.9		

Note: NA = not applicable.

Table T2. Expanded coring summary, Site 1197. (**See table notes.** Continued on next six pages.)

Core	Date (Feb 2001)	Time (local)	Core depth (mbsf) Top	Core depth (mbsf) Bottom	Length (m) Cored	Length (m) Recovered	Recovery (%)	Section	Length (m) Liner	Length (m) Curated	Section depth (mbsf) Top	Section depth (mbsf) Bottom	Catwalk samples	Comment
194-1197A-														
1H	6	1235	0.0	6.1	6.1	6.15	100.8							
								1	1.50	1.50	0.00	1.50		
								2	1.50	1.50	1.50	3.00	PAL	
								3	1.50	1.50	3.00	4.50	IW	
								4	1.45	1.45	4.50	5.95	HS	
								CC (w/CC)	0.20	0.20	5.95	6.15	PAL	
								Totals:	6.15	6.15				
2H	6	1325	6.1	15.6	9.5	9.53	100.3							
								1	1.50	1.50	6.10	7.60		
								2	1.50	1.50	7.60	9.10		
								3	1.50	1.50	9.10	10.60		
								4	1.50	1.50	10.60	12.10	IW	
								5	1.50	1.50	12.10	13.60	HS	
								6	1.50	1.50	13.60	15.10		
								7	0.40	0.40	15.10	15.50		
								CC (w/7)	0.13	0.13	15.50	15.63	PAL	
								Totals:	9.53	9.53				
3H	6	1405	15.6	25.1	9.5	9.64	101.5							
								1	1.50	1.50	15.60	17.10		
								2	1.50	1.50	17.10	18.60		
								3	1.50	1.50	18.60	20.10		
								4	1.50	1.50	20.10	21.60	IW	
								5	1.50	1.50	21.60	23.10	HS	
								6	1.50	1.50	23.10	24.60		
								7	0.44	0.44	24.60	25.04		
								CC (w/CC)	0.20	0.20	25.04	25.24	PAL	
								Totals:	9.64	9.64				
4H	6	1455	25.1	34.6	9.5	9.79	103.1							
								1	1.50	1.50	25.10	26.60		
								2	1.50	1.50	26.60	28.10		
								3	1.50	1.50	28.10	29.60	PAL	
								4	1.50	1.50	29.60	31.10	IW	
								5	1.50	1.50	31.10	32.60	HS	
								6	1.50	1.50	32.60	34.10		
								7	0.64	0.64	34.10	34.74		
								CC (w/7)	0.15	0.15	34.74	34.89	PAL	
								Totals:	9.79	9.79				
5H	6	1525	34.6	44.1	9.5	9.62	101.3							
								1	1.50	1.50	34.60	36.10		
								2	1.50	1.50	36.10	37.60		
								3	1.50	1.50	37.60	39.10		
								4	1.50	1.50	39.10	40.60	IW	
								5	1.50	1.50	40.60	42.10	HS	
								6	1.50	1.50	42.10	43.60		
								7	0.44	0.44	43.60	44.04		
								CC (w/7)	0.18	0.18	44.04	44.22	PAL	
								Totals:	9.62	9.62				
6H	6	1550	44.1	53.6	9.5	9.71	102.2							
								1	1.50	1.50	44.10	45.60		
								2	1.50	1.50	45.60	47.10		
								3	1.50	1.50	47.10	48.60		
								4	1.50	1.50	48.60	50.10	IW	
								5	1.50	1.50	50.10	51.60	HS	
								6	1.50	1.50	51.60	53.10		
								7	0.51	0.51	53.10	53.61		
								CC (w/7)	0.20	0.20	53.61	53.81	PAL	
								Totals:	9.71	9.71				
7H	6	1610	53.6	54.6	1.0	1.01	101.0							
								1	0.84	0.84	53.60	54.44	PAL	
								CC (w/1)	0.17	0.17	54.44	54.61	PAL	
								Totals:	1.01	1.01				
8X	6	1730	54.6	59.6	5.0	0.00	0.0							
9X	6	1925	59.6	69.2	9.6	0.26	2.7							
								1	0.26	0.34	59.60	59.94	PAL	
								Totals:	0.26	0.34				
10X	6	2020	69.2	78.8	9.6	0.25	2.6							
								CC (w/CC)	0.25	0.25	69.20	69.45	PAL	
								Totals:	0.25	0.25				

Table T2 (continued).

Core	Date (Feb 2001)	Time (local)	Core depth (mbsf) Top	Core depth (mbsf) Bottom	Length (m) Cored	Length (m) Recovered	Recovery (%)	Section	Length (m) Liner	Length (m) Curated	Section depth (mbsf) Top	Section depth (mbsf) Bottom	Catwalk samples	Comment
11X	6	2125	78.8	88.5	9.7	0.05	0.5							
								CC (w/CC)	0.05	0.05	78.80	78.85		All to PAL
								Totals:	0.05	0.05				
12X	6	2230	88.5	98.1	9.6	0.00	0.0							
13X	6	2310	98.1	107.7	9.6	0.00	0.0							
14X	7	0005	107.7	117.3	9.6	0.00	0.0							
15X	7	0050	117.3	127.0	9.7	0.00	0.0							
16X	7	0135	127.0	136.6	9.6	0.00	0.0							
17X	7	0215	136.6	146.2	9.6	0.10	1.0							
								1	0.10	0.12	136.60	136.72		
								Totals:	0.10	0.12				
18X	7	0305	146.2	155.8	9.6	0.00	0.0							
19X	7	0345	155.8	165.4	9.6	0.00	0.0							
20X	7	0425	165.4	175.0	9.6	0.05	0.5							
								CC (w/CC)	0.05	0.05	165.40	165.45	PAL	
								Totals:	0.05	0.05				
21X	7	0515	175.0	184.6	9.6	0.00	0.0							
22X	7	0615	184.6	194.2	9.6	0.00	0.0							
23X	7	0725	194.2	203.8	9.6	0.00	0.0							
								1	0.00	0.00				
								Totals:	0.00	0.00				
				Totals:	203.8	56.16	27.6							
194-1197B-														
10	13	2205	0.0	50.0	0.0	0.00	NA							
1R	13	2250	50.0	59.6	9.6	0.00	0.0							
2R	13	2350	59.6	69.2	9.6	0.78	8.1							
								1	0.78	0.86	59.60	60.46	PAL	
								Totals:	0.78	0.86				
3R	14	0040	69.2	78.8	9.6	0.03	0.3							
								1	0.03	0.03	69.20	69.23	PAL	All to PAL
								Totals:	0.03	0.03				
4R	14	0120	78.8	88.5	9.7	0.00	0.0							
5R	14	0220	88.5	98.2	9.7	0.01	0.1							
								1	0.01	0.01	88.50	88.51	PAL	All to PAL
								Totals:	0.01	0.01				
6R	14	0300	98.2	107.8	9.6	0.06	0.6							
								1	0.06	0.08	98.20	98.28	PAL	
								Totals:	0.06	0.08				
7R	14	0350	107.8	117.4	9.6	0.00	0.0							
8R	14	0425	117.4	127.0	9.6	0.02	0.2							
								1	0.02	0.02	117.40	117.42	PAL	All to PAL
								Totals:	0.02	0.02				
9R	14	0500	127.0	136.6	9.6	0.10	1.0							
								1	0.10	0.10	127.00	127.10	PAL	
								Totals:	0.10	0.10				
10R	14	0550	136.6	146.2	9.6	0.00	0.0							
11R	14	0625	146.2	155.8	9.6	0.05	0.5							
								1	0.05	0.05	146.20	146.25	PAL	All to PAL
								Totals:	0.05	0.05				
12R	14	0700	155.8	165.4	9.6	0.05	0.5							
								1	0.05	0.05	155.80	155.85	PAL	All to PAL
								Totals:	0.05	0.05				
13R	14	0725	165.4	175.0	9.6	0.05	0.5							
								1	0.05	0.05	165.40	165.45	PAL	All to PAL
								Totals:	0.05	0.05				
14R	14	1055	175.0	184.6	9.6	0.30	3.1							
								1	0.30	0.42	175.00	175.42	PAL, PAL, PAL	
								Totals:	0.30	0.42				
15R	14	1140	184.6	194.2	9.6	0.45	4.7							
								1	0.45	0.52	184.60	185.12	PAL, PAL, PAL, PAL	
								Totals:	0.45	0.52				
16R	14	1215	194.2	203.8	9.6	0.50	5.2							
								1	0.50	0.58	194.20	194.78	PAL	
								Totals:	0.50	0.58				
17R	14	1250	203.8	213.4	9.6	0.42	4.4							
								1	0.42	0.66	203.80	204.46	PAL	
								Totals:	0.42	0.66				

Table T2 (continued).

Core	Date (Feb 2001)	Time (local)	Core depth (mbsf) Top	Core depth (mbsf) Bottom	Length (m) Cored	Length (m) Recovered	Recovery (%)	Section	Length (m) Liner	Length (m) Curated	Section depth (mbsf) Top	Section depth (mbsf) Bottom	Catwalk samples	Comment
18R	14	1340	213.4	223.0	9.6	0.23	2.4							
								1	0.23	0.30	213.40	213.70	PAL	
								Totals:	0.23	0.30				
19R	14	1415	223.0	232.7	9.7	0.29	3.0							
								1	0.29	0.38	223.00	223.38	PAL	
								Totals:	0.29	0.38				
20R	14	1505	232.7	242.3	9.6	0.25	2.6							
								1	0.25	0.34	232.70	233.04	PAL	
								Totals:	0.25	0.34				
21R	14	1540	242.3	251.9	9.6	0.30	3.1							
								1	0.30	0.49	242.30	242.79	PAL	
								Totals:	0.30	0.49				
22R	14	1625	251.9	261.5	9.6	0.16	1.7							
								1	0.16	0.24	251.90	252.14	PAL	
								Totals:	0.16	0.24				
23R	14	1705	261.5	271.2	9.7	0.25	2.6							
								1	0.25	0.46	261.50	261.96	PAL	
								Totals:	0.25	0.46				
24R	14	1745	271.2	280.8	9.6	0.26	2.7							
								1	0.26	0.36	271.20	271.56	PAL	
								Totals:	0.26	0.36				
25R	14	1840	280.8	290.4	9.6	1.03	10.7							
								1	1.03	1.22	280.80	282.02	PAL	
								Totals:	1.03	1.22				
26R	14	1940	290.4	300.0	9.6	0.00	0.0							
27R	14	2025	300.0	309.7	9.7	0.30	3.1							
								1	0.30	0.37	300.00	300.37	PAL	
								Totals:	0.30	0.37				
28R	14	2125	309.7	319.3	9.6	1.62	16.9							
								1	1.41	1.50	309.70	311.20		
								2	0.21	0.53	311.20	311.73	PAL	
								Totals:	1.62	2.03				
29R	14	2220	319.3	328.9	9.6	1.46	15.2							
								1	0.00	1.50	319.30	320.80		
								2	1.46	0.38	320.80	321.18	PAL	
								Totals:	1.46	1.88				
30R	14	2315	328.9	338.6	9.7	0.31	3.2							
								1	0.31	0.33	328.90	329.23	PAL	
								Totals:	0.31	0.33				
31R	14	2355	338.6	348.2	9.6	1.67	17.4							
								1	1.50	1.46	338.60	340.06		
								2	0.17	0.57	340.06	340.63	PAL	
								Totals:	1.67	2.03				
32R	15	0425	348.2	357.8	9.6	1.10	11.5							
								1	1.10	1.31	348.20	349.51	PAL	
								Totals:	1.10	1.31				
33R	15	0520	357.8	367.4	9.6	0.44	4.6							
								1	0.44	0.55	357.80	358.35	PAL	
								Totals:	0.44	0.55				
34R	15	0630	367.4	377.1	9.7	0.88	9.1							
								1	0.88	0.98	367.40	368.38	PAL	
								Totals:	0.88	0.98				
35R	15	0725	377.1	386.7	9.6	4.59	47.8							
								1	1.52	1.52	377.10	378.62		
								2	1.44	1.44	378.62	380.06		
								3	1.51	1.51	380.06	381.57	PAL	
								CC (w/CC)	0.12	0.12	381.57	381.69	PAL	
								Totals:	4.59	4.59				
36R	15	0815	386.7	396.3	9.6	4.74	49.4							
								1	1.50	1.50	386.70	388.20		
								2	1.21	1.21	388.20	389.41		
								3	1.30	1.30	389.41	390.71		
								4	0.59	0.59	390.71	391.30		
								CC (w/4)	0.14	0.14	391.30	391.44	PAL	
								Totals:	4.74	4.74				
37R	15	0930	396.3	405.9	9.6	2.00	20.8							
								1	1.47	1.47	396.30	397.77		
								2	0.53	0.53	397.77	398.30	PAL	
								Totals:	2.00	2.00				

Table T2 (continued).

Core	Date (Feb 2001)	Time (local)	Core depth (mbsf) Top	Core depth (mbsf) Bottom	Length (m) Cored	Length (m) Recovered	Recovery (%)	Section	Length (m) Liner	Length (m) Curated	Section depth (mbsf) Top	Section depth (mbsf) Bottom	Catwalk samples	Comment
38R	15	1045	405.9	415.5	9.6	6.79	70.7							
								1	1.50	1.50	405.90	407.40		
								2	1.34	1.34	407.40	408.74		
								3	1.18	1.18	408.74	409.92		
								4	1.45	1.45	409.92	411.37		
								5	1.32	1.32	411.37	412.69	PAL	
								Totals:	6.79	6.79				
39R	15	1205	415.5	425.1	9.6	9.03	94.1							
								1	1.43	1.43	415.50	416.93		
								2	1.21	1.21	416.93	418.14		
								3	1.47	1.47	418.14	419.61		
								4	1.40	1.40	419.61	421.01	IW	
								5	1.45	1.45	421.01	422.46	HS	
								6	1.25	1.25	422.46	423.71		
								7	0.57	0.57	423.71	424.28		
								CC (w/7)	0.25	0.25	424.28	424.53	PAL	
								Totals:	9.03	9.03				
40R	15	1320	425.1	434.6	9.5	6.62	69.7							
								1	1.44	1.44	425.10	426.54		
								2	1.40	1.40	426.54	427.94	IW	
								3	0.98	0.98	427.94	428.92	HS	
								4	1.23	1.23	428.92	430.15		
								5	1.20	1.20	430.15	431.35		
								CC (w/CC)	0.37	0.37	431.35	431.72	PAL	
								Totals:	6.62	6.62				
41R	15	1430	434.6	444.3	9.7	4.40	45.4							
								1	1.38	1.38	434.60	435.98		
								2	1.40	1.40	435.98	437.38	IW, IW	
								3	1.45	1.45	437.38	438.83	HS, HS	
								CC (w/CC)	0.17	0.17	438.83	439.00	PAL	
								Totals:	4.40	4.40				
42R	15	1710	444.3	453.9	9.6	4.24	44.2							
								1	1.50	1.50	444.30	445.80	IW	
								2	1.48	1.48	445.80	447.28	HS	
								3	0.98	0.98	447.28	448.26		
								CC (w/3)	0.28	0.28	448.26	448.54	PAL	
								Totals:	4.24	4.24				
43R	15	1840	453.9	463.6	9.7	2.30	23.7							
								1	1.44	1.44	453.90	455.34	IW	
								2	0.70	0.70	455.34	456.04	HS	
								CC (w/2)	0.16	0.16	456.04	456.20	PAL	
								Totals:	2.30	2.30				
44R	15	2005	463.6	473.2	9.6	9.35	97.4							
								1	1.10	1.10	463.60	464.70		
								2	1.22	1.22	464.70	465.92		
								3	1.42	1.42	465.92	467.34		
								4	1.50	1.50	467.34	468.84		
								5	1.50	1.50	468.84	470.34		
								6	1.10	1.10	470.34	471.44	IW	
								7	1.11	1.11	471.44	472.55	HS	
								CC (w/CC)	0.40	0.40	472.55	472.95	PAL	
								Totals:	9.35	9.35				
45R	15	2105	473.2	482.8	9.6	9.43	98.2							
								1	1.38	1.38	473.20	474.58		
								2	0.93	0.93	474.58	475.51		
								3	1.50	1.50	475.51	477.01		
								4	1.50	1.50	477.01	478.51		
								5	1.43	1.43	478.51	479.94	IW	
								6	1.50	1.50	479.94	481.44	HS	
								7	1.19	1.19	481.44	482.63	PAL	
								Totals:	9.43	9.43				
46R	15	2230	482.8	492.4	9.6	9.73	101.4							
								1	1.50	1.50	482.80	484.30		
								2	1.29	1.29	484.30	485.59		
								3	1.50	1.50	485.59	487.09		
								4	1.50	1.50	487.09	488.59		
								5	1.50	1.50	488.59	490.09	IW	
								6	1.32	1.32	490.09	491.41	HS	

Table T2 (continued).

Core	Date (Feb 2001)	Time (local)	Core depth (mbsf) Top	Core depth (mbsf) Bottom	Length (m) Cored	Length (m) Recovered	Recovery (%)	Section	Length (m) Liner	Length (m) Curated	Section depth (mbsf) Top	Section depth (mbsf) Bottom	Catwalk samples	Comment
								7	0.88	0.88	491.41	492.29		
								CC (w/7)	0.24	0.24	492.29	492.53	PAL	
								Totals:	9.73	9.73				
47R	15	2355	492.4	502.0	9.6	8.17	85.1							
								1	1.50	1.50	492.40	493.90		
								2	1.11	1.11	493.90	495.01		
								3	1.42	1.42	495.01	496.43	IW	
								4	1.50	1.50	496.43	497.93	HS	
								5	1.48	1.48	497.93	499.41		
								6	1.16	1.16	499.41	500.57	PAL	
								Totals:	8.17	8.17				
48R	16	0115	502.0	511.6	9.6	8.66	90.2							
								1	1.50	1.50	502.00	503.50		
								2	1.37	1.37	503.50	504.87		
								3	1.41	1.41	504.87	506.28		
								4	1.50	1.50	506.28	507.78		
								5	1.50	1.50	507.78	509.28	IW	
								6	1.38	1.38	509.28	510.66	PAL, HS	
								Totals:	8.66	8.66				
49R	16	0235	511.6	521.2	9.6	3.71	38.6							
								1	1.34	1.34	511.60	512.94		
								2	1.40	1.40	512.94	514.34	IW	
								3	0.97	0.97	514.34	515.31	PAL, HS	
								Totals:	3.71	3.71				
50R	16	0420	521.2	530.8	9.6	9.88	102.9							
								1	1.50	1.50	521.20	522.70		
								2	1.50	1.50	522.70	524.20		
								3	1.41	1.41	524.20	525.61		
								4	1.50	1.50	525.61	527.11		
								5	1.50	1.50	527.11	528.61		
								6	1.50	1.50	528.61	530.11	IW	
								7	0.79	0.79	530.11	530.90	HS	
								CC (w/7)	0.18	0.18	530.90	531.08	PAL	
								Totals:	9.88	9.88				
51R	16	0545	530.8	540.5	9.7	6.56	67.6							
								1	1.50	1.50	530.80	532.30		
								2	1.00	1.00	532.30	533.30		
								3	1.50	1.50	533.30	534.80	IW	
								4	1.47	1.47	534.80	536.27	HS	
								5	1.09	1.09	536.27	537.36	PAL	
								Totals:	6.56	6.56				
52R	16	0710	540.5	550.1	9.6	9.92	103.3							
								1	1.50	1.50	540.50	542.00		
								2	1.45	1.45	542.00	543.45		
								3	1.50	1.50	543.45	544.95		
								4	1.16	1.16	544.95	546.11		
								5	1.50	1.50	546.11	547.61		
								6	1.40	1.40	547.61	549.01	IW	
								7	1.16	1.16	549.01	550.17		
								CC (w/7)	0.25	0.25	550.17	550.42	PAL	
								Totals:	9.92	9.92				
53R	16	0840	550.1	559.8	9.7	7.17	73.9							
								1	1.23	1.23	550.10	551.33		
								2	1.50	1.50	551.33	552.83		
								3	1.50	1.50	552.83	554.33		
								4	1.50	1.50	554.33	555.83		
								5	1.31	1.31	555.83	557.14		
								CC (w/5)	0.13	0.13	557.14	557.27	PAL	
								Totals:	7.17	7.17				
54R	16	1020	559.8	569.4	9.6	9.59	99.9							
								1	1.37	1.37	559.80	561.17		
								2	1.50	1.50	561.17	562.67		
								3	1.50	1.50	562.67	564.17		
								4	0.87	0.87	564.17	565.04		
								5	1.01	1.01	565.04	566.05		
								6	1.50	1.50	566.05	567.55		
								7	1.11	1.11	567.55	568.66		
								8	0.73	0.73	568.66	569.39	PAL	
								Totals:	9.59	9.59				

Table T2 (continued).

Core	Date (Feb 2001)	Time (local)	Core depth (mbsf) Top	Core depth (mbsf) Bottom	Length (m) Cored	Length (m) Recovered	Recovery (%)	Section	Length (m) Liner	Length (m) Curated	Section depth (mbsf) Top	Section depth (mbsf) Bottom	Catwalk samples	Comment
55R	16	1710	569.4	579.0	9.6	9.95	103.6							
								1	1.36	1.36	569.40	570.76		
								2	1.50	1.50	570.76	572.26		
								3	1.50	1.50	572.26	573.76		
								4	1.50	1.50	573.76	575.26		
								5	1.33	1.33	575.26	576.59	IW	
								6	1.31	1.31	576.59	577.90	HS	
								7	1.30	1.30	577.90	579.20		
								CC (w/7)	0.15	0.15	579.20	579.35	PAL	
								Totals:	9.95	9.95				
56R	16	1945	579.0	588.6	9.6	7.32	76.3							
								1	1.50	1.50	579.00	580.50		
								2	1.50	1.50	580.50	582.00		
								3	1.50	1.50	582.00	583.50		
								4	1.50	1.50	583.50	585.00		
								5	1.32	1.32	585.00	586.32	PAL, HS	
								Totals:	7.32	7.32				
57R	16	2205	588.6	598.2	9.6	9.83	102.4							
								1	1.50	1.50	588.60	590.10		
								2	1.50	1.50	590.10	591.60		
								3	1.50	1.50	591.60	593.10		
								4	1.50	1.50	593.10	594.60		
								5	1.50	1.50	594.60	596.10	HS	
								6	1.50	1.50	596.10	597.60		
								7	0.67	0.67	597.60	598.27		
								CC (w/7)	0.16	0.16	598.27	598.43	PAL	
								Totals:	9.83	9.83				
58R	17	0005	598.2	607.9	9.7	9.17	94.5							
								1	1.50	1.50	598.20	599.70		
								2	1.50	1.50	599.70	601.20		
								3	1.50	1.50	601.20	602.70		
								4	1.50	1.50	602.70	604.20		
								5	1.50	1.50	604.20	605.70		
								6	1.00	1.00	605.70	606.70		
								7	0.67	0.67	606.70	607.37	PAL	
								Totals:	9.17	9.17				
59R	17	0115	607.9	617.2	9.3	4.60	49.5							
								1	1.50	1.50	607.90	609.40		
								2	1.45	1.45	609.40	610.85		
								3	1.49	1.49	610.85	612.34		
								CC (w/CC)	0.16	0.16	612.34	612.50	PAL	
								Totals:	4.60	4.60				
60R	17	2035	617.2	626.8	9.6	4.15	43.2							
								1	1.43	1.43	617.20	618.63		
								2	1.50	1.50	618.63	620.13		
								3	1.07	1.07	620.13	621.20		
								CC (w/3)	0.15	0.15	621.20	621.35	PAL	
								Totals:	4.15	4.15				
61R	17	0350	626.8	636.5	9.7	4.36	44.9							
								1	1.50	1.50	626.80	628.30		
								2	1.50	1.50	628.30	629.80		
								3	1.22	1.22	629.80	631.02		
								CC (w/3)	0.14	0.14	631.02	631.16	PAL	
								Totals:	4.36	4.36				
62R	17	0515	636.5	646.1	9.6	4.98	51.9							
								1	1.48	1.48	636.50	637.98		
								2	1.46	1.46	637.98	639.44		
								3	1.00	1.00	639.44	640.44		
								4	0.85	0.85	640.44	641.29		
								CC (w/4)	0.19	0.19	641.29	641.48	PAL	
								Totals:	4.98	4.98				
63R	17	0635	646.1	655.7	9.6	4.96	51.7							
								1	1.44	1.44	646.10	647.54		
								2	1.38	1.38	647.54	648.92		
								3	1.23	1.23	648.92	650.15		
								4	0.91	0.91	650.15	651.06	PAL	
								Totals:	4.96	4.96				

Table T2 (continued).

Core	Date (Feb 2001)	Time (local)	Core depth (mbsf) Top	Core depth (mbsf) Bottom	Length (m) Cored	Length (m) Recovered	Recovery (%)	Section	Length (m) Liner	Length (m) Curated	Section depth (mbsf) Top	Section depth (mbsf) Bottom	Catwalk samples	Comment
64R	17	0805	655.7	665.3	9.6	2.64	27.5							
								1	1.37	1.37	655.70	657.07		
								2	1.27	1.27	657.07	658.34	PAL	
								Totals:	2.64	2.64				
65R	17	0920	665.3	674.9	9.6	1.43	14.9							
								1	1.43	1.43	665.30	666.73		
								Totals:	1.43	1.43				
				Totals:	624.9	213.64	34.2							

Notes: CC = core catcher (number in parentheses indicates which section the core catcher is stored with). Catwalk samples: PAL = paleontology sample, IW = interstitial water, HS = headspace. NA = not applicable.

Table T3. Lithological units and subunits, Site 1197.

		Hole 1197A				Hole 1197B					
		Core, section, interval (cm)		Depth (mbsf)		Core, section, interval (cm)		Depth (mbsf)			
Unit	Subunit	Top	Base	Top	Base	Top	Base	Top	Base	Description	Interpretation
I		1H-1, 0	7H-2,15	0.0	59.6					Skeletal grainstone and packstone rich in planktonic foraminifers, with bivalves and pteropods as minor components. White to yellow color.	Hemipelagic setting, minor cyclicity observed
II		9X-1, 0	?	59.6	?					Dolomitized skeletal packstone to grainstone with planktonic foraminifers, abundant larger benthic foraminifers, and neritic material. Fine grained. White to pale gray. Hardground at top.	Proximal periplatform setting (fine shed detritus)
II						2R-1, 0	14R-1, 0	59.6	175.0		
III						14R-1, 0	22R-1, 0	175.0	261.5	Dolomitized skeletal grainstone with abundant *Lepidocyclina* sp. larger benthic foraminifers and rare coralline algae and bryozoa. Glauconite present and common toward the base. Coarse grained. Pale gray. Hiatus at top.	Proximal periplatform setting (coarse shed detritus)
IV	IVA					22R-1, 0	33R-1, 0	261.5	367.4	Dolomitized silt-sized and very fine sand skeletal grainstone, homogeneous, lacking internal cyclicity, and strongly bioturbated. Unidentified fine skeletal detritus dominates.	Distal periplatform setting (predominantly silt-sized neritic detritus)
	IVB					33R-1, 0	58R-3, 50	367.4	601.7	Fine sand to silt-sized skeletal packstone/grainstone/ wackestone. Unidentifiable fine skeletal detritus dominates. Light and dark colored intervals noted suggesting long-term cyclicity and fluctuating clay content. Graded beds and sharp-based turbidites.	Distal periplatform setting (predominantly silt-sized neritic detritus) or hemipelagic setting (clays with deepening-upward trend)
V						58R-3, 50	64R-1, 40	601.7	656.1	Skeletal grainstone/rudstone rich in benthic foraminifers and branching coralline algae remains. Glauconite is abundant, quartz is present and increases in abundance towards the base. Graded bed units and parallel lamination are common. Cyclicity is well developed.	Proximal periplatform to neritic setting (with oysters at the base)
VI	VIA					64R-1, 40	65R-1, 129	656.1	666.6	Matrix-supported volcaniclastic breccia conglomerate with large angular basalt clasts and a range of altered green-colored volcanic clasts.	Debris flow—marine/continental?
	VIB					65R-1, 129	?	666.6	?	Olivine basalt, medium gray, with olivine phenocrysts and small plagioclase laths, highly altered.	Basement

Note: ? = not defined.

Table T4. Biostratigraphic datums, Site 1197.

Datum	Core, section, interval (cm)	Depth (mbsf)		Mean depth (mbsf)	Age (Ma)
		First absence or presence	Last presence or absence		
	194-1197A-				
Acme *Emiliania huxleyi*	1H-1, 0 to 1H-2, 136	0.00	2.86	1.43	0.08
LO *Globigerinoides ruber* (pink)	1H-1, 0 to 1H-CC	0.00	6.13	3.07	0.12
FO *Emiliania huxleyi*	1H-2, 136 to 1H-CC	2.86	5.95	4.41	0.26
LO *Pseudoemiliania lacunosa*	1H-CC to 2H-CC	5.95	15.50	10.73	0.46
LO *Globorotalia tosaensis*	1H-CC to 2H-CC	6.13	15.61	10.87	0.65
FO *Pulleniatina finalis*	3H-CC to 4H-CC	25.22	34.87	30.05	1.30
LO *Calcidiscus macintyrei*	4H-CC to 5H-CC	34.87	44.20	39.54	1.70
LO *Globigerinoides fistulosus*	4H-CC to 5H-CC	34.87	44.20	39.54	1.77
LO *Globigerinoides extremus*	4H-3, 12–14 to 5H-CC	29.22	54.59	41.91	1.80
LO *Discoaster brouweri*	6H-CC to 7H-1, 28–30	53.61	53.88	53.75	2.00
LO *Globorotalia pseudomiocenica*	7H-1, 28–30 to 7H-CC	53.88	54.59	54.24	2.30
	194-1197B-				
Dentoglobigerina altispira, Globoquadrina baroemoenensis, Globorotalia siakensis	Assemblage depth range (mbsf): 69.2–175; Age range (Ma): 4.8–11.4				
LO *Sphenolithus heteromorphus*	37R-CC to 38R-CC	398.28	412.67	405.48	13.6
FO *Sphenolithus heteromorphus*	57R-CC to 58R-CC	598.41	607.36	602.89	18.2
Range of *Sphenolithus belemnos*	Found in 61R-CC	631.14	631.14	631.14	18.5–19.3

Note: FO = first occurrence, LO = last occurrence.

Table T5. Summary of biostratigraphic and paleoenvironmental interpretations, Site 1197. (**See table notes.** Continued on next page.)

Core, section, interval (cm)	Depth (mbsf)	Foraminiferal assemblages					Comments on core catcher samples, >63-µm fraction	Paleowater depth (m)	Depositional setting	Lithologic unit
		PF	ONBF	SBF	LBF	Pres				
194-										
1197A-1H-CC, 18–20	6.13	Dom	Div, C			G	PF, pteropods; common bryozoan colonies/debris	>200	Hemipelagic	I
1197A-2H-CC, 11–13	15.61	Dom	Div, C			G	PF, pteropods; common bryozoan colonies/debris, solitary corals	>200	Hemipelagic	
1197A-3H-CC, 18–20	25.22	Dom	Div, C			G	PF, pteropods; common bryozoan colonies/debris, solitary corals	>200	Hemipelagic	
1197A-4H-CC, 13–15	34.87	Dom	C			G	PF, pteropods; common bryozoan colonies/debris, solitary corals	>200	Hemipelagic	
1197A-5H-CC, 16–18	44.20	Dom	C			G	PF; common bryozoan colonies/debris, alcyonarian spicules	>200	Hemipelagic	
1197A-6H-CC, 18–20	53.79	Dom	Div, C			G	PF; common bryozoan colonies/debris, alcyonarian spicules	>200	Hemipelagic	
1197A-7H-CC, 15–17	54.59	Dom	A			G	Sorted bioclastic sands, PF dominate, common bryozoans, etc.	>200	Hemipelagic	
1197A-9X-1, 31–34	59.91	A	?			VP	Recrystallized, sorted medium sand–sized neritic debris, PF hard to identify	>150	Proximal periplatform	II
1197B-2R-1, 84–86	60.44	R	?	C	A	P	Neritic debris dominates, common LBF, especially *Amphistegina*, SBF	?	Proximal periplatform	
1197B-3R-1, 0–3	69.20	C	C	C	VA	P	Abundant LBF, worn *A. radiata* dominant, finer neritic and nondescript debris	>150	Proximal periplatform	
1197A-10X-CC, 23–25	69.43	R	C	A	A	VP–M	Assorted neritic fragments including LBF in a very fine chalky neritic debris	>150	Proximal periplatform	
1197A-11X-CC, 0–5	78.80	R	C	A	A	P	Assorted neritic fragments including LBF in a very fine chalky neritic debris	>150	Proximal periplatform	
1197B-5R-1, 0–1	88.50	C	C?	A?	A	VP	Abundant LBF, worn *A. radiata* dominant, finer neritic and nondescript debris	?	Proximal periplatform	
1197B-6R-1, 6–8	98.26	C	C?	C	A	VP	Neritic debris, common LBF, especially *Amphistegina*, SBF	?	Proximal periplatform	
1197B-8R-1, 0–2	117.40	C	R?	C	A	VP	Neritic debris, common LBF, especially *A. papillosa*-type, SBF	>150	Proximal periplatform	
1197B-9R-1, 8–10	127.08	C	C	A	A	VP–M	Neritic debris, common LBF, especially *Amphistegina*, SBF	>150	Proximal periplatform	
1197A-17X-1, 10–12	136.60		R	A	A	P–M	Assorted neritic fragments including LBF in a very fine chalky neritic debris	>150	Proximal periplatform	
1197B-11R-1, 0–5	146.20	A	C?	A	A	VP–M	Highly recrystallized; *Amphistegina* and *Lepidocyclina* recognizable; PF	?	Proximal periplatform	
1197B-12R-1, 0–5	155.80	A	C?	C	C	VP–M	Highly recrystallized; *Amphistegina* and *Lepidocyclina* recognizable; PF	?	Proximal periplatform	
1197A-20X-CC, 0–5	165.40	Dom	C		A	P–G	Assorted neritic fragments in a very fine chalky dolomitic debris	>150	Proximal periplatform	
1197B-13R-1, 0–5	165.40	A	R	C	C	VP–M	PF abundant, neritic material highly recrystallized	>150	Proximal periplatform	
1197B-14R-1, 40–42	175.40	R	R	C	C	VP–M	Highly recrystallized; *Amphistegina* and *Lepidocyclina* recognizable; PF	>150	Proximal periplatform	
1197B-15R-1, 43–45	185.03	C	C	C	A	M	Neritic debris with 3 morphotypes of *Lepidocyclina*	>150	Proximal periplatform	III
1197B-16R-1, 56–58	194.76	R	C?	C?	A	VP	Neritic debris, abundant MBF, especially *Lepidocyclina*	?	Proximal periplatform	
1197B-17R-1, 64–66	204.44	A	C?	A	A	VP	Neritic debris, abundant *Lepidocyclina*, fines are crystals, PF, SBF, debris	?	Proximal periplatform	
1197B-18R-1, 28–30	213.68	A	C?	A	A	VP	Neritic debris, abundant *Lepidocyclina*, bryozoans, fines are crystals, PF, SBF, debris	?	Proximal periplatform	
1197B-19R-1, 36–38	223.36	A	C	A	A	P	Neritic debris, abundant *Lepidocyclina*, bryozoans, fines are crystals, PF, MBF, debris	>150	Proximal periplatform	
1197B-20R-1, 32–34	233.02			?	A	P	Lithified neritic debris, abundant *Lepidocyclina*, bryozoans	?	Proximal periplatform	
1197B-21R-1, 47–49	242.77	A	A	A	A	P	Neritic debris, abundant *Lepidocyclina*, bryozoans, fines are crystals, PF, SBF, debris	>150	Proximal periplatform	
1197B-22R-1, 22–24	252.12			?	A	P	Lithified neritic debris including *Lepidocyclina* filled with glauconite	?	Proximal periplatform	
1197B-23R-1, 44-46	261.94	A	A	C	C	VP–M	PF/ONBF abundant in fines, not recrystallized; coarse is mostly brown dolomite	>200	Distal periplatform	IVA
1197B-24R-1, 34–36	271.54	A	C		R	P	Fine neritic debris, PF, ONBF; neritics, including bryozoans, echnoid, juvenile *Lepidocyclina*	>200	Distal periplatform	
1197B-25R-1, 120–122	282.00	A	C		R	P	Fine neritic debris, PF, ONBF; neritics, including bryozoans, echnoid, juvenile *Lepidocyclina*	>200	Distal periplatform	
1197B-27R-1, 35–37	300.35	A	C	R	R	P	Fine neritic debris, PF, ONBF; neritics, including bryozoans, echnoid, juvenile *Lepidocyclina*	>200	Distal periplatform	
1197B-28R-2, 50–53	311.70	A	C			P	Fine neritic debris, PF, ONBF; neritics, including bryozoans, echnoid, juvenile *Lepidocyclina*	>200	Distal periplatform	
1197B-29R-2, 35–38	321.15						Lithified fine neritic debris		Distal periplatform	
1197B-30R-1, 31–33	329.21	A	C			P	Fine neritic debris, PF, ONBF; neritics, including bryozoans, echnoids, bivalves	>200	Distal periplatform	
1197B-31R-2, 55–57	340.61	A	?			VP	Fine neritic debris, PF, ONBF; neritics, including bryozoans, echnoids, bivalves		Distal periplatform	
1197B-32R-1, 129–131	349.49	A	C?	C	A	VP	Lithified LBF, bryozoans, bivalves, glauconite or pyrite infilled; fines are neritic debris and PF	>200	Distal periplatform	
1197B-33R-1, 52–55	358.32	A	C?		C	VP	Fine neritic debris, PF, ONBF; neritics, including bryozoans, echnoid, juvenile *Lepidocyclina*	>200	Distal periplatform	
1197B-34R-1, 96–98	368.36						Fine neritic and PF debris, nothing definitively recognizable		Distal periplatform	IVB
1197B-35R-CC, 10–12	381.67	A	A		R	P	Fine neritic debris, PF, ONBF; neritics, including bryozoans, echnoid, juvenile LBF	>200	Distal periplatform	
1197B-36R-CC, 12–14	391.42						Lithified medium/fine neritic and PF debris, nothing definitively recognizable		Distal periplatform	
1197B-37R-2, 51–53	398.28	A	A			P	Fine neritic debris, PF, ONBF, particularly *Cibicidoides*, minor coarse neritics	>200	Distal periplatform	
1197B-38R-5, 130–132	412.67						Lithified fine neritic and PF debris, nothing definitively recognizable		Distal periplatform	

Table T5 (continued).

Core, section, interval (cm)	Depth (mbsf)	Foraminiferal assemblages					Comments on core catcher samples, >63-µm fraction	Paleowater depth (m)	Depositional setting	Lithologic unit
		PF	ONBF	SBF	LBF	Pres				
1197B-39R-CC, 23–25	424.51	A	A		A	P	Fine neritic and planktonic debris, some partly lithified, ONBF	>200	Distal periplatform	
1197B-40R-CC, 35–37	431.70						Fine neritic and planktonic debris, some partly lithified		Distal periplatform	
1197B-41R-CC, 15–17	438.98	A	A		A	P	Fine neritic and planktonic debris, some partly lithified, ONBF	>200	Distal periplatform	
1197B-42R-CC, 26–28	448.52						Partly lithified fine mudstone		Distal periplatform	
1197B-43R-CC, 14–16	456.18						Partly lithified fine mudstone		Distal periplatform	
1197B-44R-CC, 38–40	472.93					VP	Lithified medium/fine neritic and PF debris		Distal periplatform	
1197B-45R-7, 117–119	482.61						Partly lithified fine mudstone		Distal periplatform	
1197B-46R-CC, 22–24	492.51	A	C	?	Juv?	P	Neritic debris, tiny foraminifers—PF, MBF, crystals are major components, ostracods	>200	Distal periplatform	
1197B-47R-6, 11–116	500.55						Lithified medium/fine neritic and PF debris		Distal periplatform	
1197B-48R-6, 136–138	510.64						Lithified medium/fine neritic and PF debris		Distal periplatform	
1197B-49R-3, 95–97	515.29						Lithified medium/fine neritic and PF debris		Distal periplatform	
1197B-50R-CC, 16–18	531.06	A	C	?	Juv?	P	Tiny foraminifers—PF, MBF; neritic debris, crystals are major components, ostracods	>200	Distal periplatform	
1197B-52R-CC, 23–25	550.40						Lithified medium/fine neritic and PF debris		Distal periplatform	
1197B-53R-CC, 11–13	557.25	A	C	?	Juv?		Tiny forams—PF, MBF; neritic debris, crystals are major components	>200	Distal periplatform	
1197B-54R-8, 71–73	569.37	A	C	?	Juv?		Tiny foraminifers—PF, MBF; neritic debris, crystals are major components, ostracods	>200	Distal periplatform	
1197B-55R-CC, 13–15	579.33						Partly lithified fine mudstone		Distal periplatform	
1197B-56R-5, 130–132	586.30						Partly lithified fine mudstone		Distal periplatform	
1197B-57R-CC, 14–16	598.41						Partly lithified fine mudstone		Distal periplatform	
1197B-58R-7, 66–67	607.36				A	M	Lithified coarse grainstone with glauconite-filled, rounded *Lepidocyclina* and other LBF	<100?	Open shelf or proximal periplatform	V
1197B-59R-CC, 14–16	612.48				A	M	Lithified coarse grainstone with glauconite-filled, rounded *Lepidocyclina* and other LBF	<100?	Open shelf or proximal periplatform	
1197B-60R-CC, 13–15	621.33	R		C	A	M	Lithified coarse grainstone with glauconite-filled, rounded *Lepidocyclina* and other LBF	<100?	Open shelf or proximal periplatform	
1197B-61R-CC, 12–14	631.14	R		C	A	M	Similar to Cores 58 and 59 but finer grained, beautifully preserved *Amphistegina*	<100?	Open shelf or proximal periplatform	
1197B-62R-CC, 17–19	641.46				A	M	Two lithologies, one similar to Core 61, also coarse gold grainstone with *Heterostegina*	<100?	Open shelf or proximal periplatform	
1197B-63R-4, 89–91	651.04				C	?	Bottom of core is dark, volcanic sandstone with bryozoans, bivalves and *Operculina*	<30	Inner neritic	
1197B-64R-2, 125–127	658.32				?		Black volcanic-rock conglomerate; may have some *Operculina* and oysters	<30	Inner neritic	VI

Notes: Based on microscopic analysis of biogenic sediment constituents >63 µm, particularly benthic foraminifers, from core catcher samples. Foraminiferal assemblages: PF = planktonic foraminifers, ONBF = outer neritic/upper bathyal benthic foraminifers, SBF = smaller benthic foraminifers from inner to middle neritic depths, LBF = larger benthic foraminifers, Pres = preservation; Dom = dominant, Div = diverse, A = abundant, C = common, G = good, M = moderate, R = rare, P = poor, VP = very poor, Juv = juvenile, ? = uncertain.

Table T6. Magnetic polarity transitions, Site 1197.

Chron	Top observation		Bottom observation		Average		
	Core, section, interval (cm)	Depth (mbsf)	Core, section, interval (cm)	Depth (mbsf)	Depth (mbsf)	Error	Age (Ma)
	194-1179A-		194-1179A-				
C1n (O)	2H-6, 135	14.95	2H-7, 15	15.25	15.100	0.150	0.780
C1r1r1n (T)	3H-3, 110	19.70	3H-3, 135	19.95	19.825	0.125	0.990
C1r1r1n (O)	3H-6, 135	24.45	3H-6, 145	24.55	24.500	0.050	1.070
C2n (T)	5H-7, 40	44.00	6H-1, 5	44.15	44.075	0.075	1.770
C2n (O)	6H-7, 5	53.15	6H-7, 35	53.45	53.300	0.150	1.950

Note: (T) = termination, (O) = onset.

Table T7. Age-depth control points, Site 1197.

Source	Datum	Age (Ma)	Top: FO presence or LO absence		Bottom: LO presence or FO absence		Average depth (mbsf)	Uncertainty (m)	
			Core, section, interval (cm)	Depth (mbsf)	Core, section, interval (cm)	Depth (mbsf)		Up-section	Down-section
			194-1197A-		194-1197A-				
CN	Acme *Emiliania huxleyi*	0.08	1H-1, 0	0.00	1H-2, 136	2.86	1.43	1.43	1.43
PF	LO *Globigerinoides ruber* (pink)	0.12	1H-1, 0	0.00	1H-CC	6.13	3.07	3.07	3.07
CN	FO *Emiliania huxleyi*	0.26	1H-2, 136	2.86	1H-CC	5.95	4.41	1.55	1.55
CN	LO *Pseudoemiliania lacunosa*	0.46	1H-CC	5.95	2H-CC	15.50	10.73	4.78	4.78
PF	LO *Globorotalia tosaensis*	0.65	1H-CC	6.13	2H-CC	15.61	10.87	4.74	4.74
PF	FO *Pulleniatina finalis*	1.30	3H-CC	25.22	4H-CC	34.87	30.05	4.83	4.83
CN	LO *Calcidiscus macintyrei*	1.7	4H-CC	34.87	5H-CC	44.20	39.54	4.67	4.67
PF	LO *Globigerinoides fistulosus*	1.77	4H-CC	34.87	5H-CC	44.20	39.54	4.67	4.67
PF	LO *Globigerinoides extremus*	1.80	4H-3, 13	28.23	5H-CC	44.20	36.70	7.50	7.50
CN	LO *Discoaster brouweri*	2	6H-CC	53.61	7H-1, 29	53.89	53.75	0.14	0.13
PF	LO *Globorotalia pseudomiocenica*	2.30	7H-1, 29	53.89	7H-CC	54.59	54.24	0.35	0.36
			194-1197B-		194-1197B-				
PF	Range of Zones N16–N18 assemblage	4.8–11.0	3R-CC	69.21	13R-BCI	175.00			
PF	LO *Globorotalia siakensis*	11.4	14R-CC	175.40	15R-BCI	193.71	184.56	9.16	9.16
CN	LO *Sphenolithus heteromorphus*	13.6	37R-CC	398.28	38R-BCI	415.50	406.89	8.61	8.61
CN	FO *Sphenolithus heteromorphus*	18.2	57R-CC	598.41	58R-BCI	607.90	603.16	4.75	4.75
CN	Range of *Sphenolithus belemnos*	18.5–19.3	61R-CC	631.14	61R-BCI	636.50	633.82	2.68	2.68

Notes: Source: CN = calcareous nannoplankton, PF = planktonic foraminifers. Datum: LO = last occurrence, FO = first occurrence. Core, section, interval: BCI = bottom of cored interval.

Table T8. Interpolated ages of lithologic unit boundaries and seismic reflectors, Site 1197.

	Top of unit		
	Depth (mbsf)	Age (Ma)	Comments
Lithologic unit:			
I	0	0	
II	59.6	>2.1 (?6 to 2.1)	Hiatus
III	175.0	<11.3 (11.3 to 8?)	Hiatus
IVA	261.5	12.2	
IVB	367.4	13.2	
V	601.7	18.2	
VIA	656.1	19.3	Extrapolated
VIB	666.6	19.5	Extrapolated
Seismic sequences and reflectors:			
Megasequence D	0	0	
D-black	Not present		
D-turquoise	Not present		
Megasequence C	59	>2.1 (?6 to 2.1)	Hiatus
Megasequence B	175	<11.3 (11.3 to 8?)	Hiatus
Megasequence A	Not present		
Basement	667	19.5	Extrapolated

Table T9. Headspace gas composition, Site 1197.

Core, section	Depth (mbsf)	C_1 (ppmv)
194-1197A-		
1H-4	4.50	1.6
2H-5	12.10	2.3
3H-5	21.60	2.0
4H-5	31.10	1.8
5H-5	40.60	1.6
6H-5	50.10	1.9
194-1197B-		
39R-5	421.01	2.1
40R-3	427.94	1.7
41R-3	437.38	1.9
42R-2	445.80	2.0
43R-2	455.34	2.1
44R-7	471.44	2.1
45R-6	479.94	2.2
46R-6	490.09	2.3
47R-4	496.43	2.2
48R-6	509.28	3.1
50R-7	530.11	2.5
51R-4	534.80	3.1
55R-6	576.59	2.0
56R-5	585.00	2.7
57R-5	594.60	2.4

Note: C_1 = methane.

Table T10. Interstitial water chemistry, Site 1197.

Core, section, interval (cm)	Depth (mbsf)	pH	Alk (mM)	Salinity	Cl^- (mM)	SO_4^{2-} (mM)	Na^+ (mM)	Mg^{2+} (mM)	Ca^{2+} (mM)	K^+ (mM)	NH_4^+ (μM)	Sr^{2+} (μM)	Li^+ (μM)	Mn^{2+} (μM)	Fe^{2+} (μM)
194-1197A-															
1H-3, 140–150	4.40	7.65	2.45	35.5	561	29.78	475	54.56	12.71	11.08	3	159	28.78	0.10	18.75
2H-4, 140–150	12.00	7.68	1.67	35.5	563	29.56	476	52.36	15.24	11.21	12	188	31.35	0.10	19.12
3H-4, 140–150	21.50	7.58	1.81	35.7	566	29.43	478	50.06	17.57	11.28	15	177	30.50	0.10	21.74
4H-4, 140–150	31.00	7.88	1.57	35.7	564	29.06	476	50.24	16.81	11.56	19	154	31.71	0.08	3.31
5H-4, 140–150	40.50	7.50	1.79	36.0	565	29.78	476	50.35	18.14	11.22	69	141	31.25	0.09	14.74
6H-4, 140–150	50.00	7.45	1.78	36.0	561	29.55	470	49.80	19.57	11.16	73	123	31.02	0.13	16.21
194-1197B-															
39R-4, 130–140	420.91	7.39	2.64	35.0	562	21.59	479	39.36	19.70	8.19	477	594	123.27	0.12	2.49
40R-2, 130–140	427.84	7.44	2.82	35.5	562	20.81	476	39.25	20.21	8.25	497	613	130.83	0.18	2.65
41R-2, 130–140	437.28	7.43	2.94	34.5	561	19.60	477	37.92	19.72	7.92	521				
42R-1, 140–150	445.70	7.37	3.29	34.5	559	18.67	476	37.04	19.29	7.59	566	687	146.02	0.11	0.95
43R-1, 134–144	455.24	7.32	3.10	34.0	557	16.95	473	35.81	19.52	7.11	588	754	159.76	0.14	1.20
45R-5, 131–143	479.82			34.0	558	14.38	477	33.12	18.36	6.31	693	819	171.00	0.21	17.95
46R-5, 140–150	489.99			32.5	541	13.44	454	34.41	20.12	4.90	559				
47R-3, 127–142	496.28	7.34	3.31	34.0	563	14.25	477	34.11	20.12	5.80	743	976	188.95	0.15	3.58
48R-5, 140–150	509.18			33.0	552	13.20	467	32.97	20.39	4.95	716	1074	204.90	0.20	2.70
49R-2, 131–140	514.25	7.29	3.55	33.5	555	13.02	474	32.10	18.78	5.41	782	806	160.33	0.15	1.60
51R-3, 140–150	534.70			33.5	554	11.33	471	30.57	19.64	4.86	781	1124	216.46	0.22	0.00
52R-6, 130–140	548.91			33.0	556	10.66	473	29.89	19.77	4.60	856				

Note: Alk = alkalinity.

Table T11. Percentages of aragonite, calcite, dolomite, and noncarbonate minerals, Site 1197.

Core, section, interval (cm)	Depth (mbsf)	Aragonite (wt%)	Calcite (wt%)	Dolomite (wt%)	Non-carbonate (wt%)
194-1197A-					
1H-2, 62–63	2.12	21	70	0	9
1H-4, 62–63	5.12	15	73	0	12
2H-2, 62–63	8.22	16	71	0	13
2H-4, 62–63	11.22	13	75	0	12
2H-6, 62–63	14.22	15	72	0	13
3H-2, 62–63	17.72	12	73	0	15
3H-4, 62–63	20.72	8	82	0	10
3H-6, 62–63	23.72	11	77	2	9
4H-2, 62–63	27.22	0	89	0	11
4H-4, 62–63	30.22	9	79	0	13
4H-6, 62–63	33.22	0	90	0	10
5H-2, 62–63	36.72	0	92	0	8
5H-4, 62–63	39.72	0	94	0	6
5H-6, 62–63	42.72	15	76	1	8
6H-2, 62–63	46.22	0	87	0	13
6H-4, 62–63	49.22	0	89	0	11
6H-6, 62–63	52.22	0	94	0	6
194-1197B-					
2R-1, 43–44	60.03	0	92	5	3
6R-1, 3–4	98.23	0	24	74	2
14R-1, 14–15	175.14	0	23	75	2
15R-1, 9–10	184.69	0	62	35	3
16R-1, 36–37	194.56	0	47	51	2
17R-1, 13–14	203.93	0	44	54	2
18R-1, 17–18	213.57	0	62	37	1
19R-1, 4–5	223.04	0	54	43	3
20R-1, 20–21	232.90	0	38	60	2
21R–1, 35–36	242.65	0	45	53	2
22R-1, 19–20	252.09	0	35	62	3
23R-1, 20–21	261.70	0	36	61	3
24R-1, 32–33	271.52	0	56	40	4
25R-1, 23–24	281.03	0	65	33	2
27R-1, 20–21	300.20	0	82	16	2
35R-1, 61–62	377.71	0	93	2	5
35R-3, 75–76	380.81	0	93	1	6
36R-1, 41–42	387.11	0	89	1	10
36R-2, 41–42	388.61	0	87	1	11
36R-3, 40–41	389.81	0	89	2	8
37R-1, 61–62	396.91	0	94	4	3
38R-2, 100–101	408.40	0	80	1	18
38R-4, 99–100	410.91	0	87	3	11
39R-2, 101–102	417.94	0	85	2	13
39R-4, 96–97	420.57	0	78	15	7
39R-6, 91–92	423.37	0	87	5	8
40R-2, 103–104	427.57	0	90	4	5
40R-4, 99–101	429.91	0	84	8	8
41R-1, 124–125	435.84	0	92	2	6
41R-3, 105–106	438.43	0	88	3	9
42R-1, 134–135	445.64	0	91	2	7
43R-1, 126–127	455.16	0	94	0	6
44R-2, 103–104	465.73	0	85	2	13
44R-4, 101–102	468.35	0	78	6	17
44R-6, 79–80	471.13	0	79	9	13
45R-2, 85–86	475.43	0	63	2	35
45R-4, 101–102	478.02	0	89	6	6
45R-6, 83–84	480.77	0	76	11	13
46R-2, 82–83	485.12	0	70	6	23
46R-4, 103–104	488.12	0	89	1	10
46R-6, 81–82	490.90	0	80	5	15
47R-2, 68–69	494.58	0	58	1	41
47R-4, 106–107	497.49	0	77	12	11
47R-6, 78–79	500.19	0	88	7	5
48R-1, 67–68	502.67	0	81	6	13
48R-3, 36–37	505.23	0	81	5	14
48R-5, 53–54	508.31	0	67	10	23
49R-1, 21–22	511.81	0	78	10	12
49R-2, 39–40	513.33	0	79	3	18
49R-3, 45–46	514.79	0	82	5	13
50R-2, 81–82	523.51	0	80	6	14
50R-4, 82–83	526.43	0	73	9	18
50R-6, 65–66	529.26	0	83	5	12
51R-1, 86–87	531.66	0	84	6	10
51R-4, 82–83	535.62	0	74	12	14
52R-1, 81–82	541.31	0	49	28	23
52R-3, 74–75	544.19	0	64	7	28
52R-5, 52–53	546.63	0	87	4	9
53R-2, 81–82	552.14	0	88	3	9
53R-4, 80–81	555.13	0	78	7	15
53R-5, 78–79	556.61	0	99	0	1
54R-2, 82–83	561.99	0	93	2	6
54R-4, 80–81	564.97	0	88	3	10
54R-6, 80–81	566.85	0	89	4	7
55R-2, 73–74	571.49	0	96	0	4
55R-4, 73–74	574.49	0	90	0	10
55R-6, 73–74	577.32	0	88	0	12
56R-2, 72–73	581.22	0	85	6	9
56R-4, 72–73	584.22	0	93	1	6
57R-2, 67–68	590.77	0	80	12	8
57R-4, 90–91	594.00	0	55	31	15
57R-6, 80–81	596.90	0	91	3	6
58R-2, 76–77	600.46	0	81	10	10
58R-4, 87–88	603.57	0	92	0	8
58R-6, 63–64	606.33	0	90	0	10
59R-2, 120–121	610.60	0	97	0	3
60R-2, 101–102	619.64	0	98	0	2
61R-2, 121–122	629.51	0	98	0	2
62R-1, 60–61	637.10	0	92	0	8
62R-3, 68–69	640.12	0	98	0	2
63R-1, 27–28	646.37	0	92	0	8
63R-1, 53–54	646.63	0	93	0	7
63R-3, 24–25	649.16	0	68	0	32
63R-3, 32–33	649.24	0	63	0	37
64R-1, 24–25	655.94	0	66	0	34
64R-2, 32–32	657.39	0	4	0	96

Table T12. Carbon, nitrogen, sulfur, and hydrogen values in sediments and C/N and C/S ratios, Site 1197. (See table notes. Continued on next page.)

Core, section	Depth (mbsf)	IC (wt%)	$CaCO_3$ (wt%)	TC (wt%)	TOC (wt%)	Total N (wt%)	Total S (wt%)	Total H (wt%)	C/N ratio	C/S ratio
194-1197A-										
1H-2	2.12	10.93	91.1	—	—	—	—	—	—	—
1H-4	5.12	10.62	88.4	—	—	—	—	—	—	—
2H-2	8.22	10.48	87.3	10.48	0.00	0.04	0.07	0.15	0.00	0.00
2H-4	11.22	10.56	87.9	—	—	—	—	—	—	—
2H-6	14.22	10.50	87.5	—	—	—	—	—	—	—
3H-2	17.72	10.23	85.2	10.29	0.06	0.01	0.00	0.19	4.29	—
3H-4	20.72	10.86	90.5	—	—	—	—	—	—	—
3H-6	23.72	10.87	90.6	—	—	—	—	—	—	—
4H-2	27.22	10.73	89.4	—	—	—	—	—	—	—
4H-4	30.22	10.49	87.4	10.59	0.10	0.05	0.09	0.17	2.22	1.10
4H-6	33.22	10.86	90.5	—	—	—	—	—	—	—
5H-2	36.72	11.07	92.2	—	—	—	—	—	—	—
5H-4	39.72	11.23	93.6	—	—	—	—	—	—	—
5H-6	42.72	11.05	92.1	—	—	—	—	—	—	—
6H-2	46.22	10.39	86.6	10.41	0.02	0.02	0.05	0.18	0.87	0.42
6H-4	49.22	10.71	89.3	—	—	—	—	—	—	—
6H-6	52.22	11.23	93.6	11.19	0.00	0.01	0.08	0.10	0.00	0.00
194-1197B-										
2R-1	60.03	11.62	96.8	—	—	—	—	—	—	—
6R-1	98.23	12.49	104.1	—	—	—	—	—	—	—
14R-1	175.14	12.54	104.5	—	—	—	—	—	—	—
15R-1	184.69	12.13	101.1	—	—	—	—	—	—	—
16R-1	194.56	12.41	103.4	—	—	—	—	—	—	—
17R-1	203.93	12.53	104.4	—	—	—	—	—	—	—
18R-1	213.57	12.16	101.3	—	—	—	—	—	—	—
19R-1	223.04	12.10	100.8	—	—	—	—	—	—	—
20R-1	232.90	12.27	102.2	—	—	—	—	—	—	—
21R-1	242.65	12.31	102.5	—	—	—	—	—	—	—
22R-1	252.09	12.17	101.3	—	—	—	—	—	—	—
23R-1	261.70	12.28	102.3	—	—	—	—	—	—	—
24R-1	271.52	12.06	100.4	—	—	—	—	—	—	—
25R-1	281.03	11.73	97.7	11.75	0.03	0.01	0.00	0.05	2.60	—
27R-1	300.20	12.04	100.3	—	—	—	—	—	—	—
28R-1	310.09	11.50	95.8	—	—	—	—	—	—	—
28R-2	311.44	11.27	93.9	—	—	—	—	—	—	—
29R-1	319.73	11.24	93.7	—	—	—	—	—	—	—
29R-2	320.96	11.66	97.2	—	—	—	—	—	—	—
30R-1	329.05	11.71	97.5	—	—	—	—	—	—	—
31R-1	338.83	11.28	94.0	—	—	—	—	—	—	—
31R-2	340.26	11.56	96.3	—	—	—	—	—	—	—
32R-1	348.32	11.81	98.4	—	—	—	—	—	—	—
33R-1	358.23	11.94	99.4	—	—	—	—	—	—	—
34R-1	367.82	11.21	93.4	—	—	—	—	—	—	—
35R-1	377.70	11.36	94.7	—	—	—	—	—	—	—
35R-3	380.80	11.27	93.9	—	—	—	—	—	—	—
36R-1	387.10	10.81	90.1	—	—	—	—	—	—	—
36R-2	388.60	10.63	88.6	10.86	0.22	0.03	0.18	0.13	7.49	1.25
36R-3	389.82	10.98	91.5	—	—	—	—	—	—	—
37R-1	396.91	11.67	97.2	—	—	—	—	—	—	—
38R-2	408.39	9.79	81.5	10.11	0.32	0.03	0.37	0.20	10.69	0.86
38R-4	410.91	10.73	89.4	—	—	—	—	—	—	—
39R-2	417.93	10.43	86.9	10.61	0.18	0.04	0.09	0.16	4.45	1.98
39R-4	420.56	11.19	93.2	—	—	—	—	—	—	—
39R-6	423.36	11.04	92.0	—	—	—	—	—	—	—
40R-2	427.57	11.39	94.9	—	—	—	—	—	—	—
40R-4	429.91	11.05	92.0	—	—	—	—	—	—	—
41R-1	435.84	11.27	93.9	—	—	—	—	—	—	—
41R-3	438.43	10.95	91.2	11.03	0.08	0.04	0.00	0.11	1.96	—
42R-1	445.64	11.19	93.2	—	—	—	—	—	—	—
43R-1	455.16	11.26	93.8	—	—	—	—	—	—	—
44R-2	465.73	10.47	87.2	10.58	0.11	0.03	0.00	0.16	3.97	—
44R-4	468.35	10.00	83.3	10.24	0.24	0.04	0.08	0.20	5.89	2.95
44R-6	471.13	10.49	87.4	10.72	0.23	0.03	0.13	0.17	8.14	1.79
45R-2	475.42	7.83	65.2	8.29	0.46	0.09	0.47	0.41	5.11	0.98
45R-4	478.02	11.32	94.3	—	—	—	—	—	—	—

Table T12 (continued).

Core, section	Depth (mbsf)	IC (wt%)	$CaCO_3$ (wt%)	TC (wt%)	TOC (wt%)	Total N (wt%)	Total S (wt%)	Total H (wt%)	C/N ratio	C/S ratio
45R-6	480.77	10.47	87.2	—	—	—	—	—	—	—
46R-2	485.13	9.22	76.8	9.54	0.32	0.07	0.26	0.27	4.55	1.22
46R-4	488.13	10.82	90.1	—	—	—	—	—	—	—
46R-6	490.89	10.18	84.8	10.46	0.28	0.03	0.18	0.15	8.27	1.54
47R-2	494.58	7.09	59.1	7.76	0.67	0.08	0.83	0.45	8.36	0.81
47R-4	497.49	10.67	88.9	—	—	—	—	—	—	—
47R-6	500.19	11.38	94.8	—	—	—	—	—	—	—
48R-1	502.66	10.40	86.6	—	—	—	—	—	—	—
48R-3	505.23	10.35	86.2	—	—	—	—	—	—	—
48R-5	508.31	9.25	77.0	9.48	0.24	0.06	0.16	0.27	3.96	1.50
49R-1	511.79	10.51	87.6	—	—	—	—	—	—	—
49R-2	513.32	9.84	82.0	10.05	0.21	0.06	0.18	0.22	3.45	1.18
49R-3	514.78	10.49	87.4	—	—	—	—	—	—	—
50R-2	523.51	10.36	86.3	—	—	—	—	—	—	—
50R-4	526.43	9.86	82.1	9.85	0.00	0.07	0.07	0.24	0.00	0.00
50R-6	529.26	10.57	88.1	—	—	—	—	—	—	—
51R-1	531.66	10.80	90.0	—	—	—	—	—	—	—
52R-1	541.31	9.26	77.2	—	—	—	—	—	—	—
52R-3	544.19	8.63	71.9	8.68	0.05	0.04	1.56	0.22	1.23	0.03
52R-5	546.63	10.91	90.9	—	—	—	—	—	—	—
53R-2	552.13	10.88	90.7	—	—	—	—	—	—	—
53R-4	555.13	10.25	85.4	10.23	0.00	0.06	0.11	0.19	0.00	0.00
53R-5	556.63	11.75	97.9	—	—	—	—	—	—	—
54R-2	561.99	11.34	94.5	—	—	—	—	—	—	—
54R-4	564.97	10.84	90.3	11.00	0.15	0.03	0.04	0.12	5.05	3.79
54R-6	566.85	11.19	93.2	—	—	—	—	—	—	—
55R-2	571.48	11.55	96.2	—	—	—	—	—	—	—
55R-4	574.48	10.81	90.1	—	—	—	—	—	—	—
55R-6	577.31	10.54	87.8	10.94	0.40	0.04	0.23	0.17	9.90	1.71
56R-2	581.22	10.97	91.4	—	—	—	—	—	—	—
56R-4	584.22	11.26	93.8	—	—	—	—	—	—	—
57R-2	590.77	10.99	91.6	—	—	—	—	—	—	—
57R-4	594.00	10.26	85.5	10.56	0.30	0.06	0.09	0.21	4.97	3.31
57R-6	596.90	11.24	93.6	—	—	—	—	—	—	—
58R-2	600.46	10.84	90.3	—	—	—	—	—	—	—
58R-4	603.57	11.01	91.7	—	—	—	—	—	—	—
58R-6	606.33	10.75	89.5	10.68	0.00	0.02	0.08	0.09	0.00	0.00
59R-2	610.60	11.67	97.2	—	—	—	—	—	—	—
60R-2	619.64	11.80	98.3	—	—	—	—	—	—	—
61R-2	629.50	11.80	98.3	—	—	—	—	—	—	—
62R-1	637.10	11.07	92.2	10.95	0.00	0.01	0.07	0.09	0.00	0.00
62R-3	640.12	11.79	98.2	—	—	—	—	—	—	—
63R-1	646.37	11.00	91.7	—	—	—	—	—	—	—
63R-1	646.63	11.18	93.1	—	—	—	—	—	—	—
63R-3	649.16	8.16	68.0	7.37	0.00	0.01	0.16	0.17	0.00	0.00
63R-3	649.24	7.55	62.9	—	—	—	—	—	—	—
64R-1	655.94	7.97	66.4	—	—	—	—	—	—	—
64R-2	657.39	0.52	4.3	0.47	0.00	0.02	0.00	0.43	0.00	—

Notes: IC = inorganic carbon, TC = total carbon, TOC = total organic carbon, C/N = carbon/nitrogen, C/S = carbon/sulfur. — = not analyzed.

Table T13. Results of Rock-Eval analyses on sediments, Site 1197.

Core, section	Depth (mbsf)	T_{max}	S_1	S_2	S_3	HI	OI	TOC (wt%)
194-1197A-								
1H-2	2.12	—	0.00	0.00	15.16	—	—	0.00
1H-4	5.12	—	0.00	0.00	12.87	—	—	0.00
2H-2	8.22	—	0.00	0.00	13.44	—	—	0.00
2H-4	11.22	—	0.00	0.00	13.59	—	—	0.00
2H-6	14.22	369	0.00	0.01	15.69	—	—	0.00
3H-2	17.72	—	0.00	0.00	13.68	—	—	0.00
3H-4	20.72	—	0.00	0.00	12.87	—	—	0.00
3H-6	23.72	—	0.00	0.00	12.03	—	—	0.00
4H-2	27.22	374	0.01	0.02	14.52	—	—	0.00
4H-4	30.22	—	0.00	0.00	12.87	—	—	0.00
4H-6	33.22	—	0.01	0.01	13.97	—	—	0.00
5H-2	36.72	305	0.01	0.01	12.27	—	—	0.00
5H-4	39.72	—	0.01	0.01	12.81	—	—	0.00
5H-6	42.72	349	0.00	0.01	15.15	—	—	0.00
6H-2	46.22	—	0.00	0.00	14.74	—	—	0.00
6H-4	49.22	—	0.00	0.00	14.15	—	—	0.00
6H-6	52.22	—	0.00	0.00	13.78	—	—	0.00
194-1197B-								
2R-1	60.03	—	0.00	0.00	1.19	0	11,900	0.01
6R-1	98.23	—	0.00	0.00	1.10	—	—	0.00
14R-1	175.14	—	0.00	0.00	3.67	0	18,350	0.02
15R-1	184.69	—	0.00	0.00	5.11	0	51,100	0.01
16R-1	194.56	—	0.00	0.00	3.47	0	34,700	0.01
17R-1	203.93	—	0.00	0.00	5.01	0	50,100	0.01
18R-1	213.57	—	0.00	0.00	4.74	0	47,400	0.01
19R-1	223.04	—	0.00	0.00	4.49	0	22,450	0.02
20R-1	232.90	—	0.00	0.00	4.01	0	40,100	0.01
21R-1	242.65	—	0.00	0.00	11.24	—	—	0.00
22R-1	252.09	—	0.00	0.00	3.65	0	36,500	0.01
23R-1	261.70	407	0.00	0.01	4.33	25	10,825	0.04
24R-1	271.52	412	0.00	0.03	4.56	150	27,800	0.02
25R-1	281.03	409	0.00	0.06	3.24	110	6,480	0.05
27R-1	300.20	413	0.00	0.01	2.23	100	22,300	0.01
28R-1	310.09	409	0.01	0.05	8.86	100	17,720	0.05
28R-2	311.44	412	0.01	0.08	8.97	160	17,940	0.05
29R-1	319.73	410	0.01	0.07	9.01	140	18,020	0.05
29R-2	320.96	414	0.00	0.03	8.15	150	40,750	0.02
30R-1	329.05	412	0.00	0.03	8.46	150	42,300	0.02
31R-1	338.83	407	0.01	0.06	8.88	120	17,760	0.05
31R-2	340.26	410	0.02	0.06	8.48	167	32,561	0.03
32R-1	348.32	409	0.01	0.02	9.00	100	45,000	0.02
33R-1	358.23	412	0.00	0.01	7.41	100	—	0.01
34R-1	367.82	410	0.01	0.12	10.57	109	9,609	0.11
35R-1	377.70	410	0.01	0.04	2.82	100	7,050	0.04
35R-3	380.80	407	0.02	0.06	2.37	150	5,925	0.04
36R-1	387.10	407	0.03	0.09	4.66	171	8,137	0.06
36R-2	388.60	406	0.04	0.15	8.34	150	8,340	0.10
36R-3	389.82	409	0.02	0.11	3.65	110	3,650	0.10
37R-1	396.91	405	0.01	0.02	1.70	66	5,666	0.03
38R-2	408.39	409	0.02	0.15	7.01	64	3,105	0.23
38R-4	410.91	406	0.01	0.05	3.23	62	4,037	0.08
39R-2	417.93	408	0.01	0.09	7.05	75	5,875	0.12
39R-4	420.56	408	0.00	0.08	3.15	80	3,150	0.10
39R-6	423.36	405	0.00	0.04	2.92	80	5,840	0.05
40R-2	427.57	409	0.00	0.05	2.16	83	3,600	0.06
40R-4	429.91	406	0.00	0.05	2.45	83	4,083	0.06
41R-1	435.84	404	0.02	0.04	2.32	100	5,800	0.04
41R-3	438.43	405	0.03	0.07	6.19	77	6,877	0.09
42R-1	445.64	406	0.03	0.06	2.58	100	4,300	0.06
43R-1	455.16	406	0.03	0.05	2.58	83	4,300	0.06
44R-2	465.73	409	0.05	0.10	3.17	90	2,881	0.11
44R-4	468.35	409	0.06	0.10	7.88	111	8,755	0.09
44R-6	471.13	409	0.18	0.21	7.36	119	4,273	0.18
45R-2	475.42	410	0.15	0.20	12.11	80	4,844	0.25
45R-4	478.02	408	0.03	0.05	1.78	100	3,560	0.05
45R-6	480.77	408	0.07	0.05	2.82	83	4,700	0.06
46R-2	485.13	414	0.00	0.17	2.53	70	1,054	0.24
46R-4	488.13	412	0.01	0.12	9.55	75	5,968	0.16
46R-6	490.89	411	0.00	0.13	10.44	59	4,745	0.22
47R-2	494.58	414	0.05	0.31	8.93	53	1,555	0.54
47R-4	497.49	409	0.00	0.04	8.11	66	13,576	0.06
47R-6	500.19	411	0.01	0.02	3.01	88	21,912	0.02
48R-1	502.66	407	0.03	0.08	2.52	61	1,938	0.13
48R-3	505.23	403	0.01	0.04	3.63	42	4,196	0.09
48R-5	508.31	410	0.00	0.14	4.53	60	1,969	0.23
49R-1	511.79	411	0.00	0.05	9.07	62	11,337	0.08
49R-2	513.32	405	0.00	0.13	4.72	81	2,950	0.16
49R-3	514.78	409	0.01	0.11	9.46	57	4,978	0.19
50R-2	523.51	410	0.01	0.09	8.92	45	4,460	0.20
50R-4	526.43	409	0.01	0.12	4.85	48	1,940	0.25
50R-6	529.26	406	0.01	0.07	3.32	50	2,371	0.14
51R-1	531.66	409	0.02	0.06	9.26	60	9,260	0.10
51R-4	535.62	407	0.01	0.08	10.30	53	6,866	0.15
52R-1	541.31	406	0.01	0.11	13.19	52	6,280	0.21
52R-3	544.19	406	0.01	0.07	4.06	53	3,123	0.13
52R-5	546.63	408	0.01	0.04	7.93	66	13,216	0.06
53R-2	552.13	409	0.01	0.07	6.96	77	7,733	0.09
53R-4	555.13	418	0.01	0.10	3.84	71	2,903	0.14
53R-5	556.63	—	0.00	0.00	2.24	0	21,750	0.01
54R-2	561.99	408	0.00	0.03	6.94	60	13,880	0.05
54R-4	564.97	409	0.02	0.15	5.45	90	5,498	0.11
54R-6	566.85	408	0.01	0.10	7.38	55	4,100	0.18
55R-2	571.48	407	0.00	0.03	6.06	83	20,183	0.03
55R-4	574.48	413	0.00	0.17	9.07	54	2,925	0.31
55R-6	577.31	412	0.01	0.15	5.51	44	1,713	0.33
56R-2	581.22	410	0.00	0.04	7.14	66	11,900	0.06
56R-4	584.22	409	0.00	0.05	1.44	71	2,057	0.07
57R-2	590.77	410	0.01	0.14	8.07	73	4,247	0.19
57R-4	594.00	412	0.02	0.16	3.50	76	1,666	0.21
57R-6	596.90	400	0.01	0.02	4.72	66	15,733	0.03
58R-2	600.46	416	0.02	0.08	7.58	72	6,890	0.11
58R-4	603.57	395	0.03	0.01	7.51	33	25,033	0.03
58R-6	606.33	—	0.01	0.00	2.75	0	13,750	0.02
59R-2	610.60	—	0.01	0.00	2.10	—	—	0.00
60R-2	619.64	—	0.00	0.00	4.98	—	—	0.00
61R-2	629.50	—	0.00	0.00	3.84	—	—	0.00
62R-1	637.10	389	0.01	0.01	7.61	17	28,488	0.03
62R-3	640.12	—	0.01	0.00	3.54	—	—	0.00
63R-1	646.37	—	0.00	0.00	6.43	—	—	0.00
63R-1	646.63	—	0.01	0.00	5.90	—	—	0.00
63R-3	649.16	—	0.00	0.00	7.18	0	14,360	0.05
63R-3	649.24	376	0.02	0.01	4.03	14	5,757	0.07
64R-1	655.94	376	0.01	0.01	12.59	20	25,180	0.05
64R-2	657.39	—	0.00	0.00	4.73	—	—	0.00

Notes: T_{max} = temperature of maximum hydrocarbon generation during pyrolysis in °C, S_1 = milligrams of free hydrocarbons per gram of rock, S_2 = milligrams of pyrolyzed hydrocarbons per gram of rock, S_3 = milligrams of carbon dioxide per gram of rock, HI = hydrogen index in milligrams of hydrocarbon per gram of TOC, OI = milligrams of carbon dioxide per gram of TOC, TOC = total organic carbon. — = not available.